The imprinted mouse *Kcnk9* gene - expression analysis in specific brain regions and phenotypic analysis of knockout mice

Das geprägte *Kcnk9*-Gen der Maus – Expressionsanalyse in spezifischen Hirnregionen und phänotypische Analyse von Knockout-Mäusen

D I S S E R T A T I O N

Zur Erlangung des Grades

Doktor der Naturwissenschaften

Am Fachbereich Biologie

Der Johannes Gutenberg-Universität Mainz

Alexis Cooper

geb. am 27.11.1985 in Kansas, Fort Riley, USA

Mainz, 2019

Contents

Zusammenfassung

Kcnk9/KCNK9 ist ein geprägtes maternal exprimiertes Gen in Maus und Mensch, dessen Mutationen ursächlich für das Birk-Barel Intellectual Disability-Syndrom (BBIDS) sind. Es kodiert für TASK3/KCNK9, ein Mitglied der Superfamilie der K^+-Kanalproteine mit zwei Poren-bildenden Domänen und ist in die Modulation des Ruhemembranpotenzials und der Erregbarkeit neuronaler Zellen involviert.

In den bisherigen Studien wurde ausschließlich der Phänotyp von homozygoten *Kcnk9*-Knockout-Mäusen (*Kcnk9*KO^{hom}) untersucht, bei denen beide elterliche Allele des *Kcnk9*-Gens inaktiviert vorliegen. Aufgrund der Literaturbefunde zur maternal-spezifischen Expression des *Kcnk9/KCNK9*-Gens und der dazu passenden maternalen Vererbung des BBIDS, ist es jedoch von hoher Relevanz, auch heterozygote *Kcnk9*-Knockout-Mäuse mit maternal vererbtem Knockout-Allel (*Kcnk9*KO^{mat}) phänotypisch zu charakterisieren. Es ist zu erwarten, dass diese Mäuse ähnliche oder identische phänotypische Auffälligkeiten wie homozygote Knockout-Mäuse aufweisen. In der Tat zeigten *Kcnk9*KO^{hom}- und *Kcnk9*KO^{mat}-Mäuse im Vergleich zu Wildtyp-Mäusen ein deutlich beeinträchtigtes Arbeitsgedächtnis und eine abnormale Präpulsinhibition auf. Überraschenderweise wurde bezüglich der akustischen Schreckreaktion und der nächtlichen Bewegungsaktivität bei den *Kcnk9*KO^{mat}-Tieren ein zwischen denen der *Kcnk9*KO^{hom}- und WT-Tiere liegender Phänotyp beobachtet.

Die Allel-spezifische Expressionsanalyse von *Kcnk9*-mRNA in (C57BL / 6JxCast / Ei) F1-Hybridtieren ergab eine unvollständige paternale Stilllegung von *Kcnk9* im Gehirn mit einer signifikanten restlichen väterlichen Expression insbesondere im Locus coeruleus. Weiterhin wiesen *Kcnk9*KO^{mat}-Tiere im Vergleich zu (C57BL/6xCast/Ei) F1-Wildtyp-Tieren eine erhöhte väterliche *Kcnk9*-Expression im Gehirn auf, was eine regulatorische Rückkopplungsschleife zwischen der mütterlichen und der väterlichen *Kcnk9*-Expression nahelegt.

Die tägliche intraperitoneale Injektion des Histondeacetylase-Inhibitors CI-994 erhöhte die *Kcnk9*-Expression vom inhibierten paternalen *Kcnk9*-Allel zusätzlich, was zu einer vollständigen Rettung des Verhaltensphänotyps von *Kcnk9*KO^{mat}-Tieren führte. Diese Rettung korrelierte mit einer Erhöhung der Histon-3-Lysin-27-Acetylierung (H3K27ac) am Promotor und der intronischen Region von *Kcnk9* in mehreren Gehirnregionen.

Zusammenfassend zeigen die Ergebnisse dieser Dissertation dass das väterliche *Kcnk9*-Allel im Gehirn unvollständig stillgelegt ist, in Abwesenheit des mütterlichen Allels zusätzlich dereprimiert wird und durch exogene epigenetische Modulation mit CI-994 substanziell aktiviert wird, was zu einer vollständigen Rettung des neurokognitiven Phänotyps von *Kcnk9*KO^{mat}-Mäusen nach der Behandlung führt. Meine Doktorarbeit verdeutlicht somit einen vielversprechenden therapeutischen Effekt des Inhibitors CI-994 in einem Mausmodell für BBIDS und stellt die erste epigenetische Therapie zur Verbesserung kognitiver Funktionsstörungen in einem Mausmodell mit einer genomischen Imprintingstörung dar.

Abstract

Kcnk9/KCNK9 is a paternally silenced and maternally expressed imprinted gene in mouse and human, whose heterozygous pathogenic variants on the maternal allele are causative for the maternally inherited Birk-Barel intellectual disability syndrome (BBIDS). It encodes a two-pore domain potassium (K2P) channel (TASK3 or KCNK9) and is involved in the modulation of the resting membrane potential and excitability of neurons.

In the previous studies, only the phenotype of homozygous *Kcnk9* knockout mice (*Kcnk9*KO^{hom}) was investigated in which both parental alleles of the *Kcnk9* gene are inactivated. Based on the literature findings on the maternal-specific expression of the *Kcnk9 / KCNK9* gene and the matching maternal inheritance of BBIDS, it is highly relevant to phenotypically characterize heterozygous *Kcnk9* knockout mice with a maternally inherited knockout allele (*Kcnk9*KO^{mat}). It is expected that these mice have similar or identical phenotypic abnormalities as homozygous knockout mice. Indeed, in a study comparing *Kcnk9*KO^{hom} with *Kcnk9*KO^{mat} and wildtype littermates in a behavioral battery, a clearly impaired working memory and abnormal sensorimotor gating of *Kcnk9*KO^{mat} and *Kcnk9*KO^{hom} mice in comparison to WT mice was observed. Surprisingly, however, the phenotype of *Kcnk9*KO^{mat} animals regarding acoustic startle response and nocturnal locomotor activity was intermediate between those of *Kcnk9*KO^{hom} and WT mice in. Allele-specific expression analysis of *Kcnk9* mRNA in (C57BL/6JxCast/Ei)F1 hybrid animals revealed non-canonical imprinting of *Kcnk9* in the brain with significant residual paternal expression particularly in the LC, suggesting that the paternal *Kcnk9* imprint is leaky. In addition *Kcnk9*KO^{mat} animals displayed paternal *Kcnk9* expression in the brain further increased compared to that of (C57BL/6xCast/Ei)F1 wild-type animals, suggesting a regulatory feedback-loop between maternal and paternal *Kcnk9* expression.

Daily intraperitoneal injection of the second-generation histone deacetylase (HDAC) inhibitor CI-994 further increased expression from the paternally repressed *Kcnk9*

allele, which resulted in a full rescue of the behavioral phenotype of *Kcnk9*KO^{mat} animals. This rescue was accompanied by an increase of histone 3 lysine 27 (H3K27ac) acetylation at the promoter and intronic region of *Kcnk9* in several brain regions. Taken together, the findings of my thesis demonstrate that the paternal allele of *Kcnk9* is not fully silenced in the brain, further derepressed in the case of loss of the maternal allele and substantially activated upon exogenous epigenetic modulation with CI-994 leading to a full rescue of the behavioral phenotype of *Kcnk9*KO^{mat} animals after treatment. Thus, my thesis provides evidence for a promising therapeutic effect of the inhibitor CI-994 in a mouse model for BBIDS and introduces the first epigenetic therapy to improve cognitive dysfunctions in a mouse model of an imprinting disorder.

1. Introduction

1.1. Epigenetics

The modern definition of epigenetics involves mitotic and meiotic inheritance and reversibility of biochemical modifications of DNA and chromatin structures, without a change in DNA sequence (Egger et al., 2004). The definition of the word “epigenetics” originates from the terms “epi-” (upon, beyond) and genetic” (genome), which represents a layer of information, that exists additionally to the DNA sequence. Epigenetic regulatory mechanisms mediated by chromatin and DNA modifications can promote distinctive expression patterns of individual cells and contribute to the major diversity of different cell types, although their DNA is identical. These epigenetic modifications allow cells that share the same genome to undergo separate differentiation processes and influence various biological phenomena (Payer and Lee, 2008). Each cell type has accordingly, different epigenomes, influenced by environmental and age-related dynamics (Fraga et al., 2005).

Historically, the term was first used in 1942 by the embryologist Conrad Hal Waddington. In his publication "The epigenotype" he postulated: "The phenotype of an organism is created by a program that comes from the genome regulated and influenced by the environment" (Waddington, 1942). Originally, Waddington defined epigenetics as the branch of biology that studies causal interactions between genes and their products, that eventually lead to a phenotype (Waddington, 1942). C. H. Waddington's concept combines classical genetics and embryology and describes the interaction between cell differentiation and genetic mutations during development, presenting the relationship as a hillside with bifurcating canals (creodes).

Covalent modifications of histone proteins and methylation of DNA cytosine residues are the two most studied non-sequence-dependent mechanisms of transmitting information epigenetically. Both modification types are stable through cell division, allowing long-term control over gene expression. There is complex cross-talk

between histone modifications and DNA methylation, which cooperate to coordinate complex transcriptional responses (Cedar and Bergman, 2009; Schultz et al., 2002). Despite their longevity, the majority of epigenetic modifications are also reversible and highly sensitive to environmental perturbation (Cedar and Bergman, 2009). Epigenetic regulatory mechanisms can be divided into two functional groups, *cis*-and *trans*-acting factors, according to their molecular approach of influencing gene expression (Bonasio et al., 2010). Feedback mechanisms and other auto-regulatory networks of gene transcription are very common epigenetic control mechanisms. Among a large number of previously characterized trans-acting short non-coding RNAs, miRNA, siRNAs and piRNAs have been described in association with RNA interference (RNAi) and RNAi-mediated chromatin silencing, which represent the third common epigenetic regulatory system and are described elsewhere (Fire et al., 1998; Taft et al., 2010). A comprehensive introduction to the *cis*-operating factors, DNA methylation and histone modifications, is given in the following chapters 1.1.1 and 1.1.2, respectively.

1.1.1 DNA Modifications

The covalent attachment of a methyl group to the C5 atom of cytosine is one of the most comprehensively studied epigenetic regulatory mechanisms and is catalyzed by DNA methyltransferases (DNMTs) (Hotchkiss, 1948; Li et al., 1992). Cell-specific methylation patterns are established during early embryonic development and play a role in the regulation of gene expression after and during cell differentiation (Robinson et al., 2010). In somatic cells, methylation of cytosine predominantly occurs symmetrically at the palindromic CpG context (Mandel and Chambon, 1979; McGhee and Ginder, 1979). These may be either non-coding regions including repetitive elements such as satellite sequences, and transposons or CpG islands in promoter regions of the genes. A distinction is made between CpG-poor regions, which are predominantly methylated, and predominantly hypomethylated CpG islands (Gruenbaum et al., 1981; Takai and Jones, 2002). Hypermethylated CpG-poor regions are located in intergenic regions, while CpG islands are detectable in

the regulatory regions, such as gene promoters of the majority of all mammalian genes (Saxonov et al., 2006). Methylation in CpG context is mainly associated with gene silencing (Lister et al., 2009; Stadler et al., 2011). In addition, so-called "CpG island shores", where most of the tissue-specific DNA methylation occurs, have a significant impact on the transcription of certain genes. These regions are up to 2 kb away from the CpG island and are associated with transcriptional inactivation (Irizarry et al., 2009; Zilberman and Henikoff, 2007).

Regulation of expression by DNA methylation of promoters can be accomplished by two main mechanisms. Either the methylation alters the biophysical property of the base, resulting in a reduction in the binding affinity of DNA binding proteins (for detailed description see chapter 1.2.2. CTCF and the *H19 / Igf2* locus, Figure 3) or DNA methylation can serve as a signal for chromatin modification (Gibney and Nolan, 2010; Watt and Molloy, 1988). In the second case, the repression of transcription takes place by recruitment of so-called methyl-CpG-binding proteins such as MECP2 (methyl-CpG-binding protein) to methylated DNA regions. This can initiate heterochromatization, which can lead to chromatin compaction and thus, gene inactivation (Bird and Wolffe, 1999; Meehan et al., 1989). In addition to the control of specific gene activity, DNA methylation is involved in a number of other mechanisms, such as X chromosome inactivation in female marsupial and eutherian mammals, silencing of transposable elements, genomic imprinting (chapter 1.2), and maintenance of genome stability, presumably by contributing to correct chromosome segregation and preventing non-disjunction (Barr and Bertram, 1949; Bourc'his and Bestor, 2004; Csankovszki et al., 2001; Kaneda et al., 2004; Portela and Esteller, 2010; Walsh et al., 1998; Wutz and Jaenisch, 2000).

1.1.2 Histone Modifications

The smallest unit of chromatin is the nucleosome, which is composed of a histone-DNA complex. The complex consists of 147 bp double-stranded DNA wrapped in a left-handed superhelix around an octameric protein complex, forming a so-called

“nucleosomal core particle” (Oudet et al., 1975). Each histone-DNA complex is formed from two copies each of the proteins H2A/H2B dimers, H3/H4 dimers and with one H1 linker histone (Kornberg and Thomas, 1974; Luger et al., 1997). Nucleosomes are found every ± 60 bp genomic DNA (Olins and Olins, 1974). In particular, the amino acid chains at the N-termini of H2A, H2B, H3, and H4 histones can be post-translationally modified by acetylation, methylation, phosphorylation, ubiquitinylation, sumoylation, ADP ribosylation, propionylation, butyrylation, 2-hydroxyisobutyrylation, succinylation, malonylation, glutarylation, crotonylation, β-hydroxybutyrylation and deamination of amino acid residues (Kebede et al., 2015; Kouzarides, 2007; Sabari et al., 2017). Histone modifications ultimately result in changes in the superior chromatin structure and thus, contribute to the chromatin compaction and accessibility as well as to regulation of gene transcription (Berger, 2002; Luger et al., 1997). Generally, butyrylation of lysine, the phosphorylation of serine and threonine and acetylation of lysine residues (for detailed description, see chapter 1.1.2.1) are associated with euchromatisation and subsequent gene activation. In contrast histone methylations, ubiquitinations, and sumoylations lead predominantly to heterochromatization and inactivation of gene transcription (Goudarzi et al., 2016; Mahadevan et al., 1991; Schultz et al., 2002). In addition, recent studies have shown that histone modifications can act indirectly and recruit effector proteins to activate downstream signaling, block the access of remodeling complexes, or influence the recruitment of chromatin modifiers and transcription factors (Clements et al., 2003; Lawrence et al., 2016; Margueron et al., 2005; Wysocka et al., 2006). More recent studies have shown, that central globular domains of the histones also contain a high number of modification sites (Tropberger and Schneider, 2013). For schematic representation of known post-translational histone tail modifications and their role in gene regulation, see Figure 1 and Table 1.

1.1.2.1 Histone Acetylation and Deacetylation

Acetylation of histones is one of the best-studied and most widespread histone modifications, which takes place on different lysine residues. Acetylation is a key modulator of chromatin structure and gene regulation and is generally associated with the activation of transcription (Kouzarides, 2007). The dynamic balance between acetylation and deacetylation in the cell is critically important and controlled by two antagonistic enzymes, histone acetyltransferases (HATs) and histone deacetylases (HDACs) (Bannister and Kouzarides, 2011).

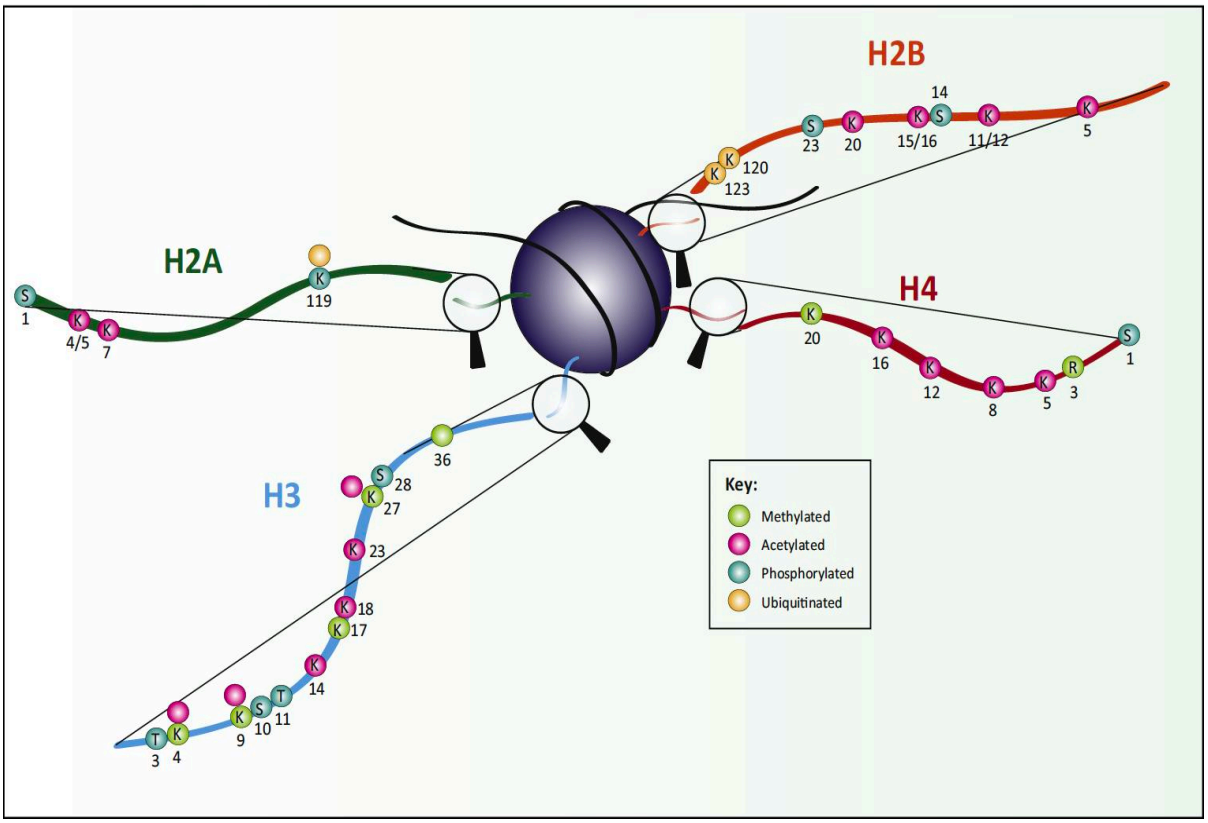

Figure 1: Post-Translational Modifications of the Histone Tails. Schematic showing post-translational changes that include the N-terminal side chains of H2A, H2B, H3 and H4 histones. The position of each amino acid modified is given by black numbers and the amino acid modified at the respective position is also shown (K = lysine, R = arginine, S = serine, T = threonine). Colors depict the respective modification (green = methylated, pink = acetylated, turquoise = phosphorylated, beige = ubiquitinated) (Lawrence et al., 2016).

In the non-acetylated state, lysine residues are protonated and strongly interact with the negatively charged phosphate group of the DNA, resulting in a compact chromatin structure (Borisenko et al., 2000). HATs transfer acetyl groups from acetyl-CoA to the lysine residues of histones. By attaching the acetyl group, the positive charge of the lysine is neutralized. This disturbs the electrostatic interactions between the histones and the negatively charged phosphate groups of the DNA (Shahbazian and Grunstein, 2007). This leads to a loosening of the densely packaged chromatin and thus results in higher accessibility of chromatin and binding of transcription factors to genomic DNA (Strahl and Allis, 2000). The histone acetyltransferases (HATs) can be classified into several groups, based on sequence similarity, including the GNAT family, the MYST family, the p300/cAMP response element binding protein (CREB)-binding protein family, some nuclear receptor coactivators (like SRC-1, ACTR, TIF2), and other general transcription factors (Bannister and Kouzarides, 2011; Roth et al., 2001).

HDACs remove the acetyl groups from lysine residues, thereby increasing the affinity between protonated lysine residues and DNA again. This leads to the formation of a tightly packed chromatin (transcriptionally inactive heterochromatin) structure that is less accessible to the transcription machinery (Fischle et al., 2003). HDAC molecules can be classified into four classes (class I, IIa, IIb and IV), which differ in structure, enzymatic function, subcellular localization and expression patterns. In addition to the mentioned HDACs, mammalian genomes also encode the sirtuins, which represent another group of deacetylases, referred to as class III HDACs (Bordone and Guarente, 2005). In this study, we focus on the class I HDAC family, which consists of HDAC1, 2, 3 and 8. These enzymes are expressed ubiquitously in the cell, but mainly localized to the nucleus where they display high affinity towards histones (Yang and Seto, 2003).

Table 1: Histone Tail Modifications (adapted from Lawrence et al., 2016)

Histone	Modification	Role
H2A	H2A H2AS1P	Mitosis; chromatin assembly
	H2AK4/5ac	Transcriptional activation
	H2AK7ac	Transcriptional activation
	H2AK119P	Spermatogenesis
	H2AK119uq	Transcriptional repression
H2B	H2BS14P	Apoptosis
	H2BS33P	Transcriptional activation
	H2BK5ac	Transcriptional activation
	H2BK11/12ac	Transcriptional activation
	H2BK15/16ac	Transcriptional activation
	H2BK20ac	Transcriptional activation
	H2BK120uq	Spermatogenesis/meiosis
	H2BK123uq	Transcriptional activation
H3	H3K4me1	Transcriptional activation, enriched at active enhancers
	H3K4me2	Permissive euchromatin
	H3K4me3	Transcriptional elongation; active euchromatin
	H3K9me3	Transcriptional repression; imprinting; DNA methylation
	H3R17me	Transcriptional activation
	H3K27me3	Transcriptional silencing; X-inactivation; bivalent genes/gene poising
	H3K36me3	Transcriptional elongation
	H3K4ac	Transcriptional activation
	H3K9ac	Histone deposition; transcriptional activation
	H3K14ac	Transcriptional activation; DNA repair
	H3K23ac	Transcriptional activation; DNA repair
	H3K27ac	Transcriptional activation
	H3T3P	Mitosis
	H3S10P	Mitosis; meiosis; transcriptional activation
	H3T11/S28P	Mitosis
H4	H4R3me	Transcriptional activation
	H4K20me1	Transcriptional silencing
	H4K20me3	Heterochromatin
	H4K5ac	Histone deposition; transcriptional activation; DNA repair
	H4K8ac	Transcriptional activation; DNA repair; transcriptional elongation
	H4K12ac	Histone deposition; telomeric silencing; transcriptional activation; DNA repair
	H4K16ac	Transcriptional activation; DNA repair
	H4S1P	Mitosis
	H4S1P	Mitosis

Both HATs and HDACs, which lack intrinsic DNA-binding activity, are recruited to the respective gene regions in multi-protein complexes consisting of sequence-specific transcription factors and their cofactors (Grunstein, 1997). The modifications induced by HDACs and HATs are both reversible and play a significant role in the regulation of transcription, as shown in Figure 2. The imbalance of HAT/HDAC activity can lead to altered gene expression profiles, changes in certain signaling pathways, proteasomal degradation and alterations in DNA methylation status (Hull et al., 2016).

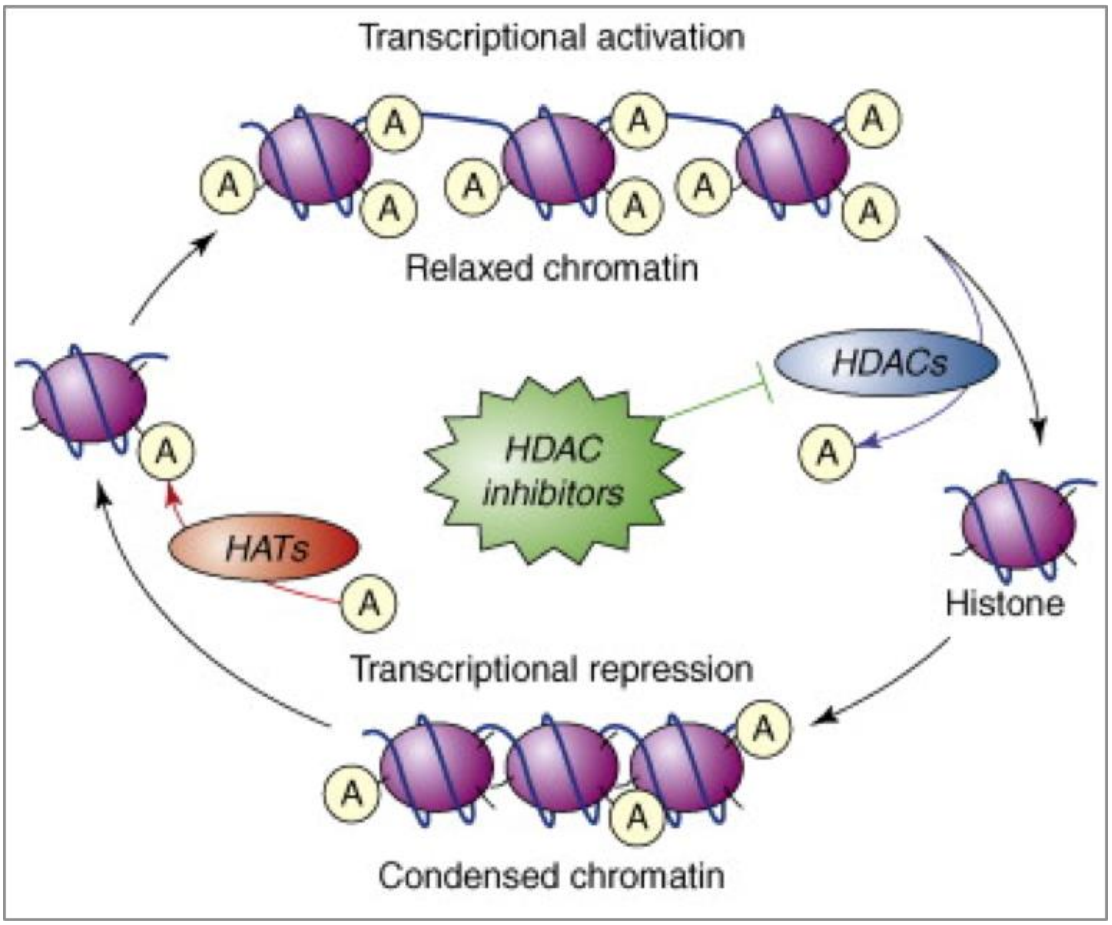

Figure 2: The antagonistic actions of HDACs and HATs. HATs transfer acetyl groups onto histones, which modulates the chromatin structure and accessibility of promoter regions to the transcriptional machinery, resulting in transcriptional activation. In contrast, HDACs remove the acetyl groups, leading to condensed chromatin and transcriptional repression (Chuang et al., 2009).

1.1.2.2 Histone Deacetylase Inhibitors

Histone deacetylase inhibitors (HDACi) block the activity of histone deacetylases by interacting with the catalytic domain of the enzymes. The prevention of deacetylation of histones leads to an increase in acetylation and thus to decondensation of chromatin. Subsequently, the relaxed chromatin structure is more accessible for processes resulting in altered gene expression profiles (Li et al., 2010; Margueron et al., 2005). Furthermore, HDACi can also inhibit the deacetylation of other proteins, such as structural proteins, chromatin remodeling proteins, DNA-binding nuclear receptors, signaling mediators, transcription co-regulators and DNA-binding transcription factors (Eckschlager et al., 2017). Whole-transcriptome analyses using microarrays, showed that only a fraction (2-5%) of the transcriptome is activated or repressed by HDAC inhibitors (Emanuele et al., 2008). This indicates that gene regulation modulated by HDACi is a specific process. Histone deacetylase inhibitors can be divided into five distinct classes, based on their chemical structure: hydroxamic acids (hydroxamates), short chain fatty acids (aliphatic), benzamides, cyclic tetrapeptides and sirtuin inhibitors including nicotinamide, sirtinol and cambinol (Eckschlager et al., 2017). In addition, the different HDACi differ in their spectrum of activity. HDAC isoform-selective inhibitors only inhibit several types of HDACs, whereas certain HDACis, pan-inhibitors, act against all types of HDACs (Table 2). Generally, treatment with HDAC inhibitors causes a higher abundance of hyperacetylated histones, which is accompanied by derepression of inhibited genes and increased expression of activated genes. Some HDACi have been approved by the United States Food and Drug Administration (FDA) and have great potential in the treatment of several diseases, such as cancer and neurodegenic diseases (Bolden et al., 2006; Hahnen et al., 2008).

1.1.2.3 Histone Methylation

Histone methylation can take place on both lysine (mono-, di- or trimethylation) and arginine (mono-or dimethylation) residues. In this work, we focus on lysine methylation. Depending on the position of the histone lysine residues and degree of methylation, lysine methylation can have a different effect on the regulation of transcription. Thus, modifications such as monomethylation on lysine 4 of histone H3 (H3K4me) and trimethylation on lysine 4 of histone H3 (H3K4me3) are associated with transcriptionally active gene regions and enhancers, whereas trimethylation on lysine 9 of histone H3 (H3K9me3) and lysine 27 of histone H3 (H3K27me3) induces transcriptional inactivation (Kouzarides, 2007; Local et al., 2018). Lysine methylation is performed by histone methyltransferases, which use the S-adenosylmethionine cofactor to transfer the methyl group onto the lysine. In contrast to histone acetylation, histone methylation does not alter the charge of the histone tails. In contrast, it affects the basicity and hydrophobicity of histones and their affinity for transcription factors. Altered methylation of the histones H3K9 and H3K27 are associated with aberrant gene repression in many types of tumors (Leszinski et al., 2012). Dysregulations of histone methyltransferase and demethylases can lead to pathological alteration of the histone methylation pattern and thus to deregulation of gene expression (Wong et al., 2011).

Table 2: Overview of selected histone deacetylase (HDAC) inhibitors (Eckschlager et al., 2017)

Class	HDAC Inhibitor	Target HDAC Class*	Clinical Status
Hydroxamic acids	Trichostatin A	pan	preclinical
	SAHA	pan	approved for cutaneous T-cell lymphoma
	Belinostat	pan	approved for peripheral T-cell lymphoma
	Panabiostat	pan	approved for multiple myeloma
	Givinostat	pan	phase II clinical trials—relapsed leukemia and multiple myeloma
	Resminostat	pan	phase I and II clinical trials—hepatocellular carcinoma
	Abexinostat	pan	phase II clinical trial—B-cell lymphoma
	Quisinostat	pan	phase I clinical trial—multiple myeloma
	Rocilinostat	II	phase I clinical trial—multiple myeloma
	Practinostat	I, II and IV	phase II clinical trial—prostate cancer
	CHR-3996	I	phase I clinical trial—advanced/metastatic solid tumors refractory to standard therapy
Short chain fatty acids	Valproic acid	I, IIa	approved for epilepsy, bipolar disorders and migraine, phase II clinical trials—several studies
	Butyric acid	I, II	phase II clinical trials—several studies
	Phenylbutyric acid	I, II	phase I clinical trials—several studies
Benzamides	Entinostat	I	phase II clinical trials—breast cancer, Hodgkin´s lymphoma, non-small cell lung cancer, phase III clinical trial—hormone receptor positive breast cancer
	Tacedinaline (CI-994)	I	phase III clinical trial—non-small cell lung cancer and pancreatic cancer
	4SC202	I	phase I clinical trial—advanced hematological malignancies
	Mocetinostat	I, IV	phase II clinical trials—Hodgkin´s lymphoma
Cyclic tetrapeptides	Romidepsin	I	approved for cutaneous T-cell lymphoma
Sirtuin inhibitors	Nicotinamide	all class III	phase III clinical trial—laryngeal cancer
	Sirtinol	SIRT 1 and 2	preclinical
	Cambinol	SIRT 1 and 2	preclinical
	EX-527	SIRT 1 and 2	cancer preclinical, phase I and II clinical trials—Huntington disease, glaucoma

*pan-inhibitors= act against all types of HDACs

1.2 Genomic Imprinting

Genomic imprinting is an epigenetically regulated process that causes approximately 1-2% of the genes in mammalian diploid cells to be expressed in a monoallelic fashion, either from the maternal or paternal chromosome only (Barlow and Bartolomei, 2014). Imprints are epigenetic modifications, which distinguish the maternally and paternally inherited alleles. A number of epigenetic modifications play a role in the regulation of allele-specific expression of imprinted genes. The two main epigenetic DNA modifications known in mammals are 5-methylcytosine and 5-hydroxymethylcytosine (Li and Zhang, 2014). The most frequently characterized regulator in imprinting is the methylation of cytosine bases at CpG positions of DNA, mostly found in the context of CpG islands (For further description see chapter 1.1.1, DNA methylation).

Genomic imprinting in mammals was discovered in the 1980s. Particularly important for the discovery were a series of pronucleus transplantation experiments in the mouse showing that maternal and paternal autosomes are not functionally equivalent in an individual (McGrath and Solter, 1984a, b; Surani et al., 1984), and that the contribution of both parental genomes is crucial for the normal development of an embryo (McGrath and Solter, 1984a, b; Surani et al., 1984). Thus, artificially generated murine zygotes with a diploid maternal (gynogenetic) genome developed to conceptuses with predominantly embryonic tissues and defective formation of extraembryonic structures (Surani et al., 1984). In contrast, artificially generated murine zygotes with a diploid paternal (androgenetic) genome developed to conceptuses that predominantly consisted of extraembryonic structures, while embryonic components were absent or severely retarded (Surani et al., 1986). In both cases, embryos died around the middle of gestation (McGrath and Solter, 1984a, b; Surani et al., 1984). This led to the hypothesis that the two parental genomes fulfilled complementary functions during early embryonic development via so-called parentally imprinted genes and that the lack or overexpression of these imprinted genes caused the observed developmental disorders (Ferguson-Smith, 2011). After complex crossbred experiments using mouse lines with different

chromosomal translocations, these parent-specific effects could be assigned to certain regions of the genome (Cattanach and Kirk, 1985). Several years later, in the early 1990's the existence of genomic imprinting of both parental genomes as a special type of epigenetic regulation was confirmed by the identification and characterization of the first imprinted genes, *Igf2r, Igf2,* and *H19,* in the mouse (Barlow et al., 1991; Bartolomei et al., 1991; DeChiara et al., 1991). This deviation from the rules of Mendelian inheritance is possible through parental allele-specific modification leading to the transcriptional inactivation of one allele and thus to the exclusive or preferential expression of the other allele (Moore and Haig, 1991; Reik and Walter, 2001). Many of the meanwhile identified imprinted genes show a development- and / or tissue-specific regulation of genomic imprinting (Santoro and Barlow, 2011).

In contrast to the findings of Surani et al. (1986), as well as McGrath and Solter (1984), a more recent study demonstrated that injecting sperm or an oocyte with cultured imprint-free hypomethylated androgenetic and parthenogenetic haploid embryonic stem cells (haESCs) harbouring deletions of specific imprinted regions, results in alive bipaternal and normally growing bimaternal mice. These innovative experiments indicate the possibility of unisexual reproduction in mammals, using specific gene manipulation tools (Li et al., 2018).

1.2.1 Evolutionary Theories of Genomic Imprinting in Mammals

To date numerous theories have attempted to elucidate the phenomenon of genomic imprinting in mammals from an evolutionary point of view. In principle, genomic imprinting in mammals should have a negative effect on the individual, since the advantage of diploidy is given up by the monoallelic expression of imprinted genes (Otto and Gerstein, 2008). However, this does not seem to be the case. Although genomic imprinting has also been found in some insects and plants, it is most prevalent among placental mammals (placentalia) including humans, mice and marsupials (Renfree et al., 2009a). They differ from egg-laying vertebrates and in

invertebrates (ovipar) in terms of their strategy of nourishing the growing embryo, such as to which extent the embryo uses the maternal resources for developmental purposes (Renfree et al., 2009b). Oviparity is often associated with parthenogenesis, an asexual reproduction form in which a female gamete develops into an organism without fertilization, resulting in an individual with two identical maternal genomes and absence of imprinting (Kono, 2006). In mammals, the paternal genome is necessary and sexual reproduction is inevitable, which gives an indication of the importance of genomic imprinting in the evolution of mammals. Placentalia are known to have the highest degree of complexity concerning genomic imprinting, compared to other infraclasses of mammals (Suzuki et al., 2005).

Many evolutional theories attempt to interpret the purpose of genomic imprinting in mammals, and try to explain why this phenomenon is absent in ovipar animals. The most common model, the “parental conflict hypothesis” or “kinship theory” is based on the conflict between the two parental genomes and antagonistic interactions in the embryo (Moore and Haig, 1991). Moreover, Moore and Haig hypothesize, that the paternally expressed genes allow the father a maximum exploitation of maternal resources to increase fetal growth and optimize the fitness of his progeny, accepting a compromisation of the mother’s health (Wilkins and Haig, 2003). This theory is based on the promiscuous behavior of females, where the father is not necessarily related to all the offspring of the female, and has the goal to ensure the survival of his own progeny. Counteracting, the maternal genome is determined to preserve the female organism and suppress these embryonic growth factors. The main objective of the female genome is to balance equal nutrient distribution to all offspring in the current pregnancy and to have sufficient resources for later pregnancies (Moore and Haig, 1991; Renfree et al., 2009a).

The “trophoblast defense theory” describes the risk of spontaneous female internal reproduction, which consequentially leads to the development of an embryo without paternal contribution and possibly ovarian trophoblast disease (Varmuza and Mann, 1994). This is not the case for males, since they do not possess the appropriate reproduction anatomy. Varmuza and Mann propose that the maternally silenced

imprinted genes support placental development and maternally expressed genes reduce placental growth. After fertilization, genes of the paternal genome then induce placental development, ensuring an adequate environment for the fetus.

In contrast, the "coadaptation hypothesis" attempts to explain the development of genomic imprinting as a coadaptive regulation between maternal behavior during pregnancy and embryonic development (Keverne and Curley, 2008; Wolf and Hager, 2006). Keverne and Curley describe a transgenerational model, in which the placenta plays a decisive role, as it not only promotes the embryonic prenatal nutrient supply, but also influences the maternal metabolism and sexual behavior pre- and postnatally. For example, multiple imprinted genes are paternally expressed and maternally silenced in the hypothalamus and in the placenta. The imprints associated with these genes are set in the germline of the mother and contribute significantly to the development of the fetoplacental unit, which has a counter-productive effect for the mother (exploitation of maternal resources) (Keverne and Curley, 2008; Ubeda and Gardner, 2015).

A more recent hypothesis postulates, that imprinting in placentalia has also been established, partly as a response to the significantly greater incidence of LTR (long terminal repeat) retrotransposons in the mammalian genome (Pask et al., 2009). These and other described theories cannot entirely explain the phenomenon of genomic imprinting, but allow an insight of the role of imprinted genes in embryonic and placental development (Wilkins and Haig, 2003). However it is conceivable that a combination of these main theories reflects the reality (Renfree et al., 2009a; Ubeda and Gardner, 2015).

1.2.2 Organization of Imprinting Clusters

The number of imprinted genes has now increased to over 150 in the mouse genome and over 250 genes in humans (http://www.geneimprint.com). Reciprocal crossbreeding between hybrid mouse strains and identification of single nucleotide

polymorphisms (SNPs) between the two strains is a common method to investigate novel imprinted genes in mice (DeVeale et al., 2012). The search for new imprinted genes is ongoing, but only a few new genes have been identified in recent screens (Bonaldi, 2017; Henckel and Arnaud, 2010).

The main feature of genomic imprinting is the *cis*-acting regulatory mechanism, which is restricted to one chromosome. Therefore, a regulatory factor, such as a silencing factor on one parental allele, cannot freely move within the nucleus and target the active parental allele. Imprinting is not reduced to silencing mechanisms and can regulate on all levels of gene regulation to ensure allele-specific gene expression. To provide differential expression, certain marks or “imprints” on one of the parental chromosomes are necessary, in order to direct transcription factors and mRNA processing factors.

Most of all known imprinted genes (more than 80%) are localized in one of 16 known genomic regions and organized in imprinted gene clusters, containing 3-12 imprinted genes in a span from 100-3700 kb of genomic DNA (Barlow and Bartolomei, 2014; Wan and Bartolomei, 2008). However, there are also cases of individual and co-organized imprinted genes in the genome (Cowley and Oakey, 2010). The existence of an imprinted long non-coding RNA (lncRNA) surrounded by several paternally and maternally expressed protein-coding genes is very characteristic of an imprinting cluster. . A further typical element of an imprinting cluster is a DNA sequence carrying a gametic methylation imprint, also known as a differentially methylated region (DMR) (Reik and Walter, 2001). In many cases the germline DMR regulates the expression of several or all imprinted genes in the cluster and is therefore often classified as an imprinting control element (ICE) or imprinting control region (ICR) (Wutz et al., 1997). A deletion in an imprinted region including the ICE, leads to the loss of ICE-dominated regulation throughout the cluster, only when the deletion occurs on the parental allele expressing the lncRNA (Buiting, 2010; Horsthemke and Buiting, 2006; Thorvaldsen et al., 1998).

The mechanisms by which the ICEs perform their regulatory functions vary from region to region. Two main *cis*-operating silencing mechanisms at imprinted gene clusters have been extensively described. One mechanism is the insulator model, that was postulated for the first time to explain imprinting control at the *Igf2-H19* locus (Fig. 3A). The CCCTC binding factor (CTCF) protein binds to the unmethylated ICE on the maternal chromosome and serves as an insulator, which inhibits the common enhancers from activating transcription of the distant *Igf2* and *Ins2* genes and instead activates transcription at the nearby *H19* lncRNA promoter (Bell and Felsenfeld, 2000; Leighton et al., 1995). These processes do not occur on the paternal allele, where the ICEs methylated which prevents CTCF binding and further confers methylation and transcriptional inactivation of the nearby *H19* lncRNA promoter (Hark et al., 2000). Another *cis*-operating silencing mechanism described thoroughly is the lncRNA model, which was suggested for the first time to explain imprinting control at the *Igf2r* cluster (Fig. 3B). The methylated ICE on the maternal allele harbors the *Air* lncRNA promoter, which is silenced by DNA methylation and thus allows maternal expression of the *Igf2r*, *Slc22a2* and *Slc22a3* genes (Sleutels et al., 2002). On the other hand, expression of the *Air* lncRNA on the paternal inhibits the expression of these three imprinted genes in *cis* by transcriptional interference (Mancini-Dinardo et al., 2006; Martienssen and Moazed, 2015), (Fig. 3B.).

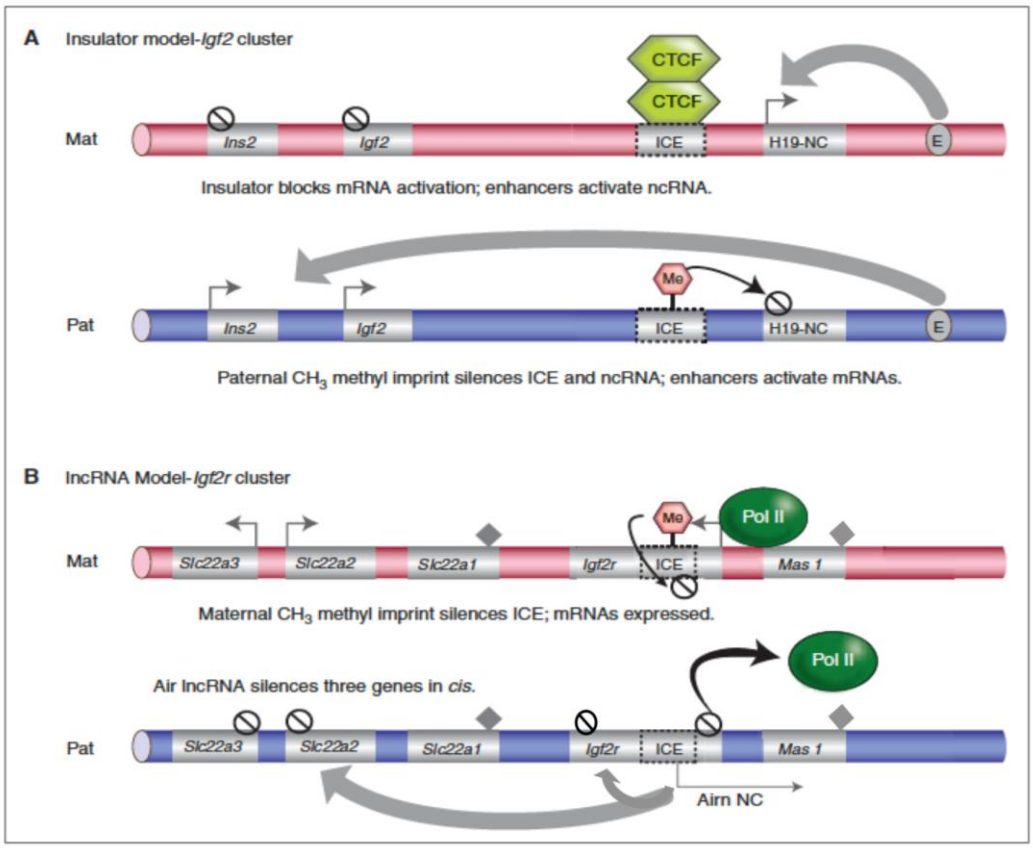

Figure 3: Two *cis*-silencing mechanisms for imprinted genes. (A) Endodermal insulator model in the *Igf2* cluster **(B)** Placental lncRNA model in the *Igf2r* cluster. For description see chapter 1.2.2. ICE: imprint control element; slashed circle, repressed allele of an imprinted gene; gray arrow, expressed allele of an imprinted gene; thick gray arrows, long distance effect in *cis;* filled diamonds, not expressed in placenta (adapted from Barlow and Bartolomei, 2014).

1.2.3 Epigenetic Reprogramming of Imprints

The imprints must be erasable in the germline during sex determination in order to reset the imprint for the next generation and generate imprinted haploid parental-specific gametes (Barlow and Bartolomei, 2014). In mammalian development, there are two crucial phases in which extensive epigenetic reprogramming takes place, gametogenesis and embryogenesis (Fig. 4). Genome-wide DNA demethylation also including imprinted gene DMRs occurs in developing mouse primordial germ cells (PGCs) between E8.5 and E11.5 and is accompanied by dynamic changes in

chromatin structure (Hayashi and Surani, 2009; Seki et al., 2005) (Guibert et al., 2012; Hajkova et al., 2008; Reik and Walter, 2001). Sex-specific remethylation processes follow during gametogenesis which also involve the establishment of new methylation imprints at DMRs/ICEs (Ferguson-Smith, 2011; Reik and Walter, 2001). The second phase of genome-wide DNA demethylation starts directly after fertilization in the zygote, to remove the vast majority of sex-specific methylation marks of gametes with only a few regions, such as the majority of imprinted gene DMRs being excluded (Rougier et al., 1998; Smith et al., 2012; Tomizawa et al., 2011) De novo methylation processes leading to the establishment of somatic methylation patterns follow around the time of implantation. Parental allele-specific DNA methylation during gametogenesis occurs in the majority of imprinting clusters (Bartolomei et al., 1993). DNA methylation imprints are introduced prenatally in prospermatogonia and postnatally during oocyte development, mediated by the *de novo* DNA methyltransferase DNMT3A and DNMT3L (Bourc'his and Bestor, 2004; Kelsey and Feil, 2013; Lucifero et al., 2002). Thus, two types of recognition system are required, one sperm-specific and one oocyte-specific, allowing imprint establishment and maintenance, throughout fertilization and mitosis in embryogenesis and adulthood (Reik and Walter, 2001). It is not fully elucidated, how exactly DNA methylation marks at imprinted genes escape the genome-wide reprogramming that occurs after fertilization. However, it is possible that *cis*-acting factors and *trans*-operating elements are responsible for the preservation of imprints (Li and Zhang, 2014). Allele-specifically unmethylated CpGs of imprinted genes must be shielded against *de novo* DNA methylation in the morula stage to ensure parental allele-specific gene expression (Li and Zhang, 2014; Nakamura et al., 2012). Specific maintenance mechanisms including molecules such as Arid4a-b, MBD3, ZFP57 and PGC7/STELLA (through interactions with H3K9me2), ensure imprint manifestation throughout active demethylation processes of the paternal genome in the zygote and passive demethylation of the maternal genome in the two-cell embryo (Nakamura et al., 2012; Reik and Walter, 2001; Santos and Dean, 2004). The erasure of imprints in PGCs is accomplished by a combination of DNA-replication-dependent passive processes and active demethylation through enzymatic oxidation of 5-methylcytosine

(5mC) to 5-hydroxymethylcytosine (5hmC) by ten-eleven translocation family of enzymes (TET1-3 enzymes) together with the excision of 5mC by base excision repair (BER) mechanisms throughout the cell cycle (Li and Zhang, 2014; Tahiliani et al., 2009; Tan and Shi, 2012).

In addition to DNA methylation, post-translational modifications of histone proteins, such as histone methylation, acetylation, phosphorylation, sumoylation, and ubiquitylation are involved in the regulation of genomic imprinting (Sadakierska-Chudy et al., 2015). For instance, H3K9me and H3K20me were found at the promoter region on the methylated maternal allele of the imprinted human *SNRPN* gene, while the active paternal allele is characterized by monomethylation of H3 (H3K4me) and acetylation of histones 3 and 4 (Fournier et al., 2002; Horsthemke and Buiting, 2008).

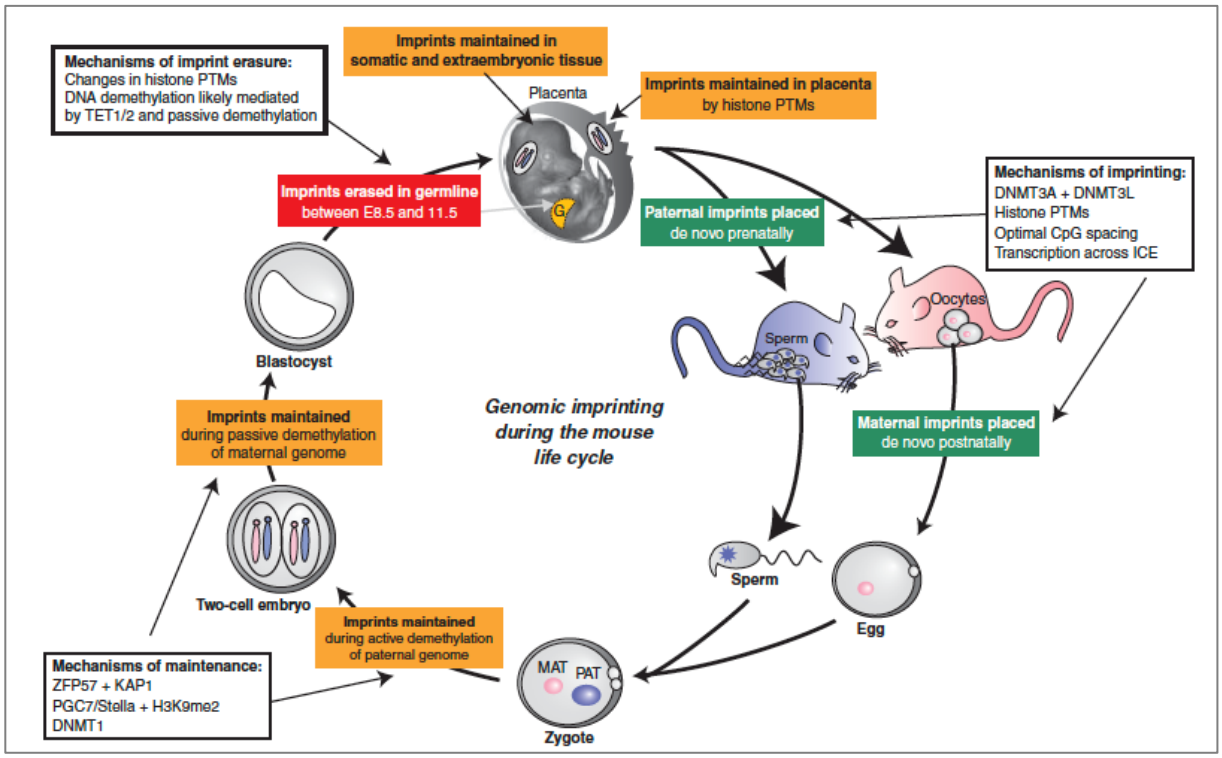

Figure 4: Establishment, maintenance, and erasure of genomic imprints in mouse development. See chapter 1.2.3 for further description (Barlow and Bartolomei, 2014).

1.2.4 Neurological Imprinting Disorders

The study of genes regulated in a parental-specific manner has contributed to the understanding of various so-called imprinting disorders. Current evolutionary theories attempting to explain the purpose of imprinted genes focus mainly on the influence of the parental alleles in embryonic nourishment and maternal resource distribution during pregnancy (see chapter 1.2.1). However, following the discovery of two neurological disorders associated with imprinting dysregulation in the human chromosomal region 15q11-13, Prader-Willi syndrome and Angelman syndrome, the role of imprinted genes in brain-specific processes gained strong significance (Nicholls et al., 1989). The relevance of imprinting in the brain has been further strengthened by several studies showing that the majority of imprinted genes are expressed most abundantly in the brain (Gregg et al., 2010). Brain function and behavioral phenotype can be affected by numerous genetic abnormalities involving imprinted genes, including duplications, deletions, null mutations, uniparental disomies and epimutations (Eggermann et al., 2015). Imprinting dysregulation has been further associated with a number of other diseases with neurological manifestations, e.g. Alzheimer's disease, asthma, autism, diabetes (type 1 and 2) schizophrenia and numerous imprinting disorders (Morison et al., 2005).

The human chromosomal region 15q11-q13, includes certain paternally expressed protein-coding genes and noncoding RNAs, together with the brain-specific maternally expressed *UBE3A* (Angulo et al., 2015; Sahoo et al., 2008). Angelman syndrome (AS) is a neurogenic disorder characterized by intellectual disability, developmental delay, hypermotoric behavior, seizures, happy demeanor and frequent laughter, also known as the "Happy Puppet Syndrome" (Bird, 2014; Williams and Frias, 1982). It is caused by deficient expression or function of the *UBE3A* gene through a maternal deletion of the 15q11-q13 region (65%-75% of cases), paternal uniparental disomy 15 (3%-7% of cases), an imprinting defect (3% of cases) or a pathogenic *UBE3A* variant (5-11% of cases)(Buiting, 2010).

Prader-Willi syndrome (PWS) is characterized by intellectual disability, hypogenitalism, low birth weight, hypotonia and adiposity. It is due to deficiency of paternally expressed genes in 15q11-13. Several molecular causes for this deficiency are known. In the majority of PWS patients (~ 70%), a paternal deletion of 15q11-13 is causative. Approximately 25% and 1% of cases have maternal uniparental disomy 15 and an imprinting defect, respectively, as molecular causes (Buiting, 2010).

The Silver-Russell syndrome (SRS) is a further well studied imprinting disorder and characterized by a small, triangular face with distinctive facial features including a prominent forehead, narrow chin, small jaw, and downturned corners of the mouth as well as pre- and postnatal growth abnormalities and childhood dwarfism. In about 44% of all SRS cases, aberrant hypomethylation of the ICR1 regulating imprinting of the *H19* and *IGF2* genes on human chromosome 11p15.5 can be diagnosed as molecular genetic cause (Binder et al., 2011; Russell, 1954). Maternal uniparental disomy 7 may cause disease in 5-10% of patients (Kotzot et al., 1995). In almost half of all SRS cases, the molecular causes cannot yet be determined using standard laboratory techniques (Binder et al., 2011).

Furthermore, Beckwith-Wiedemann syndrome (BWS) is a well described imprinting disorder associated with the imprinted region on human chromosome 11p15.5. The clinical features of BWS patients are inconsistent and include characteristics such as macroglossia, microcephaly, macrosomia, hemihyperplasia and omphalocele, (Beckwith, 1963; Wiedemann, 1964). Patients are likely to develop embryonal tumors (particularly Wilms tumor (nephroblastoma)), facial dysmorphia and hypoglycaemia (Weksberg et al., 2010). Known molecular causes of BWS are paternal uniparental disomy 11, mutations in the maternally expressed *CDKN1C* gene as well as imprinting defects in 11p15, i.e. gain of methylation at the ICR1 resulting in biallelic expression of *IGF2* or loss of methylation at the ICR2 leading to reduced expression of *CDKN1C* (Bliek et al., 2001; Cooper et al., 2005; Soejima and Higashimoto, 2013).

In addition, genomic imprinting is an important model system for the molecular analysis of epigenetic regulatory mechanisms during ontogenesis (Barlow, 2011).

Further recent studies have linked imprinted genes to additional neurological disorders. The 7q21–31 region is reported to be associated with autism spectrum disorder (Schanen, 2006). Allele-specific mutations in *SGCE* lead to myoclonus-dystonia syndrome accompanied by anxiety, agoraphobia and depression (Peall et al., 2013; Zimprich et al., 2001). The 8q24 region harbours the imprinted *KCNK9* and *TRAPPC9* genes, whose pathogenic variants have been associated with intellectual disability in mice and humans (Barel et al., 2008; Mochida et al., 2009). *TRAPPC9/Trappc9*, a gene that is linked to non-syndromic, autosomal-recessive intellectual disability and postnatal microcephaly, undergoes isoform-specific imprinting, with one truncated isoform being paternally expressed, however, all other transcripts being maternally expressed (Gregg et al., 2010; Mochida et al., 2009). See following chapter 1.2.5 for detailed description of *KCNK9* and its role in the Birk-Barel intellectual disability dysmorphism syndrome.

1.2.5 Birk-Barel Intellectual Disability Dysmorphism Syndrome and the *KCNK9* gene

The Birk-Barel intellectual disability dysmorphism syndrome (BBIDS or KCNK9 imprinting syndrome; OMIM 612292; outdated: Birk Barel mental retardation dysmorphism syndrome) is typically associated with congenital central hypotonia, developmental delay of speech and motor skills such as sitting and walking, reduced facial movements, decreased subcutaneous fat, intellectual disability and dysphagia (severe feeding problems). Dysmorphic features of BBIDS include dolichocephaly with a narrow forehead, short and broad philtrum, abnormally shaped eyebrows, tented upperlip, cleft palate as well as mild micro/retrognathia (Fig. 5) (Barel et al., 2008; Graham et al., 2016). BBIDS is inherited autosomal dominantly with maternal-only transmission, and caused by heterozygous pathogenic variants on the maternal allele of the paternally silenced (imprinted) *KCNK9* gene on chromosome 8q24.3 (Ruf et al., 2007; Barel et al., 2008). The most common pathogenic variant is the missense variant 770G>A in exon 2, replacing glycine at amino acid position 236 by

arginine (p.G236R) (Barel et al., 2008).

Using a high-resolution approach to analyze novel imprinting cluster regions, RNA-Seq technology was performed to characterize the transcriptome of brain tissues from F1 mouse hybrids (Gregg et al., 2010). This approach identified a 700 kb imprinting domain on mouse chromosome 15, containing the maternally expressed *Kcnk9* gene together with further imprinted genes, including *Eif2c2* (also known as *Ago2*), *Chrac1* and *Trappc9* and paternally expressed ncRNA *Peg13,* which lies within intron 17 of *Trappc9*. In addition, numerous expressed sequence tags (ESTs) were detected surrounding *Peg13* (Gregg et al., 2010).

A comprehensive allele-specific expression analysis of the human orthologous region on chromosome 8q24 revealed a reciprocally imprinted expression of the *KCNK9* and *PEG13* genes, with brain-specific maternal expression of *KCNK9* and paternal expression of *PEG13* (Court et al., 2014). In the mouse, the promoter of non-coding *Peg13* overlaps with a CpG island and is associated with a maternally methylated region (DMR), which is assumed to be involved in imprinted gene regulation in the *Kcnk9* cluster on mouse chromosome 15 (Singh et al., 2011; Xie et al., 2012). Studies of the human 8q24 region further showed that CTCF-mediated allele-specific chromatin looping connects the brain-specific enhancer and the *KCNK9*/*PEG13* promoter regions (Fig. 6) (Court et al., 2014). Genome-wide ChIA-PET and CTCF ChIP-seq datasets revealed a strong CTCF enrichment at the *KCNK9* and *PEG13* promoter, suggesting an enhancer chromatin signature with the co-enrichment of histone H3 lysine 4 monomethylation (H3K4me1), H3 lysine 27 acetylation (H3K27ac) chromatin marks and p300 in brain tissue (Heintzman et al., 2009). Utilizing a combination of whole-genome bisulphite sequencing (WGBS) and ChIP-seq for meDIP and H3K4me3, the methylation status of the associated CpG islands in the imprinting locus was analyzed. The analysis revealed that promoter CpG-islands associated with *KCNK9, AGO2, CHRAC1* and *TRAPPC9* are unmethylated in the brain and are associated with abundant H3K4me3 enrichment. These findings suggest that the imprinting of *KCNK9* is dependent on other *cis*-acting regulatory mechanisms and elements. A DMR was detected only at the *PEG13* locus, with

methylation of the maternal allele and enrichment for CTCF colocalized with cohesin on the unmethylated paternal allele (Court et al., 2014).

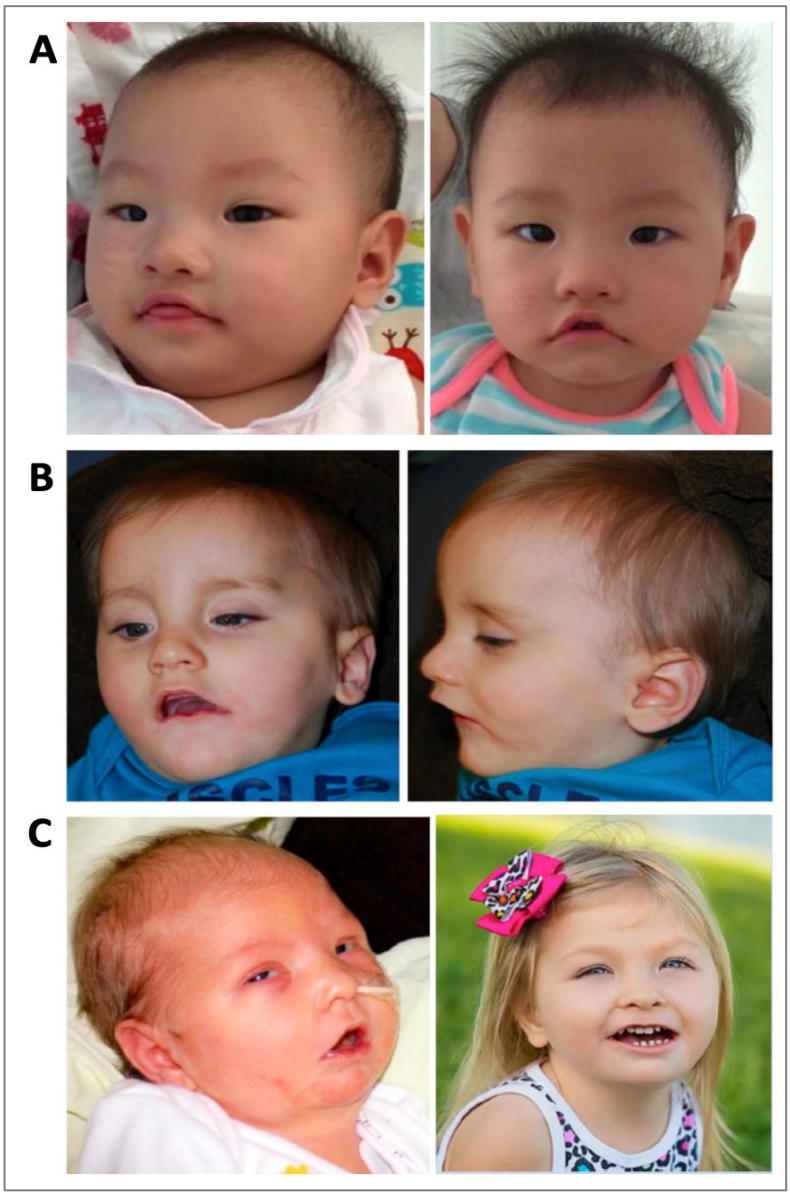

Figure 5: Patients with Birk-Barel Intellectual Disability Syndrome. (A) Young affected patient at 11 months showing mild dysmorphic features include bitemporal narrowing, tented upper lip, high arched palate, and retrognathia. **(B)** 13 month old patient with downturned open mouth, thin upper lip, broad alveolar ridges, cleft soft palate, and retognathia/micrognathia **(C)** Female patient after birth and 3 years of age displays micrognathia, high and broad nasal bridge, and a generous mouth with downturned corners. (Graham et al., 2016).

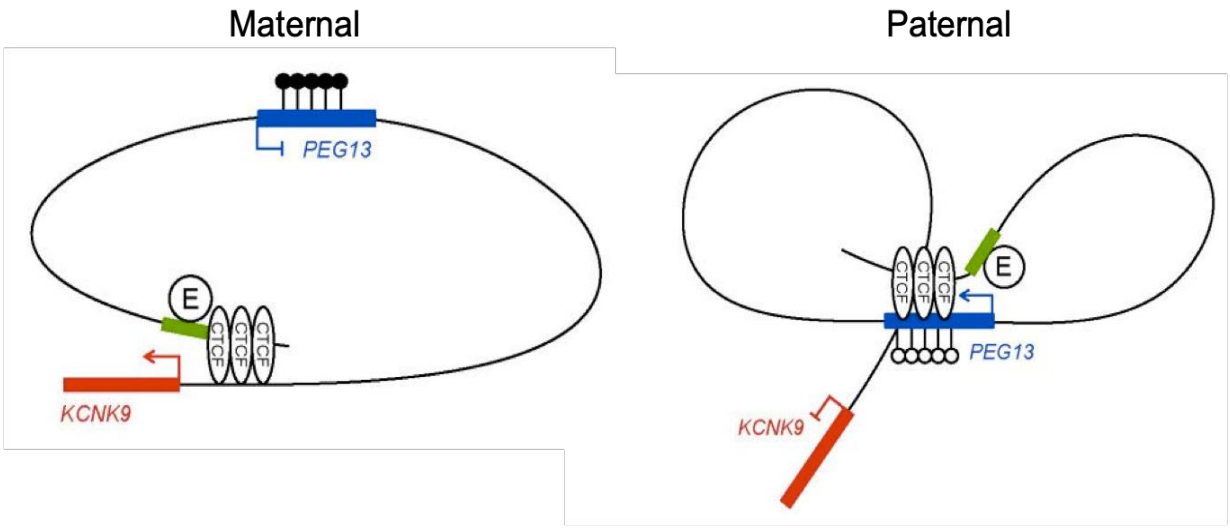

Figure 6: Schematic representation of CTCF-mediated chromatin interactions of the *KCNK9* promoter and the *PEG13*-DMR. A model of the allele-specific chromatin looping within the 8q24 domain, illustrating the organization of the *PEG13* enhancer-blocker, gene promoters, CTCF binding sites and H3K4me1/H3K27ac enhancer region. Description: (o) unmethylated cytosines, (●) methylated cytosine, (green block) histone modification site (H3K4me1/H3K27ac) associated with a brain-specific enhancer (E) (Court et al., 2014).

1.3. Potassium Channels

In animal cells potassium channels (K+ channels) are transmembrane proteins, which form a potassium ion (K+) selective pore to facilitate the specific gateway of potassium ions through the phospholipid bilayer.

The first potassium channel gene was isolated from Drosophila in 1987 and was named Shaker after a motion disorder caused by a mutation in this gene encoding for a presynaptic potassium channel in fruit flies (Papazian et al., 1987; Tempel et al., 1987). K+ channels are widely distributed throughout different cell types and comprise the most diverse family of ion channels, with 118 genes cloned or predicted from the human genome and 124 genes cloned or predicted from the mouse genome (http://www.ncbi.nlm.nih.gov). All K+ channel subunits contain common features, such as a conserved P domain, constituted by pore-forming subunits called alpha-subunits. Based on their function and structure, K+ channel subunits can be grouped

into three structural protein families, made of two, four or six transmembrane domains (TM). In order to form a functional pore region, two or four alpha-subunits have to assemble a selectivity filter consisting of four pore-lining P-loops and at least two transmembrane proteins (Patel and Honore, 2001b). Physiologically, K+ channels bring the membrane potential closer to the potassium equilibrium potential and play an essential role in the maintenance and stability of the neuronal resting membrane potential. Other fundamental ions, such as sodium and chloride, also play a key role in membrane potential, with many channel types and subtypes reported (Goldstein et al., 2001).

1.3.1 Two-Pore-Domain Potassium Channels (K2P)

The two-pore domain potassium (K2P) channels, also known as „background leakage channels“, modulate cellular excitability voltage- and time-independently and stabilize the resting membrane potential (Lesage and Lazdunski, 2000). The resting membrane potential is characterized by the equilibrium potential of intra- and extracellular ions and their conductances, in particular the predominating background conductance of K+ ions. K2P background or “leak” channels follow the Goldman-Hodgkin-Katz principal, where a high intracellular K+ concentration leads to an outflux of permeable K+ ions (Duprat et al., 1997). The K2P channel family consists of 15 members in the human genome, and are divided into six subfamilies termed as TREK, TALK, TASK, TWIK, THIK, and TRESK (Goldstein et al., 2001). The typical mammalian K2P channel consists of four transmembrane domains, M1-M4, with two pore loops, P1 and P2. Two subunits form a selective functional K2P channel (Fig. 7). However, in addition to providing passive leakage of K+ currents, the K2P channels can also be activity-modulated by physiological factors such as temperature change, pH, oxygen and binding of neurotransmitters or anesthetics (Lesage and Lazdunski, 2000; Patel and Honore, 2001b).

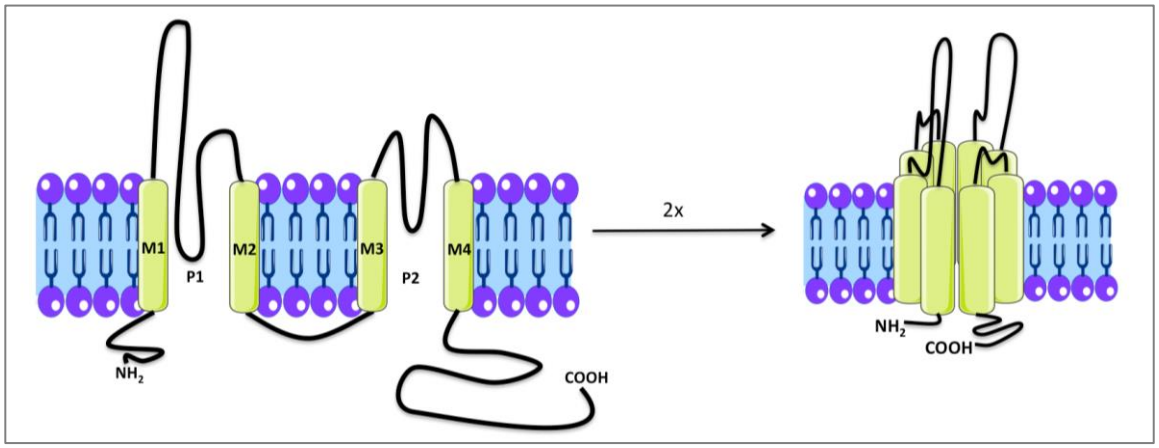

Figure 7: Schematic structure of a two-pore-domain potassium (K2P) channel subunit. The subunits of K2P channels consist of four transmembrane domains numbered M1-M4 and pore regions P1 and P2 with a short amino-terminal and a longer carboxy-terminal cytoplasmatic sequence. Two subunits form a selective functional K2P channel.

1.3.2 Characterization of KCNK9/ TASK-3 Potassium Channels

In this study, KCNK9/ TASK-3 potassium channels are the main focus of investigation. TASK-3, acronym for TWIK-related acid-sensitive K+ channel 3, is a member of the TASK family of K2P channels. The first TASK-3 channel was cloned from a rat cerebellum cDNA library and shares 54% sequence identity with TASK-1, the first TASK family member discovered (Duprat et al., 1997; Kim et al., 2000). Subsequently, the work group of Rajan introduced the human K2P channel, TASK-3, after isolating cDNA of TASK-3 from guinea pig brain and finding an orthologous sequence in a human genomic library (Rajan et al., 2000). In the nomenclature of the Human Genome Organization, TASK-3 was named KCNK9 (K2P 9.1). To date, three common nomenclatures are used for defining the protein, K2P 9.1 (International Union of Pharmacology), TASK-3 (based on physical and chemical features, TWIK-related and acid-sensitive) and KCNK9 (Human Genome Organization). Due to the commonly used *KCNK9/Kcnk9* gene nomenclature, we used KCNK9 as protein nomenclature in this work.

KCNK9 shares the typical channel structure of K2P channels. The subunits consist of four transmembrane domains (M1-M4) and two pore loops (P1 and P2). The state and conformation of KCNK9 can be altered by numerous intra- and extracellular modulators, including interacting proteins, physical and chemical stimuli, such as changes in temperature, membrane stretching, pH changes, GPCRs, kinases, 14-3-3 proteins and calcineurin (Rajan et al., 2000). The intracellular C-terminus includes a cAMP-dependent protein kinase phosphorylation site, two protein kinase C phosphorylation sites and two casein kinase phosphorylation sites (Rajan et al., 2000). In addition, KCNK9 is inhibited after activation of specific G-alpha-q-coupled receptors (Meuth et al., 2003). Moreover, KCNK9 is sensitive to extracellular acidification. The histidine residue at position 98 of KCNK9 enables the detection of slight changes in extracellular pH, resulting in a decrease of outwardly rectifying K+ current of 96% after shifting the pH from 7.2 to 6.0 (Kim et al., 2000; Rajan et al., 2000). Extracellular channel activation can be mediated by specific activators, such as halogenated ether, alcohol, alkane anesthetics, TNFa, flufenamic acid and Terbinafine (El Hachmane et al., 2014; Luethy et al., 2017; Veale et al., 2014; Wright et al., 2017). On the contrary numerous inhibitors including ruthenium red, endocannabinoids (anandamide, methanandamide), local anesthetics (lidocaine, bupiviacine), alphaxolone and Muscarinic acetylcholine agonists have been described (Czirjak and Enyedi, 2003; Maingret et al., 2001; Meadows and Randall, 2001; Patel and Honore, 2001a; Veale et al., 2014).

1.3.3 Distribution and Physiological Function of KCNK9

KCNK9 is widely distributed throughout the body and was detected in numerous tissues including brain, kidney, lung, colon, stomach, spleen, testis and skeletal muscle with RT-PCR analyses (Kim et al., 2000). High levels of *Kcnk9* mRNA were found in brain tissue (Kim et al., 2000; Rajan et al., 2000). Three major investigations indicate a wide distribution of KCNK9 throughout the rat brain. Karschian and Tally independently performed *in situ* hybridization analyses and detected *Kcnk9* mRNA expression in the majority of brain regions (Karschin et al., 2001; Talley et al., 2001).

A third study investigated the localization of KCNK9 channel proteins with specific antibodies in adult rat brains and demonstrated widespread representation of KCNK9 in the central nervous system with notably high levels in somatic motoneurons, cerebellar granule neurons, the dorsal raphe nuclei, hippocampal CA1 and CA3 pyramidal neurons and several hypothalamic nuclei (Marinc et al., 2014; Marinc et al., 2011). Furthermore, a strong immunoreactivity of neurons of the locus coeruleus has been described (Berg et al., 2004; Marinc et al., 2011). Moreover, KCNK3 and KCNK9 are also known to form heterodimers, which are co-expressed in numerous neuronal subgroups, such as motoneurons, in cerebellar granule cells, in thalamocortical relay neurons and in hippocampal CA1 neurons (Berg et al., 2004; Kang et al., 2004; Meuth et al., 2003; Torborg et al., 2006). TASK3 interacts with the adaptor protein 14-3-3, which facilitates protein-protein interaction and promotes the trafficking of TASK-1 and TASK-3 channels to specific compartments of the cell, for example to the membrane (Rajan et al., 2002).

KCNK9 channels are implicated in various pathological mechanisms associated with cancer, epilepsy and intellectual disability. Recent studies showed a role of the KCNK9 protein in the development and maturation of neurons in the cerebellum (Zanzouri et al., 2006). Amplification and overexpression of the *KCNK9* gene was found in various human carcinoma tissues, such as breast, lung, colon and prostate (Mu et al., 2003). A study in rodents, analyzing mice with a homozygous deletion of *Kcnk9,* revealed a reduction of the resting potassium conduction and revoked sustained high-frequency firing of action potentials in adult cerebellar granule neurons (Brickley et al., 2007). Further studies of homozygous *Kcnk9*KO animals revealed cognitive deficits, increased nocturnal activity, as well as a reduced sensitivity to inhalation anaesthetics, such as halothane and isoflurane, and the cannabinoid receptor agonist WIN55212-2 mesylate in *Kcnk9*KO mice (Gotter et al., 2011; Linden et al., 2007; Pang et al., 2009). In addition, RNAi-based knockdown of *Kcnk9* was demonstrated to deteriorate neuronal migration during mouse cortical development (Bando et al., 2014).

1.4. Purpose of the Thesis

Several studies have described the neuronal and behavioral phenotype of homozygous *Kcnk9* knockout mice with a deletion of both *Kcnk9* alleles (*Kcnk9*KO^{hom}). However, the phenotype of mice with heterozygous deletion of the expressed maternal *Kcnk9* allele (*Kcnk9*KO^{mat}), which mimics the genetical circumstances of patients suffering from Birk-Barel intellectual disability syndrome (BBIDS) best, has not yet been described to date.

The first objective of this thesis was to characterize *Kcnk9*KO^{mat} mice genetically and phenotypically compared to *Kcnk9*KO^{hom} mice and WT mice. Therefore, several behavioral tasks were performed to investigate working memory, acoustic startle response, pre-pulse inhibition and circadian rhythm in these mice. Furthermore, the allele-specific expression pattern of *Kcnk9* was determined in different brain regions using various molecular techniques.

The second main goal was to identify extrinsic epigenetic modifiers, which stimulate paternal *Kcnk9* expression sufficiently *in vitro.* Subsequently, it should be tested whether intraperitoneal injections of a selected epigenetic modifier in *Kcnk9*KO^{mat} mice can influence symptoms and eliminate any behavioral deficits and cognitive dysfunctions similar to those of BBIDS patients.

2. Material und Methods

2.1 Material

2.1.1 Equipment

Table 3: Devices and manufacturer

Device	Manufacturer
ABI StepOnePlusTM Real-Time PCR System	Life technologies
Electrophoresis Power Supply	Peqlab
Qubit 2.0	Invitrogen
Thermocycler MJ Research PTC-200	Biorad
UV Transilluminator Intas Gel iX Imager	Intas-Science-Imaging Instruments GmbH
Cell incubator CO2 Incubators CB 210	Binder
Centrifuge	Thermo Fisher Scientific
Work bench	Kendro Laboratory Products
PyroMark Q96 instrument	Qiagen
Brain Punch Tissue Set	Leica
Bioruptor Pico	Diagnode
Rotarod	Ugo Basile
Sound-attenuating isolation cabinets	Med Associates

2.1.2 Chemicals/Reagents

Table 4: Chemicals/Reagents and manufacturer

Reagents	Manufacturer
β-Mercaptoethanol	Roth
Acetic Acid, 100%	Roth
Agarose	AppliChem
B27 plus vitamin A	Gibco Life Technologies
Chloroform	Roth
CI-994	ApexBio
Dimethyl sulfoxide (DMSO)	Roth
DMEM	Sigma-Aldrich
Dulbecco's phosphate buffered saline (DPBS)	Gibco Life Technologies
Ethanol, Absolute	AppliChem
Ethidium bromide (EtBr)	Roth
Fastgreen	Sigma-Aldrich
FBS	Gibco Life Technologies
Formamide	Roth
GeneRuler 100bp	Thermo Scientific
GeneRuler 1kb	Thermo Scientific
Glycine	Roth
Glutamax	Gibco Life Technologies
Isopropanol	Roth
Laminin	Sigma-Aldrich
Sodium chloride	Roth
Neurobasal medium	Gibco Life Technologies
OptiMEM	Gibco Life Technologies
Paraformaldehyde	Roth
PBS	Gibco Life Technologies
Poly-L-Orhnithine	Sigma-Aldrich

RNase	NEB
RNAlater®	Sigma-Aldrich
SDS	Roth
Sepharose beads	GE Healthcare
TEMED	Invitrogen
TRIS	Roth
Triton X-100	Roth
TRizol	Thermo Scientific
Trypsin	Gibco Life Technologies
Trypton	Roth
Tween	Roth
Water	Ampuwa

2.1.3 Buffers und Solutions

Table 5: Buffers und Solutions

Buffer	Composition
Annealing buffer	30 mM Hepes pH 7,4, 100 mM Kaliumacetat, 2 mM Magnesiumacetat, ad 100 ml H_2O
Sodium citrate buffer (10mM)	1 g Natriumcitrat, 1 ml 0,2% Tx-100, ad. 500 ml H_2O, pH6
PBS-T	2 PBS tablets, 1 ml Tween, ad 1 l H_2O
Paraformaldehyde (4%)	4 g PFA in 90 ml PBS at 60°C and 1 M NaOH. Adjust pH to 6,9 with HCL
TAE buffer (50x)	242 g TRIS, 18,6 g EDTA, 57,1 ml Essigsäure (100%), add 1 l H_2O
Formaldehyde (1%)	Formaldehyde in PBS

2.1.4 Kits

Table 6: Kits

Kit	Manufacturer
PrimeScript TM Master Mix (Perfect Real Time)	TAKARA
SYBR® Premix Ex Taq (Tli RNaseH Plus (2x))	TAKARA
High Pure RNA Tissue Kit	Roche
High Pure RNA Isolation Kit	Roche
PyroGold SQA reagents	Qiagen
EZ DNA Methylation Direct ™ Kit	Zymo Research

2.1.5 Primers

Table 7: Primer sequences

Primer		Application	Sequence (5‘ – 3‘)
TASK3-P3	F	Genotyping	TGCGAGCTTCAGAGAGGATG
TASK3-P4	R	Genotyping	ATGCTCTAATCTCCAGTCTG
Kcnk9 Exon 2	F	Genotyping	CACCACGCCATGTACTTCCT
Kcnk9 Exon 2	R	Genotyping	GGACCGGAAGTAGGTGTTCC
Kcnk9-SNP	F	Allele-specific RT-qPCR	CACAACTATCGGATATGGACATGC
Kcnk9-SNP	R	Allele-specific RT-qPCR	TGCCGCGGTGTTCGAT
Kcnk9-477	F	QUASEP	GCCTGTACCTTCACCTAC
Kcnk9-477	R	QUASEP	CACAACTATCGGATATGGACATGC
Kcnk9-477	Seq	QUASEP	TGCCGCGGTGTTC
kcnk9-283/284	F	RT-qPCR	ACTATCGGATATGGACATGCTGC
kcnk9-283/284	R	RT-qPCR	GCCCAGGCTCTGGAACATAA
Bdnf	F	RT-qPCR	ATCCACTGAGCAAAGCCGAA
Bdnf	R	RT-qPCR	CCTGGTGGAACATTGTGGCT
Impa2	F	RT-qPCR	CGTGCGGGACAAATCATCAG
Impa2	R	RT-qPCR	AAGGAAACCGCTTTCGCAAC
Tyrosine hydroxylase	F	RT-qPCR	AGCCCAAGGGCTTCAGAAGAG

Tyrosine hydroxylase	R	RT-qPCR	CAATGAACCTTGGGGACGTGA
Kcnk9 promoter	F	ChIP-qPCR	CGTGTGCGCTACATCTCCTA
Kcnk9 promoter	R	ChIP-qPCR	ATTCGCCGGTTCCTTCTACT
Kcnk9 intron	F	ChIP-qPCR	AGGGCAGATGCTTAAGAGGA
Kcnk9 intron	R	ChIP-qPCR	CATCTGTTCTGTACCCCATCC
mPeg13-CpG 1-9	F	Methylation analysis	TTGGATGAGTTATTATATAAGGTTTAAAA
mPeg13-CpG 1-9	R	Methylation analysis	ACAACTACCTACATTCCAAATCT
mPeg13-CpG 1-9	Seq	Methylation analysis	AAATTTTAATAAGATGGGTTAAT
mPeg13-CpG 17-22	R	Methylation analysis	AGATTTGGAATGTAGGTAGTTGTGA
mPeg13-CpG 17-22	F	Methylation analysis	CCTCAATAAAACCATTCTAATCAACTAT
mPeg13-CpG 17-22	Seq	Methylation analysis	GGTAATTTGTTAGGTGGAGATATA

2.1.6 Software and Tools

Table 8: Software and manufacturer

Software/Tool	Manufacturer
EthoVision XT	Noldus
GraphPad Prism 6	GraphPad Software Inc.
Pyro Q CpG software	Qiagen
PyroMark Q96 ID Software 2.5	Qiagen

2.2. Methods

2.2.1 Standard Methods for Molecular Biology

Conventional standard techniques of molecular biology such as DNA extraction, polymerase chain reaction (PCR), gel electrophoresis or the preparation of standard solutions will not be discussed in detail here. Standard protocols were used unless otherwise stated (Sambrook et al., 2006).

2.2.2 Mice and Breeding

All experimental procedures were performed in accordance with institutional animal welfare guidelines and were approved by the ethical committee of the state government of Rhineland-Palatinate, Germany. *Kcnk9*KO^{hom} mice, were provided by Florian Lesage, Institut de Pharmacologie Moléculaire et Cellulaire, Valbonne, France. The gene targeting strategy of *Kcnk9*KO^{hom} mice was based on a cre-mediated deletion of exon 2 encoding pore domains P1 and P2, transmembrane domains M2 to M4 as well as the cytoplasmic C-terminus (Guyon et al., 2009). WT C57BL/6J and heterozygous *Kcnk9*KO mice with inactivation of the maternal *Kcnk9* allele (*Kcnk9*KO^{mat}) were obtained by crossing male WT (C57BL/6J) mice with female *Kcnk9*KO^{mat} mice. The mice were kept under specific-pathogen-free (SPF) conditions on a 12 h light / 12 h darkness cycle in standard polystyrene cages with free access to water and food. Using tail tip DNA, mice were genotyped by assessing exon 2 excision using the primers flanking this region (F, 5′-TGCGAGCTTCAGAGAGAGGATG-3′ and R, 5′-ATGCTCTAATCTCCAGTCTG-3′) producing fragments for WT and mutant alleles. Additional primers within exon 2 were applied to generate a control product for the WT allele (5’-CACCACGCCATGTACTTCCT-3’ and 5’- GGACCGGAAGTAGGTGTTCC -3’). 8-10 weeks old male mice were used for expression analysis and to investigate the behavioral phenotype with and without drug treatment. Allele-specific expression

analyses were carried out with total RNA from F1 offspring derived from crosses between female WT C57BL/6J or *Kcnk9*KO^{hom} mice and male Mus musculus castaneus (Cast/Ei) mice.

2.2.3 Drug Administration *in vivo*

9 weeks old male *Kcnk9*KO^{mat} and WT mice were injected intraperitoneally once daily with CI-994 (ApexBio) or dimethyl sulfoxide (DMSO) (control vehicle) for 7 consecutive days before behavior experiments were initiated (Fig. 5a). On days of testing, mice were injected 2 hours before behavior experiments. A single injection contained either 20 µl DMSO or 20 µl CI-994 (35 mg/kg) dissolved in 100 % DMSO.

2.2.4 Tissue Collection

Whole mouse brains were removed and incubated in RNAlater® (Sigma) and stored for 2 days at 4°C. After the dehydration process, several brain regions were dissected and further processed or stored at -80°C. For locus coeruleus samples, coronal brain sections (80 µm) between bregma -5.40 and -5.52 (Franklin, 1997) were generated, and 0.51 µm punches bilaterally of each brain region were collected. Accuracy of the LC tissue collection was validated by performing tyrosine hydroxylase expression analyses and comparing the expression levels to those of WT cerebellum and hippocampus samples. Tyrosine hydroxylase served as a norepinephrine marker.

2.2.5 Isolation of Primary Cortical Neurons

Female pregnant mice were anesthetized with isoflurane at embryonic day 14 (E14) and opened to obtain 5-9 embryos per mouse. Murine primary cortical neurons (mPCNs) were prepared from embryonic (E14) mouse pups. *Kcnk9*KO^{mat} mPCNs were isolated from E14 embryos derived from matings between female *Kcnk9*KO^{hom} mice and WT males. After collection of emybronic brains, cortices were dissected out

and incubated in Dulbecco's Modified Eagle Medium (DMEM, Gibco) at 37 °C and mechanically separated into single cortical cells through resuspendation. After dissecting the cortices and removing their meninges, cortices were transferred to 50 ml Falcon tubes containing ice cold DMEM. The tissue was dissociated using Trypsin solution (0,5 ml/Embryo, Gibco) and incubated for 6 minutes at 37°C. The reaction was stopped using a DMEM-FBS solution. Cells were centrifuged (2 min, 200g), washed 2x with DMEM and resuspended with culture medium, containing neurobasal medium (Gibco), supplemented with 2% B27 plus vitamin A (Gibco) and 1% Glutamax (Gibco), until no cell pellet was visible. After staining 10 µl of cell lysate with trypan blue, living cells were counted manually on a Neubauer chamber. Around 0,7 x 106 mPCNs were plated on 100 µg/ml poly-L-ornithine (Sigma) and 10 µg/ml laminin (Sigma) precoated 6- or 12-well plates and maintained in culture medium in a humidified incubator at 37 °C and 5% CO_2.

2.2.6 *In vitro* Drug Treatment

mPCNs were cultured in culture medium for a 4 days cell differentiation period in 6-or 12 well-plates and treated with epigenetic compounds or vehicle controls, DMSO or H_2O, diluted in culture medium for 24 or 72 hours.

2.2.7 Total RNA Isolation

Total RNA extraction from brain tissue was performed with TRIzol reagent as recommended by Invitrogen Life Technologies. Brain tissue was stored at -80° C and in RNAlater, respectively, and the isolation was carried out using TRIzol, chloroform, isopropanol and 70% ethanol. The isolated RNA was eluted in elution buffer of the Agilent RNA nanoprep kit. All RNA isolation steps were performed under a hood and only sterile pipettes, tips, tubes, pedestals, etc. were used. First, 1 ml of TRIzol was added to the frozen tissue, followed by homogenous suspension using a mortarand incubation for 5 min at RT. After the addition of 200 µl of chloroform, the solution was vigorously shaken until it turned pink to milky and then incubated at RT for 2 min. The

suspension was centrifuged at 12,000 rpm and 4° C for 15 min to effect phase separation. The upper, colorless aqueous phase of the centrifuged sample was transferred into initially charged ice-cold isopropanol in fresh reaction tubes. The mixture was gently mixed and incubated at RT for 10 min. This was followed by another centrifugation at 12,000 rpm and 4 ° C. for 15 min. The supernatant was discarded, the precipitate washed with 1 ml of 70% ethanol and then centrifuged at 12,000 rpm and 4° C. for 5 min. This washing was repeated and subsequently the precipitate was air-dried until it appeared glassy. The precipitate was then dissolved in 50-100 µl elution buffer (Agilent RNA nanoprep kit) and the RNA samples immediately stored on ice. The long-term storage of the RNA samples was carried out at -80 ° C. The High Pure RNA Tissue Kit (Roche) and High Pure RNA Isolation Kit (Roche) were used to extract total RNA from small tissue and cell samples using spin columns. The purity, quantity and integrity of the RNA were measured with a NanoDrop 1000 spectrophotometer and an Agilent 2100 Bioanalyzer.

2.2.8 Reverse Transcription and cDNA-Synthesis

The cDNA samples were synthesized from 200-1000 ng total RNA using the PrimeScript™ RT Master Mix cDNA (Takara) as recommended by the manufacturer. Each cDNA sample was stored with a final volume of 10 µl or 20 µl at -20°C. The working concentration for RT-qPCR amplification experiments was 5-10 ng/ µl.

2.2.9 Real-Time Quantitative PCR (RT-qPCR)

The principle of qPCR is based on that of conventional standard PCR. Furthermore, quantification is done during amplification with very high sensitivity and high linearity. A fluorescence reporter molecule is used, here SYBR Green I, which intercalates into the small groove of the DNA with each cycle, leading to an increase in fluorescence, which can be detected via a CCD (Charge-Coupled Device) sensor. The fluorescence increases in proportion to the amplified amount of DNA. When the amplification reaches the exponential phase, the amplicon-specific Ct (threshold

cycle) is determined. After completion of the PCR, a melting curve analysis is performed to check for possible non-specific PCR products and contaminations based on the specific melting temperature of each amplicon.

Quantitative real-time PCR (qRT-PCR) was carried out using SYBR® Premix Ex Taq™ II (Tli RNaseH Plus) and 10 µM primers (final concentration), according to the manufacturer's instructions. The final reaction solution per well contained of 5 µl SYBR® Premix Ex Taq (Tli RNaseH Plus (2x)), 0,4 µl of a primer mix (10 µM forward & 10 µM reverse primers), 2,6 µl of HPLC grade water and 2 µl of diluted template cDNA. RT-qPCR reactions were performed on an ABI StepOnePlus™ Real-Time PCR System using exon-exon junction primers with the following conditions: 95 °C/30 sec, 40 cycles of 95 °C/5 s, 60 °C/30 s, 72 °C/30 s. All reactions were measured in triplicates, and median cycles to threshold (Ct) values were used for analysis. The primers used in this study were exon-exon junctioned and are listed in the table 2.1.5. The housekeeping genes *Impa2* and *Gapdh* was used to normalize against experimental genes, and relative gene expression was determined using the 2−ΔΔCT method (Livak and Schmittgen, 2001).

2.2.10 Allele-specific RT-qPCR

To quantify the relative expression of the maternally and paternally inherited allele in (C57BL/6JxCast/Ei)F1 hybrid mice, genes were amplified in a specific manner. Two different allele-specific forward primers were designed to bind either to the C57BL/6J C allele or the Cast/Ei T allele of the single-nucleotide polymorphism (SNP) and used for PCR together with a reverse primer under stringent conditions (Fig. 8). This method enriches amplicons, whose alleic ratio is proportional to the ratio in the starting material, regardless of the number of cycles of amplification. The analyses of expression levels of the gene of interest were normalized with a reference gene, resulting in relative gene quantification.

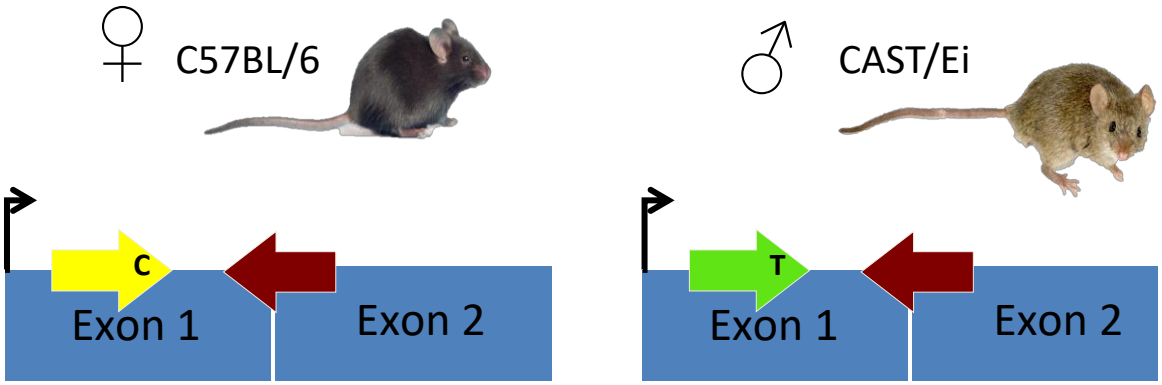

Figure 8: Assay design and melt curve analysis for the allele-specific RT-qPCR. Allele-specific primers bind to the strain-specific SNP at the 3´-prime end, allowing only the complementary primer to elongate.

2.2.11 Quantification of Allele-Specific Expression by Pyrosequencing (QUASEP)

For allele-specific expression analysis using QUASEP, the synthesized cDNA of (C57BL/6JxCast/Ei)F1 hybrid mice was amplified in a PCR applying one non-biotinylated forward primer: 5´-GCCTGTACCTTCACCTAC-3´ and one biotinylated reverse primer: 5´-CACAACTATCGGATATGGACATGC-3´. To distinguish the parental origin of the alleles the RT-PCR products using the C/T-SNP rs225149059 (ensembl; GRCm38.p5) the QUASEP method was used as previously described (Ruf et al., 2007). A *Kcnk9*-specific pyrosequencing primer: 5´-TGCCGCGGTGTTC-3´ flanking the allele-specific SNP was designed with the PyroMark Q96 ID Software 2.5. Pyrosequencing was carried out on a PyroMark Q96 instrument (Qiagen) and results were displayed as percentage (%) allelic expression.

2.2.12 Pyrosequencing

Pyrosequencing is a "sequencing by synthesis" method, that allows real-time detection of nucleotides, newly synthesized by DNA polymerase, and was initially described in 1993 (Nyren et al., 1993). The method is routinely used in a variety of fields, for example in genotyping, identification of microorganisms (Marsh 2007) and analysis of DNA methylation patterns. In this work, pyrosequencing was used for SNP analysis and is based on the detection of measurable light emission by released pyrophosphate (PPi) during nucleotide synthesis. In a defined order of dispensation, the four deoxynucleotide triphosphates (dNTP) are added to the DNA template primer hybrid. If a nucleotide is successfully incorporated into the DNA strand, which is complementary to the primer template, an equimolar amount of PPi is released. The pyrophosphate is enzymatically converted to ATP by the ATP sulfurylase. The presence of ATP causes the conversion of luciferin to oxyluciferin, which is processed by the luciferase. This results in the release of a quantum of light detected by the device's internal light-sensitive CCD (Charge-Coupled Device) sensor. The light signal is displayed as a peak in the pyrogram. The more frequently a base occurs consecutively in the sequence, the higher is the peak. Excess dNTPs and unincorporated nucleotides are degraded by the apyrase. However, since dATP is a natural substrate of luciferase, dATPalphaS is used for pyrosequencing. This is also recognized by the DNA polymerase and incorporated into the DNA (Fig. 9).

Preparation of single-stranded PCR products with the Vacuum Prep Tool and preparation of the pyrosequencing plate were performed using the standard protocol recommended by Qiagen as follows:

1. The following volumes were pipetted per sample into a 96-well PCR plate:

4 µl Streptavidin-Sepharose beads (GE Healthcare, Uppsala, Sweden)

20 µl binding buffer (Qiagen)

22 µl of PCR product

The PCR plate was sealed with an adhesive seal (ThermoScientific) and vortexed for 5 min at 1400 min^{-1}.

2. 1.6 µl sequencing primer (10 µM) and 38.4 µl annealing buffer (Qiagen) were pipetted into a pyrosequencing plate.

3. The sample mixture was aspirated with the PyroMark Vacuum Prep Table (Qiagen) by applying a negative pressure on the PCR plate. The Streptavidin-Sepharose beads bound to the biotin modification of the above-mentioned reverse PCR primers were fixed by the filter tips of the aspirator.

4. The aspirator was then successively incubated for 5 each seconds first in 70% ethanol and then in denaturation buffer (0.2 M NaOH) and finally transferred in washing buffer (10 mM Tris-acetate, 7,4 pH). The whole process was used for the preparation and purification of a single-stranded PCR product.

5. The negative pressure was then switched off above the pyrosequencing plate and the Sepharose beads with the single-stranded PCR product were released in the mix of annealing buffer and sequencing primer.

6. The pyrosequencing plate was heated to 80 ° C for 2 min. This served to avoid secondary structures of the DNA. The plate was then cooled to room temperature, allowing binding of the sequencing primer.

7. A sequencing cartridge was filled with all four nucleotides (Qiagen) as well as substrate and enzyme mix (Qiagen). The volumes of the components were calculated according to the sequence to be analyzed by the Pyro Q CpG software (Qiagen).

8. Pyrosequencing plate and cartridge were placed in the sequencer and the run started. The evaluation was carried out by the Pyro Q CpG software (Qiagen). The DNA samples were previously prepared for sequencing using the PyroGold SQA reagents (Qiagen, Hilden, Germany). The quality of a sequence is also influenced by analysis parameters such as sufficient signal amplitude and peak width and indicated

by the software using color-coded quality levels.

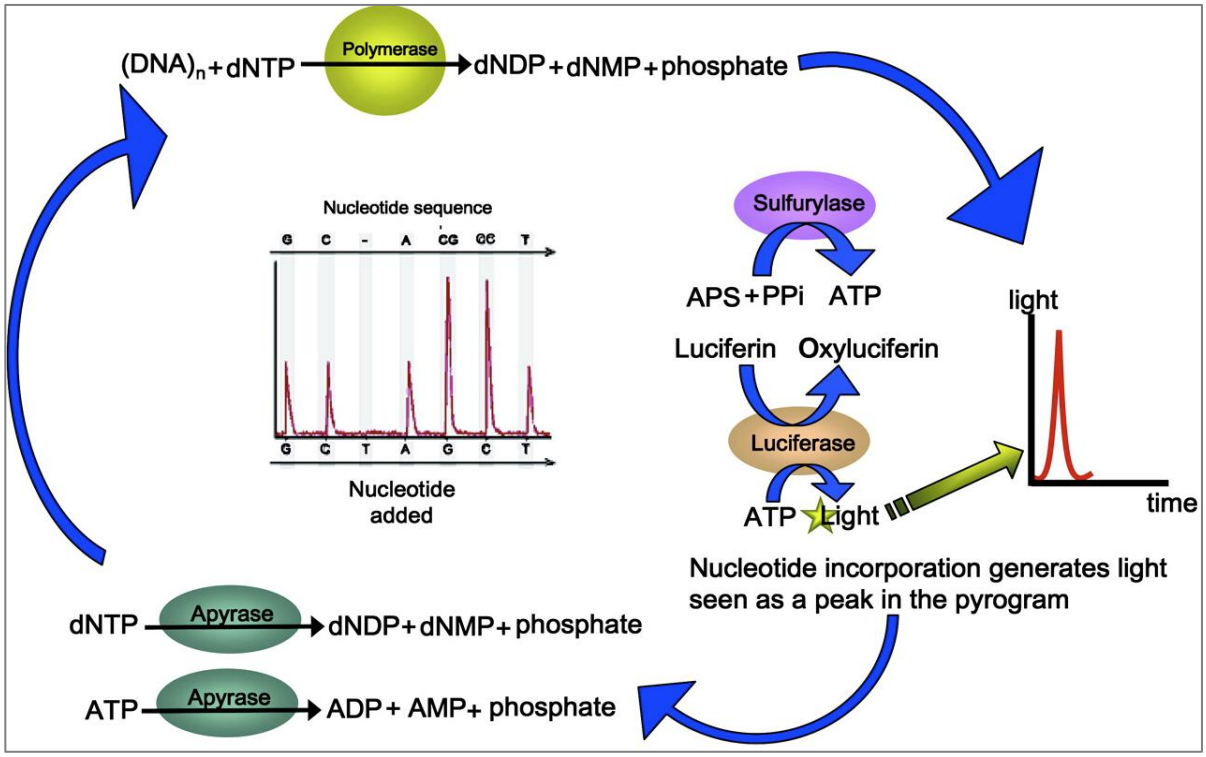

Figure 9: The principle of pyrosequencing. The biochemical reactions and enzyme cascades necessary for the generation of a flash of light. When incorporating a nucleotide into the single-stranded DNA, pyrophosphate is released. The free PPi is converted to ATP by the sulfurylase. The ATP is used by the luciferase as a substrate to generate a flash of light, which is detected by a camera. dNTP: deoxynucleoside triphosphate; dNDP: deoxynucleoside diphosphate; dNMP: deoxynucleoside monophosphate, PPi: pyrophosphate; APS: adenosine 5-phosphosulphate (Source: http://www.clinchem.org).

2.2.13 DNA Extraction

The NucleoSpin® Mini Tissue Kit (Macherey-Nagel) was used to extract DNA from brain tissue and ear biopsies for genotyping. The extraction was carried out according to the manufacturer's instructions (standard protocol for human or animal tissue and cultured cells). The DNA was then eluted in 30 µl elution buffer.

2.2.14 Bisulfite Treatment of Genomic DNA

The principle of bisulfite treatment is based on the fact that unmethylated cytosines are converted to uracil during deamination with sodium bisulfite ($NaHSO_3$) (Frommer et al., 1992). The method consists of four basic chemical steps: denaturation, hydrolytic deamination, sulfonation and alkali desulfonation.

The 5,6-double bond of cytosine binds the bisulfite ion, creating an intermediate that is converted by deamination into sulfonated uracil. Under basic reaction conditions, the sulfone group is split off and uracil is formed (Fig. 10). In the following PCR uracil is amplified as thymidine. Unlike cytosine, 5'-methylcytosine is insensitive to the above processes. This process enables the differentiation between methylated and unmethylated cytosines.

Approximately 500 ng DNA was subjected to sodium bisulphite treatment and purified using the EZ DNA Methylation Direct™ kit (Zymo Research, Irvine CA, USA), which provides a 99.5% cytosine conversion rate, with a recovery rate of more than 80% of the original DNA, according to the manufacturer. All steps were carried out according to the manufacturer's instructions.

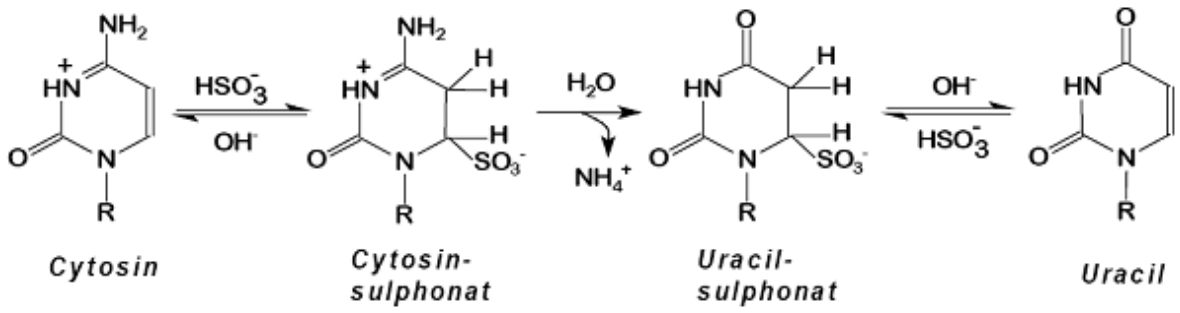

Figure 10: Bisulfite conversion of cytosine to uracil.

2.2.15 DNA-Methylation Analysis

PCR amplification of bisulfite-treated DNA was performed with 1 µg bisulphite-converted DNA and specific primers in 42 cycles. Two CpG-rich regions, *Peg13*-DMR1 and *Peg13*-DMR2, known to be involved in transcriptional regulation of the mouse *Kcnk9* gene were amplified. The pyrosequencing was carried out on the PyroMark Q96 instrument (Qiagen).

The generated pyrosequencing data was analyzed and evaluated with the Pyro Q-CpG 1.0.9 Software. See 2.2.12 for further details on pyrosequencing. The percent methylation status, (ratio mC / (mC + C)), is calculated and reported for each CpG dinucleotide by the Pyro Q-CpG software (Qiagen, Hilden, Germany). For quality control, a bisulfite control (unmethylated cytosine not followed by a guanine) is incorporated to verify complete conversion of the DNA.

2.2.16 Chromatin Immunoprecipitation (ChIP)

Chromatin immunoprecipitation (ChIP) is a technique to investigate protein-DNA interactions and understand transcriptional regulation. ChIP experiments were performed as described in Akhtar et al. (2018) with minor modifications for brain tissue processing (Akhtar et al., 2018). Briefly, brain tissues were dissected in cold PBS and homogenized with a pestle. Following dissection, tissues were fixed with 1% formaldehyde in PBS for 10 minutes at room temperature, followed by quenching of the fix with 125 mM glycine for 5 minutes. Fixed cells were resuspended in 140 mM RIPA (10 mM Tris-Cl pH 8.0, 140 mM NaCl, 0.1 mM EDTA pH8.0, 1% Triton X-100, and 0.1% SDS) and subjected to 18 cycles of sonication on Bioruptor Pico (Diagnode), with 30 Secs “ON”/ “OFF” at high settings. After sonication, samples were centrifuged at 14,000 g for 10 minutes at 4°C and supernatant was transferred to a fresh tube. The extracts were incubated overnight with 1.5 µg of a specific H3K27ac (Abcam) or IgG control (Diagnode) antibody at 4°C with head-over tail rotations. After overnight incubations, 20 µl of blocked Protein A and G Dynabeads

(Diagnode) were added to the tubes and further incubated for 3 hours to capture the antibodies. Bead separation was carried out using a magnetic rack and was washed as following; once with 140 mM RIPA (10 mM Tris-Cl pH 8.0, 140 mM NaCl, 0.1 mM EDTA pH8.0, 1% Triton X-100, and 0.1% SDS), four times with 250 mM RIPA (10mM Tris-Cl pH 8.0, 250 mM NaCl, 0.1 mM EDTA pH8.0, 1% Triton X-100, and 0.1% SDS) and twice with TE buffer pH8.0 (10 mM Tris-Cl pH 8.0 and 0.1 mM EDTA pH8.0). For reversal of cross-linking, samples were RNase-treated (NEB) and subjected to Proteinase K treatment for 12 hours at 37°C and at least 6 hours at 65°C after immunoprecipitation. After proteinase K treatment, the DNA was extracted using the phenol chloroform method. After precipitating and pelleting, DNA was dissolved in 30 µl of TE buffer pH 8. The real-time PCR was performed using SYBR Green chemistry (ABI) on the ABI StepOnePlus™ Real-Time PCR System. The input and chromatin-immunoprecipitated material were processed identically across the samples. The low amount chromatin immunoprecipitation was performed according to the pre-print of Akhtar et al. (2018) and will be described in details elsewhere.

2.2.17 Primer- and Assay Design

The primers used for QUASEP were generated using Biotage's "PyroMark Assay Design" software (Version 2.0.1.15). For bisulphite pyrosequencing PCR primers for the *Peg13*-DMR1 and *Peg13*-DMR2 (located from +195 to + 833 bp relative to the 5´ end of the *Peg13* transcript) and the sequencing primer were designed using the Pyrosequencing Assay Design Software (Qiagen). All additional primers were designed using the online tool “Primer-BLAST” (National Center for Biotechnology Information). In order to check the specificity of primer binding, electronic PCR (genome-wide primer BLAST search) with the generated primers was performed using the online PCR program "BiSearch". The primer stocks (100 mM, Sigma) were dissolved in HPLC water and the working solution adjusted to a final concentration of 10 mM with HPLC water.

2.2.18 Behavioral Analysis of *Kcnk9* Knockout and WT Mice

Littermate WT and conditional *Kcnk9* KO mice were tested in 4-8 cohorts of mice, with testing beginning at 8-10 weeks of age. All experimenters were blinded to genotype of the mice throughout the studies and the analysis of their behaviors. Immediately after the behavioral tests, animals were sacrificed and whole brains were rapidly removed and incubated in RNAlater for subsequent expression analysis. Male mice were used to minimize variability in behavior, as females can be more variated by the oestrus cycle.

2.2.18.1 Acoustic Startle Response

The test was performed in sound-attenuating isolation cabinets (Med Associates, St. Albans, VT, USA) as described previously (Radyushkin et al, 2010). Mice were placed in small metal cages (90 × 40 × 40 mm) to restrict exploratory behavior. The cages were equipped with a movable platform floor connected to a sensor to detect vertical movements.

The mice were subjected to broadband acoustic startle tones from a high-frequency speaker mounted in a light- and sound-attenuating experimental chamber. Animals were habituated in the startle chamber with a 60 dB background white noise for 5 min. A startling reaction is triggered by a randomized acoustic stimulus ranging from 60 to 120 dB from a loudspeaker. Over the duration of the experimental period (30 min), 60 acoustic stimuli of varying intensity are used. Immediately after each startle tone presentation, the startle amplitude was measured and recorded. Based on the data obtained the startle reaction is calculated and scaled in arbitrary units.

2.2.18.2 Pre-Pulse Inhibition

The arrangement of the experimental equipment is identical to the acoustic startle response setup (Fig. 11), as described previously (Radyushkin et al, 2010). Mice were exposed to an acoustic stimulus delivered from a loudspeaker which was

connected to an acoustic generator. The startle reaction to an acoustic stimulus, which evokes a movement of the platform and a transient force resulting from this movement of the platform, was recorded with a computer during a recording window of 260 milliseconds (beginning with the onset of pre-pulse) and stored for further evaluation. An experimental session consisted of a 3-min habituation to 65 dB background white noise (continuous throughout the session), followed by a baseline recording for 1 min at background noise. In the first trial, mice were exposed to 10 presentations of a 120 dB pulse intensity and 40 milliseconds duration in order to decrease the influence of within-session habituation. For tests of pre-pulse inhibition, the 120 dB/40 milliseconds startle pulse was applied either alone or applied by a pre-pulse stimulus of 70, 75 or 80 dB intensity and 20 milliseconds duration.10 trials of each kind were applied in a pseudorandom order with variable inter-trial interval ranging from 10 to 19 seconds. Amplitudes of the startle response (expressed in arbitrary units) were averaged for each individual animal, separately for each type of trials. Pre-pulse inhibition was calculated as the percentage of the startle response using the following formula: PPI (%) = 100 – [(startle amplitude after pre-pulse and pulse / startle amplitude after pulse only) × 100] (Radyushkin et al, 2010).

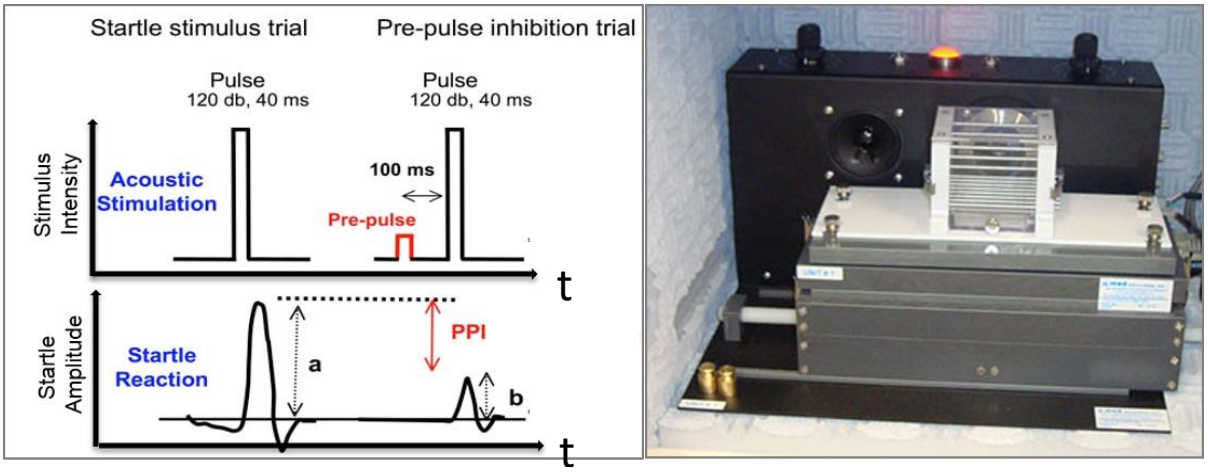

Figure 11: Pre-pulse Inhibition. Stimulus intensity and startle amplitude in the corresponding timeline of the PPI reaction. PPI (%) =100- (b (startle amplitude after pre-pulse & pulse) / a (startle amplitude after pulse only) ×100) (left). Sound-attenuating isolation cabinets (Med Associates, St. Albans, VT, USA) in which recordings took place (right). 4

2.2.18.3 Circadian Rhythm

Mice were individually placed in transparent polypropylene cages (38 x 22 x 15 cm) with standard beddings. Food and water were available and accessible at all times. The cages were placed in a sound-prove room under dimed light during the light phase and under infrared LED lights during the dark cycle. The horizontal locomotor activity of the mice was recorded in the light and in the dark phase using a video tracking software (EthovisionXT, Noldus software). The circadian rhythm activity was measured after 48 hours acclimatization for 24 hours and analysed with EthovisionXT, Noldus software. The results show the distance travelled (in cm) in the light and in the dark phase.

2.2.18.4 Spontaneous Alternation

Spatial working memory was assessed in a Y-maze test as described previously (Radyushkin et al., 2005). During a 10-min session in a Y-maze the spontaneous alternation behavior was recorded. The spontaneous alternation test is based on willingness of rodents to explore new environments, therefore to enter the arm of a Y-maze that had not been recently explored, i.e. the arm that was not entered in the previous choice. Mice were placed in a grey plexiglass Y-maze in a sound prove room. Each maze consisted of three arms. Each arm was 40 cm long, 20 cm high and 10 cm wide, and the arms converged to an equilateral triangular central area. Each mouse was placed at the end of the start arm, in which the mouse starts to explore and move freely through the maze during the 10-min session. The series and order of arm entries was observed manually and considered to be completed when the hind paws of the mouse had completely entered into the arm. Transitions between arms were scored as either correct or incorrect alternations by the observer. Healthy animals (controls) show a high change rate. This shows that the animal can remember which arm was last entered. The percentage of alternation was calculated as the ratio of actual to possible alternations multiplied by 100%. Each of the arms of the Y maze was cleaned with 70% ethanol solution between trials.

2.2.18.5 Rotarod

The rotarod test examines motor function, balance and coordination and was developed specifically for the automated measurement of neurological deficits in rodents. The Rotarod (Ugo Basile, Comerio, Varese, Italy) consists of a rotating horizontal drum, with partitions to separate several mice that are being tested simultaneously, which was accelerated from 4 to 40 r.p.m. over 5 min. Mice were placed individually on the drum and the latency of falling off the drum was recorded using a stop-watch. Mice were habituated on day 1 to the Rotarod apparatus, followed by 1 day of testing.

2.2.19 Statistical Analysis

All analyses were performed using Prism 7 (Graphpad Software, San Diego, CA). Assumptions concerning normal distribution were applied (Kolmogorov-Smirnov test) before statistical analyses were implemented. For animal studies and RT-qPCR expression analysis, data were compared using a one-way ANOVA and 2-way ANOVA with and without repeated measures by multiple comparisons followed by Tukey's or Bonferroni´s multiple comparison post hoc test. The numbers of biologically independent experiments, sample size, statistical results and ages of the animals are all indicated in the main text or figure legends. Values were only excluded if they were identified as outliers based on a Grubbs' test. Unless stated otherwise, the data given in figures and text are expressed as mean ± SEM. $P < 0.05$ was considered to be statistically significant.

3. Results

3.1 Deletion of *Kcnk9* leads to Impaired Behavior

To assess behavioral deficits along the BBIDS phenotype in *Kcnk9*KO mice, we performed *in vivo* experiments in adult wild-type (WT) as well as mice with a deletion of *Kcnk9* exon 2 on both alleles (*Kcnk9*KO^{hom}) or only the maternal allele (*Kcnk9*KO^{mat}), encoding pore domains P1 and P2, transmembrane domains M2 to M4 and the cytoplasmic C-terminus, as previously described (Guyon et al., 2009). Following the strictly monoallelic expression pattern of *Kcnk9* in mouse brain (<1% paternal expression) (Ruf et al., 2007), we expected largely concordant phenotypes in *Kcnk9*KO^{hom} and *Kcnk9*KO^{mat} mice, respectively.

3.1.1 Y-maze Test

Based on the description of intellectual disability in BBIDS patients, we first examined whether working memory was affected in *Kcnk9*KO mice. Spontaneous alternation relies on the natural tendency of rodents to explore a novel environment and can be measured in a Y-maze test. The ability to remember the immediately preceding choice is considered an indicator for active working memory. In the Y-maze, spontaneous alternation was defined as consecutive entries into all three arms without revisiting an arm. The average percentage of spontaneous alternation made by *Kcnk9*KO^{hom}, *Kcnk9*KO^{mat} and WT mice across a 10-minute trial was analyzed and revealed a significant reduction of spontaneous alternation by about 10% in *Kcnk9*KO^{hom} and *Kcnk9*KO^{mat} mice compared to WT littermates (Table 9, Fig. 12). There was no significant difference between *Kcnk9*KO^{hom} and *Kcnk9*KO^{mat} mice (Fig. 12, Table 9). Our findings indicate an impaired working memory in *Kcnk9*KO^{hom} and *Kcnk9*KO^{mat} mice, which is consistent with previously reported observations in *Kcnk9*KO^{hom} mice (Linden et al., 2007).

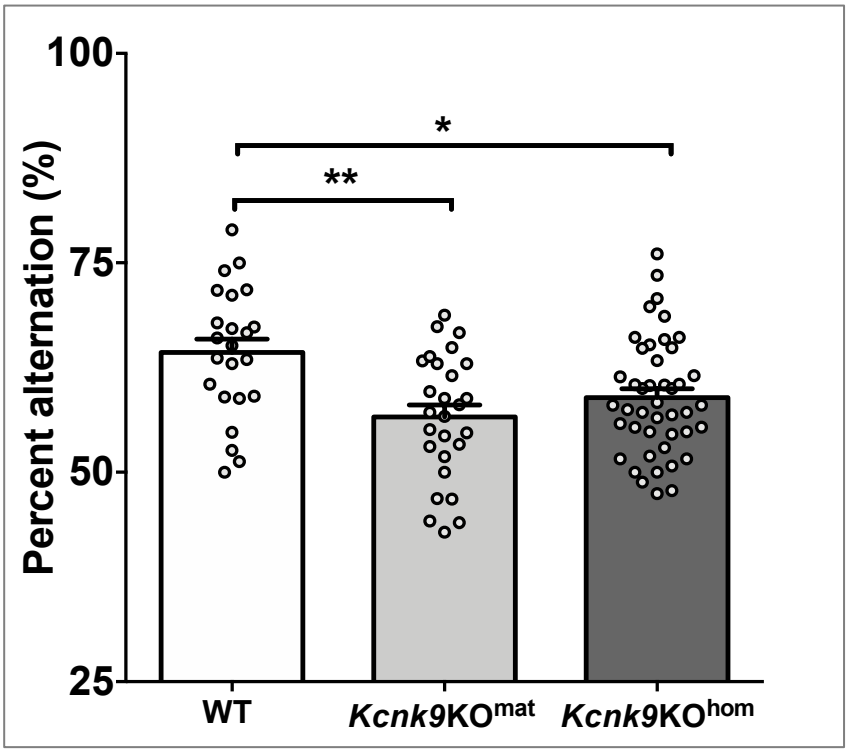

Figure 12: Y-maze results. Y-maze percentage alternation analysis of WT (n=23), *Kcnk9*KO^{mat} (n=27) and *Kcnk9*KO^{hom} (n=45) mice. A spontaneous alternation was defined as consecutive entries into all three arms without revisiting an arm. *Kcnk9*KO mice display a significant decrease in percentage alteration compared to WT mice. One-way ANOVA: F (2, 91) = 7.261, P=0.0012; followed by Bonferroni's multiple comparison post hoc test, *P<0.05, **P<0.01.

Table 9: Y-Maze

Mean ± SEM	Genotype	N	Statistics	F value	P value	Post hoc	Adjusted p-values
64.31 ± 1.619	WT	23	**One way ANOVA**	F (2, 91) = 7.261	P=0.0012	Bonferroni's multiple comparisons test	***P<0.01* *(WT vs. Kcnk9KO^{mat})* **P<0.05* *(WT vs. Kcnk9KO^{hom})*
56.62 ± 1.438	*Kcnk9*KO^{mat}	27					
59.02 ± 1.020	*Kcnk9*KO^{hom}	44					

3.1.2 Rotarod

In the second behavioral test, motor coordination of WT, *Kcnk9*KO^{mat} and *Kcnk9*KO^{hom} mice was analyzed in the light of congenital central hypotonia described in BBIDS patients. No differences in the latency to fall on the rotarod were seen between all genotypes indicating that knockout of *Kcnk*9 in the mouse does not affect motor coordination (Fig. 13, Table 10).

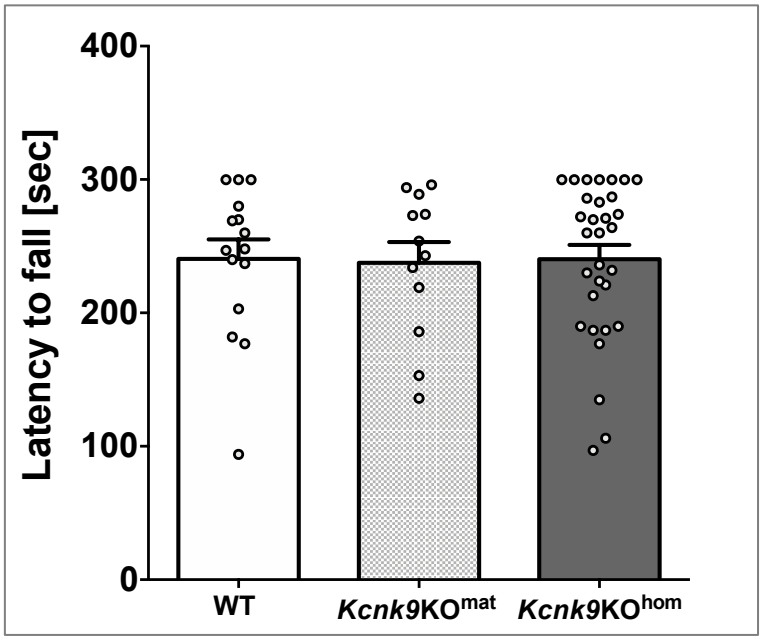

Figure 13: Latency to fall in Rotarod test. WT (n=15), *Kcnk9*KO^{mat} (n=12) and *Kcnk9*KO^{hom} (n=31) mice show no significant differences in latency to fall. Values are means ± SEM.

Table 10: Rotarod test

Mean ± SEM	Genotype	N	Statistics	F value	P value
240.5 ± 14.59	WT	15	**One way ANOVA**	F (2, 55) = 0.01168	P = 0.9884
237.6 ± 15.72	*Kcnk*9KO^{mat}	12			
240.4 ± 10.49	*Kcnk*9KO^{hom}	31			

3.1.3 Pre-Pulse Inhibition

Sensory filtering was evaluated using the well-established paradigm of pre-pulse inhibition (PPI), which is the reduction of the startle reflex by implementation of a weak intensity pre-pulse immediately before the startle stimulus. PPI is reduced in a number of neuropsychiatric disorders including schizophrenia, obsessive-compulsive disorder, Tourette's syndrome and autism (Kohl et al., 2013). The test was performed in sound-attenuating isolation cabinets (Med Associates, St. Albans, VT, USA) as described previously (Radyushkin et al., 2010). *Kcnk9* mutant mice exhibited a significant decrease of PPI ranging from 15-22% for 70 dB, 16-18% for 75 dB to 11-17% for 80 dB compared to age- and sex-matched control mice. There was no significant difference between *Kcnk9*KO^{hom} and *Kcnk9*KO^{mat} mice (Fig. 14, Table 11). Taken together the data indicates a disturbed sensorimotor gating of *Kcnk9*KO^{mat} and *Kcnk9*KO^{hom} mice at 8 weeks of age.

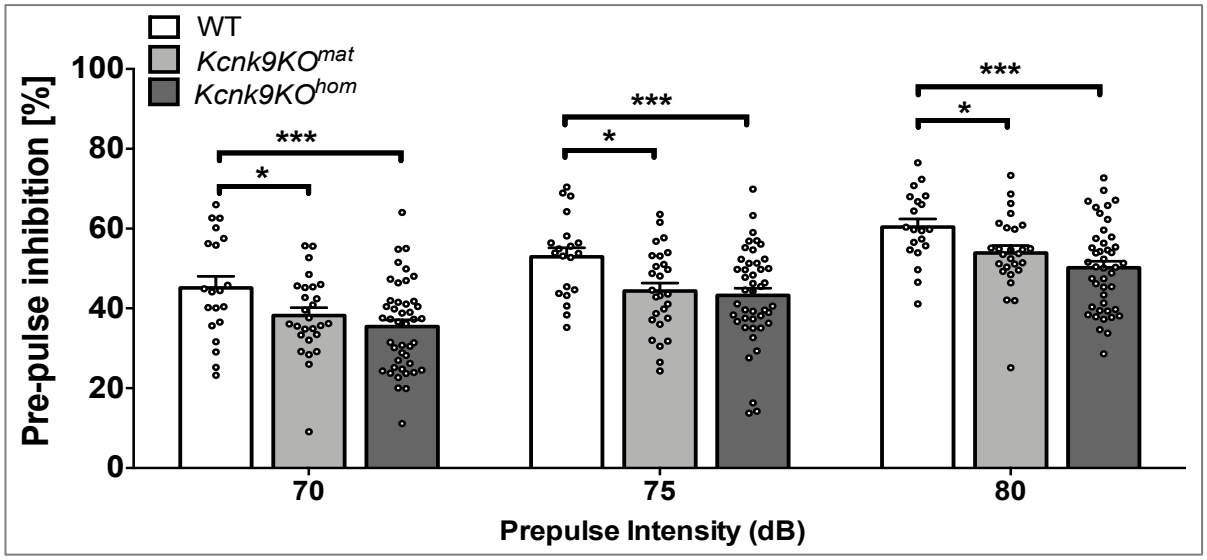

Figure 14: Pre-pulse inhibition (PPI). Graph depicts pre-pulse inhibition (PPI) percentage for WT (n=20), *Kcnk9*KO^{mat} (n=27) and *Kcnk9*KO^{hom} (n=44) mice at three different pre-pulse intensities (70, 75, and 80 dB). *Kcnk9*KO mice exhibit a significantly decreased PPI compared to WT littermates. Repeated measures 2-way ANOVA: Interaction: F (4, 176) = 0.3321, P = 0.8561; Pre-pulse intensity: F (2, 176) = 102.0, P < 0.0001; Genotype: F (2, 88) = 7.757, P = 0.0008; followed by Bonferroni's multiple comparison post hoc test, *P<0.05, ***P<0.001. Values are means ± SEM.

Table 11: Pre-pulse inhibition (PPI)

Mean ± SEM		Genotype	N	Statistics	Interaction	F value	P value	Post hoc	Adjusted p-values
70 dB 75 dB 80 dB	45.132 ± 2.908 52.900 ± 2.272 60.404 ± 1.996	WT	20		Interaction	F (4, 176) = 0.3321	P = 0.8561		
70dB 75dB 80dB	38.231 ± 1.913 44.364 ± 2.014 53.913 ± 1.811	*Kcnk9*KO^{mat}	27	**RM 2-way-ANOVA**	Pre-pulse intensity	F (2, 176) = 102.0	P < 0.0001	Bonferroni's multiple comparisons test	**P<0.05 (WT vs. Kcnk9KO^{mat})*
70dB 75dB 80dB	35.460 ± 1.676 43.285 ± 1.807 50.213 ± 1.623	*Kcnk9*KO^{hom}	44		Genotype Subjects (matching)	F (2, 88) = 7.757 F (88, 176) = 5.524	P = 0.0008 P < 0.0001		****P<0.001 (WT vs. Kcnk9KO^{hom})*

3.1.4 Acoustic Startle Response

Subsequently, mice were analyzed in an acoustic startle response (ASR) test. Acoustic startle response (ASR) is affected in a diverse spectrum of neuropsychiatric phenotypes including ADHD, a key feature in BBIDS. Analysis of the ASR showed that the startle response amplitude across all pulse-intensities (dBs) was significantly decreased in both *Kcnk9*KO^{hom} and *Kcnk9*KO^{mat} animals compared to WT littermates (Fig. 15, Table 12). Surprisingly, however, the post hoc test for multiple comparisons revealed a significant difference of ASR not only between both *Kcnk9*KO genotypes and WT animals, but also between *Kcnk9*KO^{mat} and WT animals on one hand and *Kcnk9*KO^{mat} and *Kcnk9*KO^{hom} animals on the other. This finding suggests an intermediate phenotype in the *Kcnk9*KO^{mat} mice with the *Kcnk9*KO^{hom} animals being significantly more severely affected than the *Kcnk9*KO^{mat} animals.

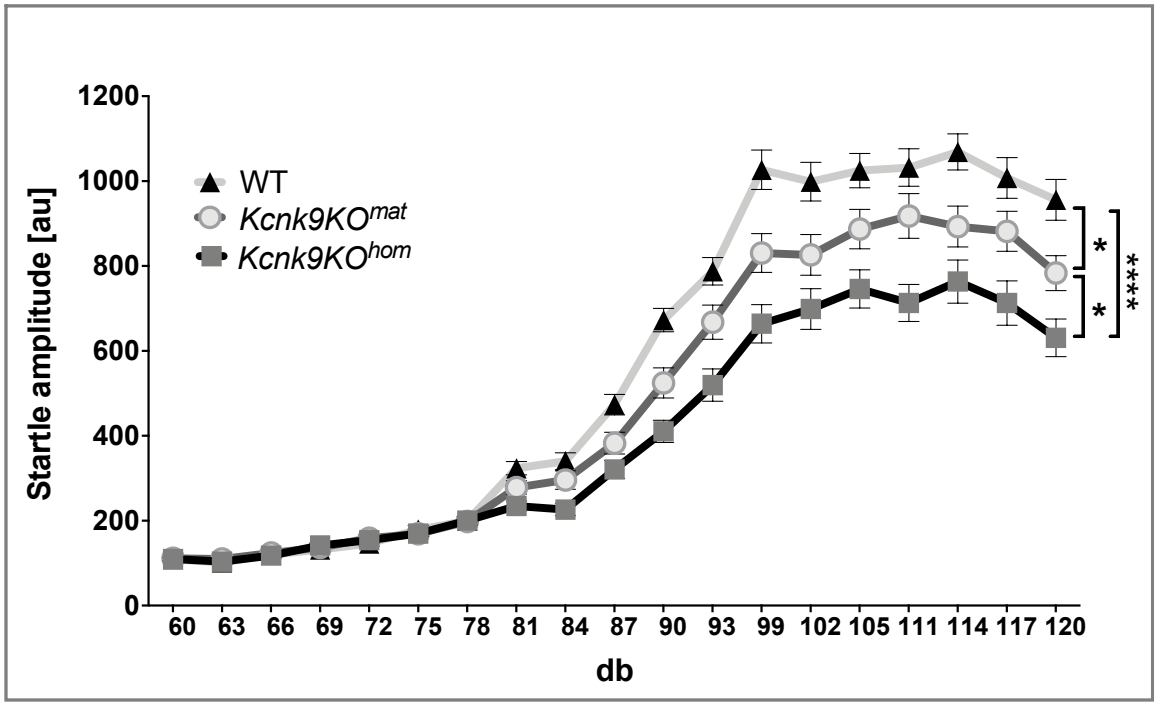

Figure 15: Acoustic startle response (ASR). ASR of WT (n=42), *Kcnk9*KO^{mat} (n=48) and *Kcnk9*KO^{hom} (n=42) mice. The repeated measure two-way ANOVA showed a significant effect of genotype (F (2, 129) = 12.94, P < 0.0001), interaction (F (36, 2322) = 9.24, P < 0.0001) and dB (F (18, 2322) = 584.9, P < 0.0001). The genotype effect was corrected with the Bonferroni's multiple comparison post hoc test, *P<0.05, ****P<0.0001. Values are means ± SEM.

Table 12: Acoustic Startle Response

Mean ± SEM	Genotype	N	Statistics	F value	F value	P value	Post hoc	Adjusted p-values
563,22 ± 25,41	WT	42	**RM 2- way ANOVA**	Interaction	F (36, 2322) = 9.24	P < 0.0001	Bonferroni's multiple comparisons test	*P<0.05 (WT vs. *Kcnk9*KO^{mat})
483,11 ± 27,03	*Kcnk9*KO^{mat}	48		dB	F (18, 2322) = 584.9	P < 0.0001		*P<0.05 (*Kcnk9*KO^{mat} vs. Kcnk9KO^{hom})
402,07 ± 25,39	*Kcnk9*KO^{hom}	42		Genotype	F (2, 129) = 12.94	P < 0.0001		****P<0.0001 (WT vs. *Kcnk9*KO^{hom})
				Subjects (matching)	F (129, 2322) = 16.48	P < 0.0001		

3.1.5 Circadian Rhythm

Circadian rhythms in mammals are endogenously coordinated rhythms that have a period length of about 24 hours (Reppert and Weaver, 2002). KCNK9 channels contribute to the activity of neurons in brain regions associated with the regulation of the circadian rhythm and arousal (Gotter et al., 2011; Linden et al., 2007; Meuth et al., 2003; Pang et al., 2009). Activity pattern analysis during light and dark phase resembling day and night was performed. A significantly increased locomotor activity during the dark phase was found in *Kcnk9*KO^{hom} and *Kcnk9*KO^{mat} mice compared to WT controls, describing an exaggerated nocturnal activity in *Kcnk9*KO animals (Fig. 16, Table 13), which is in consensus with previous observations (Linden et al., 2007). Surprisingly, an intermediate phenotype in the dark phase activity pattern was seen in the *Kcnk9*KO^{mat} animals with statistically significant differences to both, WT and *Kcnk9*KO^{hom} animals. No significant differences between genotypes were observed in the total locomotor activity during the light phase.

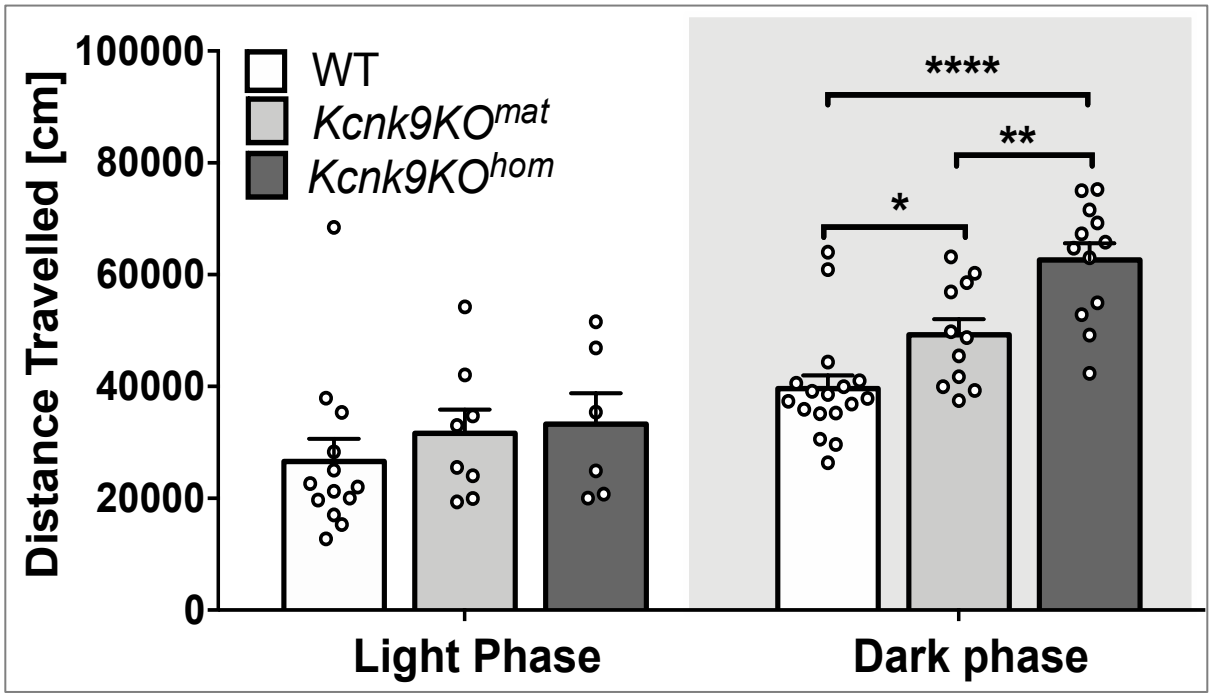

Figure 16: Total locomotor activity. Distance travelled in the home cage in light (12h)/ dark (12h) phase. The left section shows the distance travelled in the light phase of WT (n=13), *Kcnk9*KO^{mat} (n=8) and *Kcnk9*KO^{hom} (n=6) mice. One-way ANOVA: F (2, 24) = 0.6183, P = 0.5472. The right section depicts the nocturnal activity of WT (n=17), *Kcnk9*KO^{mat} (n=11) and *Kcnk9*KO^{hom} (n=12) mice. *Kcnk9*KO^{mat} and *Kcnk9*KO^{hom} mice display significantly increased nocturnal hyperactivity compared to WT littermates with activity scores of *Kcnk9*KO^{mat} mice intermediate between *Kcnk9*KO^{hom} and WT mice. One-way ANOVA: F (2, 37) = 19.23, P < 0.0001; followed by Bonferroni's multiple comparison post hoc test, *P<0.05, **P<0.01, ****P<0.0001. Values are means ± SEM.

Table 13: Circadian Rhythm

Phase	Mean ± SEM	Genotype	N	Statistics	F value	P value	Post hoc	Adjusted p-values
Light	26601,97 ± 4029.135	WT	13	**one way ANOVA**	F (2, 24) = 0.6183	P = 0.5472	n.s.	
	31630.828 ± 4255.746	*Kcnk*9KO^{mat}	8					
	33267.280 ± 5559.225	*Kcnk*9KO^{hom}	6					

Dark	39619.945 ± 2350.092	WT	17	**one way ANOVA**	F (2, 37) = 19.23	P < 0.0001	Bonferroni's multiple comparisons test	**P<0.05 (WT vs. Kcnk9KO^{mat})*
	49223.234 ± 2790.957	*Kcnk*9KO^{mat}	11					*****P<0.0001 (WT vs. Kcnk9KO^{hom})*
	62616.870 ± 3039.967	*Kcnk*9KO^{hom}	12					***P<0.01 (Kcnk9KO^{mat} vs. Kcnk9KO^{hom})*

Together, these data demonstrate that the loss of *Kcnk9* in mice results in the impairment of several behavioral parameters that resembles parts of the BBIDS phenotype. Interestingly, intermediate phenotypes for acoustic startle response and nocturnal locomotor activity was found in animals with a loss of only the actively expressed maternal allele (*Kcnk9*KO^{mat}) suggesting the involvement of the silenced paternal allele.

3.2 Non-canonical Imprinting of *Kcnk9* in the Mouse Brain

In human and mouse brain, *KCNK9/Kcnk9* was reported to be monoallelically expressed from the maternal allele while the paternal allele is silenced (Court et al., 2014; Ruf et al., 2007). To elucidate if the intermediate phenotype of *Kcnk9*KO^{mat} animals is due to residual expression from the paternal allele, we thoroughly analyzed the parent-of-origin allele-specific expression pattern of *Kcnk9* in different brain regions using the previously described QUASEP method (Ruf et al., 2007). QUASEP allows pyrosequencing-based parental allele-specific detection of *Kcnk9* transcripts through heterozygous, transcribed single nucleotide polymorphisms (SNPs) in brain regions of F1 hybrid animals from crosses between C57BL/6 (B6) and Mus musculus castaneus (Cast/Ei) mouse strains [(C57BL/6xCast/Ei)F1]. As expected, we observed predominant expression of the maternal *Kcnk9* allele in all

analyzed brain regions (Fig. 17, Table 14). However, we also detected significant expression from the repressed paternal allele, which represented 1-14% of all transcripts depending on the brain region analyzed. Highest paternal expression was observed in the locus coeruleus (LC) (Fig. 17, Table 14). The high paternal expression of *Kcnk9* in the LC could also be confirmed by the analysis of WT and *Kcnk9*KO^{mat} mice with a C57BL/6J background using RT-qPCR expression analysis of the LC (Fig. 18c).

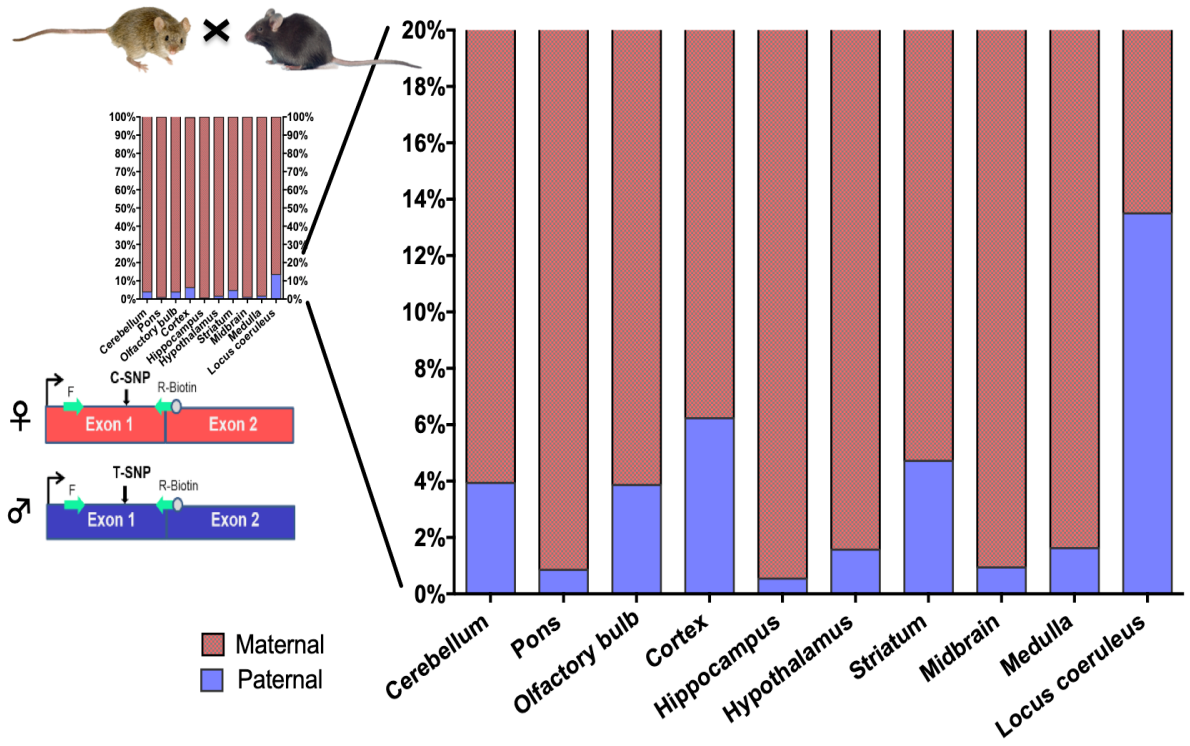

Figure 17: Non-canonical *Kcnk9* imprinting in (C57BL/6xCast/Ei)F1 hybrid mice Quantification of Allele-Specific Expression by Pyrosequencing (QUASEP) of several brain regions from (C57BL/6xCast/Ei)F1 hybrid mice; maternal allele (pink) and paternal allele (violet). Cerebellum n=14, pons n=10, olfactory bulb n=12, cortex n=14, hippocampus n=14, hypothalamus n=9, striatum n=5, midbrain n=5, medulla n=5 and locus coeruleus n=4. Lower left graph depicts the assay design and position of primers (turquoise) flanking the C/T-SNP in exon 1 for the maternal (pink) and paternal (violet) *Kcnk9* allele.

Table 14: QUASEP of several brain regions from (C57BL/6xCast/Ei)F1 hybrid mice

Maternal transcripts in %			Paternal transcripts in %			Region	N
96,1	±	0,2	3,9	±	0,2	Cerebellum	14
99,2	±	0,3	0,9	±	0,3	Pons	10
96,2	±	1,5	3,8	±	1,5	Olfactory bulb	12
93,2	±	0,3	6,8	±	0,3	Cortex	14
99,5	±	0,2	0,5	±	0,2	Hippocampus	14
98,4	±	0,4	1,6	±	0,4	Hypothalamus	9
95,3	±	0,4	4,7	±	0,4	Striatum	5
99,1	±	0,4	0,9	±	0,4	Midbrain	5
98,4	±	0,4	1,6	±	0,4	Medulla	5
86,5	±	1,8	13,5	±	1,8	Locus coeruleus	4

Accuracy of the LC tissue collection was validated, by performing tyrosine hydroxylase expression analyses and comparing the expression levels to those of WT cerebellum and hippocampus samples. Tyrosine hydroxylase, which serves as a norepinephrine marker, was expressed ~400 fold higher compared to hippocampus samples, indicating a precise tissue dissection of the LC (Fig. 18a).

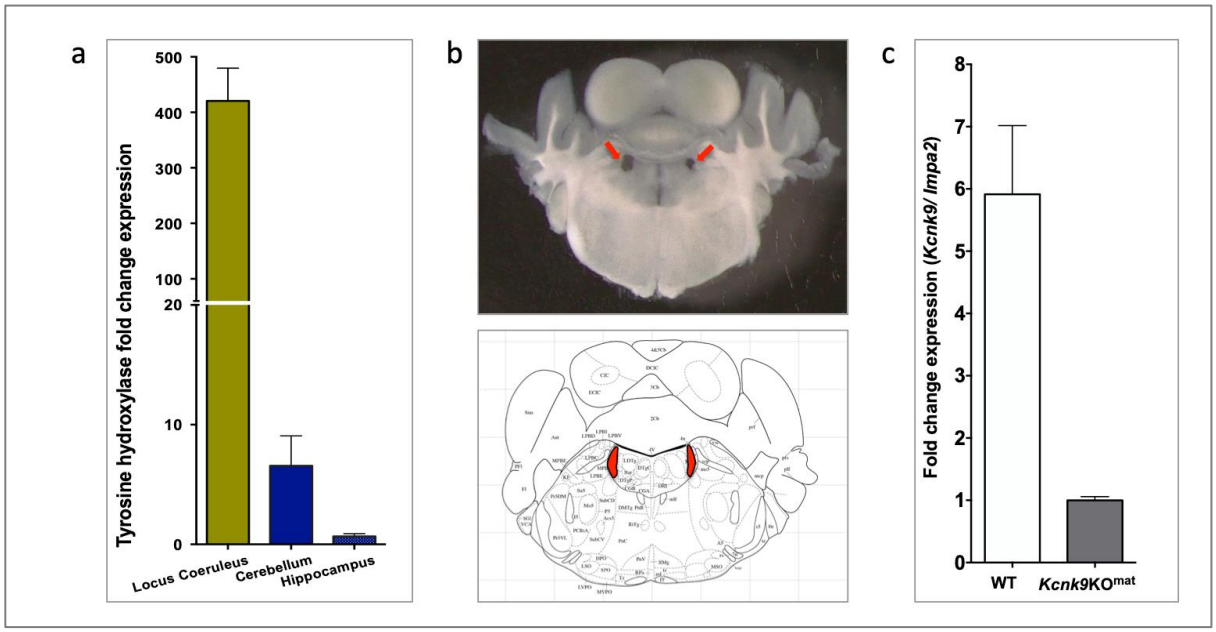

Figure 18: Locus coeruleus expression analysis. (a) Tyrosine hydroxylase (TH) RT-qPCR expression analysis. The TH expression was highly increased in Locus coeruleus (LC) compared to hippocampus and cerebellum samples of WT mice. TH serves as a norepinephrine marker. **(b)** Coronal brain slice of an adult mouse; red arrows indicate tissue excision position of LC (top) Schematic coronal brain slice of adult mouse, bregma -5.34mm, interaural -1.54 mm (Franklin, 1997), LC is depicted in red (bottom) **(c)** *Kcnk9* RT-qPCR expression analysis in LC samples of WT and *Kcnk9*KO^{mat} mice in comparison.

In addition, the relative expression levels of *Kcnk9* between different brain regions were compared. A high paternal expression was detected in the cortex and cerebellum followed by midbrain, hypothalamus, olfactory bulb, hippocampus, pons, striatum and medulla oblongata, respectively (Fig. 19a). Furthermore, (*Kcnk9*KO^{hom}xCast/Ei)F1 animals carrying only a maternal *Kcnk9* deletion (*Kcnk9*KO^{mat}) displayed paternal *Kcnk9* expression further increased compared to that of (C57BL/6xCast/Ei)F1 WT animals in several brain areas suggesting a regulatory feedback-loop between maternal and paternal *Kcnk9* expression (Fig. 19b, Table 15).

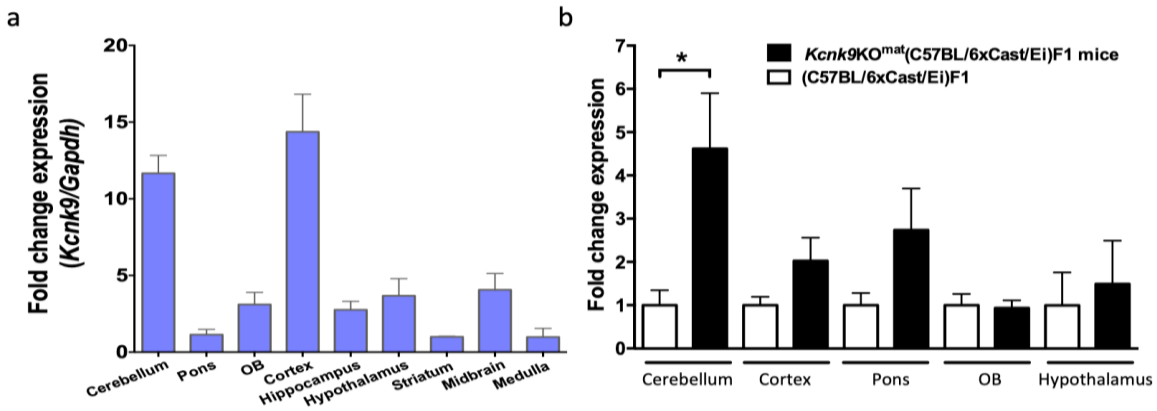

Figure 19: Paternal *Kcnk9* expression in several brain regions of (C57BL/6xCast/Ei)F1 hybrid mice and up-regulation of paternal *Kcnk9* expression in *Kcnk9*KO^{mat}(C57BL/6xCast/Ei)F1 hybrid mice (a) Relative mRNA expression of the paternal *Kcnk9* allele in cerebellum (n=6), pons (n=3), olfactory bulb (n=4), cortex (n=6), hippocampus (n=6), hypothalamus (n=6), striatum (n=2), midbrain (n=4) and medulla (n=3) **(b)** Allele-specific RT-qPCR results. Relative mRNA expression of the paternal *Kcnk9* allele in cerebellum, cortex, pons, olfactory bulb and hypothalamus of WT (C57BL/6xCast/Ei)F1 (n=5-6) and *Kcnk9*KO^{mat}(C57BL/6xCast/Ei)F1 (n=4-7) mice. Paternal *Kcnk9* expression is increased in *Kcnk9*KO^{mat} compared to WT mice. A significant increase was observed in the cerebellum (P=0,0173, Mann-Whitney U test). OB = olfactory bulb. Values are means ± SEM.

Table 15: Paternal expression of *Kcnk9 in* several brain regions

Mean ± SEM			Genotype	Region	N	Statistics	P value
1,00	±	0,34	(C57BL/6xCast/Ei)F1	Cerebellum	5	Mann-Whitney U	P=0,0173
4,62	±	1,28	*Kcnk*9KO^{mat} (C57BL/6xCast/Ei)F1		6		
1,00	±	0,19	(C57BL/6xCast/Ei)F1	Cortex	5		P=0.1596
2,02	±	0,54	*Kcnk*9KO^{mat} (C57BL/6xCast/Ei)F1		4		
1,00	±	0,28	(C57BL/6xCast/Ei)F1	Pons	6		P=0,2308
2,74	±	0,96	*Kcnk*9KO^{mat} (C57BL/6xCast/Ei)F1		7		
1,00	±	0,26	(C57BL/6xCast/Ei)F1	Olfactory bulb	5		P=0.5000
0,93	±	0,18	*Kcnk*9KO^{mat} (C57BL/6xCast/Ei)F1		3		
1,00	±	0,76	(C57BL/6xCast/Ei)F1	Hypothalamus	4		P=0.2286
1,49	±	1,00	*Kcnk*9KO^{mat} (C57BL/6xCast/Ei)F1		3		

These data demonstrate a brain region-specific relaxation of the imprint on the paternal *Kcnk9* allele with a peak in the LC, which represents a possible modifying mechanism of the phenotype in *Kcnk9*KO^{mat} animals.

3.3 Identification of Epigenetic Modulators Activating the Paternally Repressed *Kcnk9* Allele

The paternally inherited *Kcnk9/KCNK9* allele is epigenetically silenced yet structurally unimpaired. Our behavioral and gene expression experiments suggest a contribution of paternally expressed *Kcnk9* to the intermediate phenotype of the *Kcnk9*KO^{mat} mice and the possibility of up-regulation of the paternal allele in the case of loss of the maternal allele. We therefore speculated that exogenous application of epigenetic modulators may alter the structure at the *Kcnk9* promoter region and result in further derepression of the paternal *Kcnk9* allele. We hypothesized that this could possibly fully compensate the loss of the maternal allele and rescue the BBIDS-like phenotype of *Kcnk9*KO^{mat} mice.

To investigate the paternally derived *Kcnk9* transcript levels after epigenetic drug treatment, we isolated E14 mouse primary cortical neurons (mPCNs) of WT and *Kcnk9*KO^{mat} animals from crosses between WT males and *Kcnk9*KO^{hom} females (Fig. 20). We then chose six different compounds representing diverse classes of epigenetic modulators for treatment: the histone methyltransferase EZH2 inhibitor 3-deazaneplanocin A (DZNep), the DNA methyltransferase inhibitor Zebularine, the histone acetyltransferase p300/CBP inhibitor C646, and the histone deacetylase inhibitors (HDACi) Vorinostat (SAHA), Valproic acid (VPA) and Tacedinaline (CI-994) (Table 16).

Table 16: Epigenetic modulators used for treatment of mPCNs with enzymatic activities inhibited by them

Drug	Inhibition
C646	histone acetyltransferase p300/CBP inhibitor
Tacedinaline CI-994	histone deacetylase
3-deazaneplanocin A (Dznep)	histone methyltransferase EZH2 inhibitor
Vorinostat (SAHA)	histone deacetylase
Valproic acid (VPA)	histone deacetylase
Zebularine	DNA methyltransferase

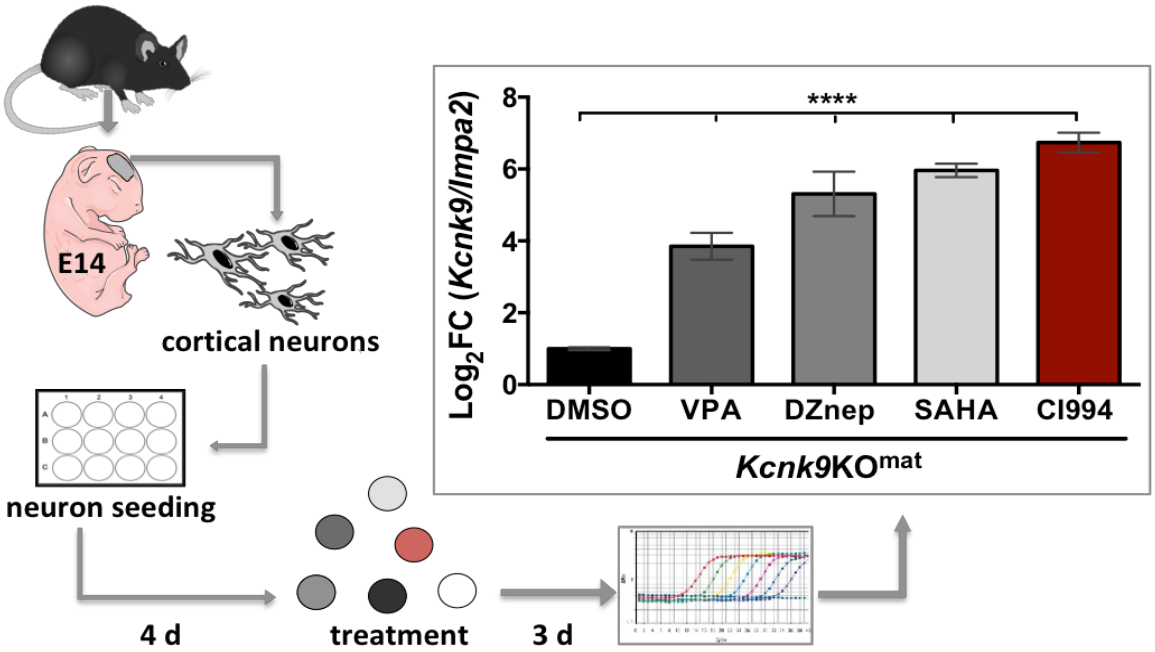

Figure 20: Identification of epigenetic modulators that up-regulate paternal *Kcnk9* expression in murine primary cortical neurons (mPCNs). Workflow of mPCN isolation, drug treatment and RT-qPCR analysis (left). Significant up-regulation of paternal allele-derived *Kcnk9* mRNA in DZnep-, SAHA-, VPA- and CI-994-treated E14 *Kcnk9*KO^{mat} mPCNs compared to DMSO-treated *Kcnk9*KO^{mat} mPCNs detected by RT-qPCR (3 day treatment, normalization to *Impa2*, DMSO n=7 cultures/group, DZnep (20 µM) SAHA (30 µM), VPA (5 mM) and CI-994 (40 µM) n=3 cultures/group) (right). One-way ANOVA: $F(5, 22) = 75.51$, $P < 0.0001$; followed by Bonferroni's multiple comparison post hoc test to *Kcnk9*KO^{mat} DMSO control, ****P<0.0001. Values are means ± SEM.

Murine PCNs were treated for three days with the epigenetic modifiers and *Kcnk9* expression was analyzed by quantitative reverse transcription PCR (RT-qPCR). Murine PCNs treated with DZNep (20 µM), SAHA (30 µM), VPA (5 mM) and CI-994 (40 µM) exhibited a significantly increased paternal *Kcnk9* expression (RT–qPCR) compared to *Kcnk9*KO^{mat} mPCNs treated with dimethyl sulfoxide (DMSO) (control vehicle) (Fig. 20, Table 17). By contrast, treatment with the compounds Zebularine and C646 did not show any altered *Kcnk9* expression in *Kcnk9*KO^{mat} mPCNs compared to control conditions (Fig. 21, Table 18).

Table 17: Treatment of cortical neurons with epigenetic drugs

Mean ± SEM	Drug	N	Statistics	F value	P value	Post hoc	Adjusted p-values
	*Kcnk*9KO^{mat}	Cultures					vs. DMSO
1.000 ± 0.0417	DMSO	7				Bonferroni's multiple comparisons test	
3.853 ± 0.3724	**VPA**	3	**one way ANOVA**	F (4, 14) = 92.00	P < 0.0001		****P < 0.0001
5.307 ± 0.6183	**DZnep**	3					****P < 0.0001
5.963 ± 0.1874	**SAHA**	3					****P < 0.0001
6.738 ± 0.2760	**CI-994**	3					****P < 0.0001

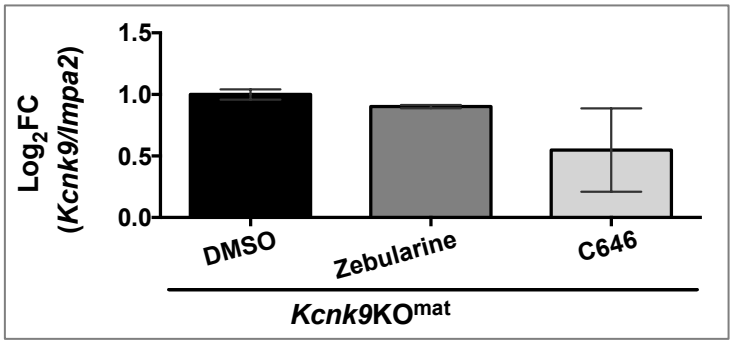

Figure 21: Epigenetic drug treatments in murine primary cortical neurons (mPCNs). The compounds Zebularine and C646 had no effect on the *Kcnk9* expression in *Kcnk9*KO^{mat} mPCNs (Zebularine P=0.0667, C646 P=0.4727, Mann-Whitney-U test. Values are means ± SEM.

Table 18: Treatment of cortical neurons with epigenetic drugs without effect

Mean ± SEM	Drug	N	Statistics	P value
	*Kcnk9*KO^{mat}	Cultures		
1.000 ± 0.0417	DMSO	7	**one way ANOVA**	vs. DMSO
0.901 ± 0.013	Zebularine	3		P= 0.0667
0.548 ± 0.338	C646	4		P =0.4727

For further investigations, we focused on the second-generation histone deacetylase inhibitor (HDACi) CI-994, a selective inhibitor of class I HDACs, which inhibits HDAC isoenzymes 1, 3, 9 and 8 (Beckers et al., 2007). CI-994 showed the most efficient up-regulation of paternal *Kcnk9* expression in *Kcnk9*KO^{mat} mPCNs (Fig. 20).

The effect of CI-994 in *Kcnk9*KO^{mat} mPCNs was further tested in a dose-response experiment. *Kcnk9*KO^{mat} mPCNs were treated with increasing concentrations of CI-994 for 24 hours and *Kcnk9* expression was analyzed using RT-qPCR in comparison to DMSO-treated *Kcnk9*KO^{mat} and WT control cells (Fig. 22, Table 19). As expected, the paternal *Kcnk9* expression in DMSO-treated *Kcnk9*KO^{mat} mPCNs was significantly reduced compared to that of WT mPCNs. After CI-994 treatment of *Kcnk9*KO^{mat} mPCNs, we observed a strong correlation between increase of paternal *Kcnk9* expression and CI-994 dosage suggesting a specific, dose-dependent effect of CI-994. Notably, *Kcnk9* expression in 80 µM CI-994-treated *Kcnk9*KO^{mat} mPCNs exceeded that of DMSO-treated WT mPCNs *in vitro* (Fig. 22, Table 19).

In addition, we investigated the effect of CI-994 on the expression of other nearby imprinted genes within the imprinted cluster on mouse chromosome 15. Intriguingly, treatment with 20 µM or 80 µM CI-994 did not affect the expression of *Eif2c2, Chrac1, Peg13* and *Trappc9 in Kcnk9*KO^{mat} mPCNs. (Fig. 23, Table 20).

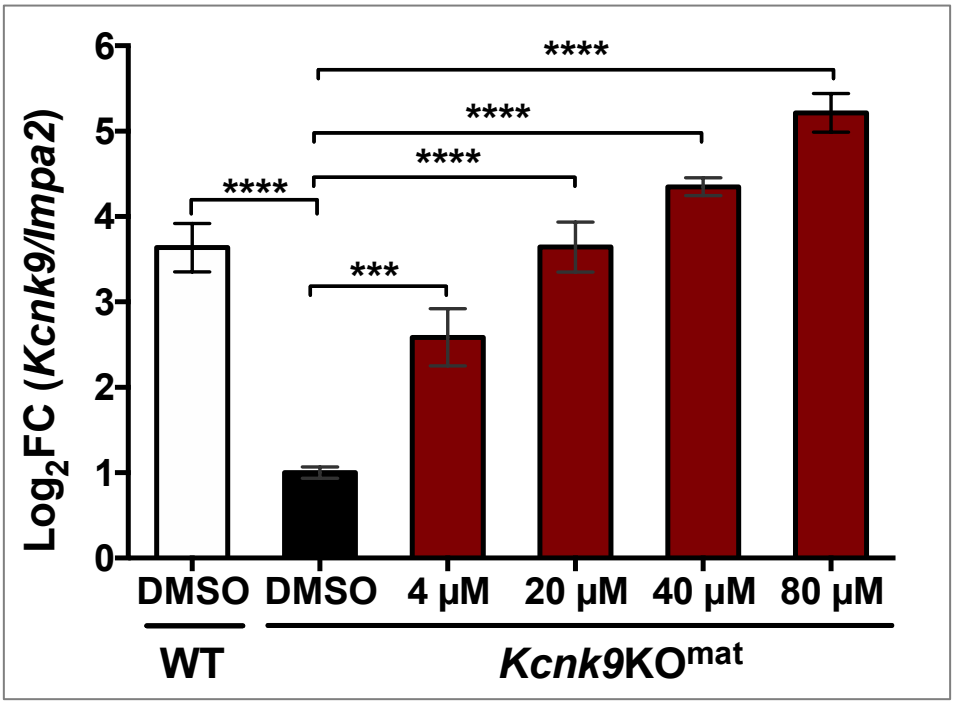

Figure 22: Treatment of mPCNs with CI-994 (dosage response). Up-regulation of paternal allele-derived *Kcnk9* mRNA after treatment of *Kcnk9*KO^{mat} mPCNs with different CI-994 concentrations compared to paternal allele-derived *Kcnk9* mRNA of DMSO-treated *Kcnk9*KO^{mat} mPCNs and *Kcnk9* mRNA of DMSO-treated WT mPCNs detected by RT-qPCR (1 day treatment, normalization to *Impa2*, *Kcnk9*KO^{mat} DMSO n=9; 4µM n=2; 20-80µM n=4 and WT DMSO n=5 cultures/group). One-way ANOVA: F (5, 22) = 75.51, P < 0.0001; corrected with Bonferroni's multiple comparison post hoc test to *Kcnk9*KO^{mat} DMSO mPCNs, ***P<0.001, ****P<0.0001. Values are means ± SEM.

Table 19: Treatment of mPCNs with CI-994 (dosage response)

Mean ± SEM	Genotype	N	Statistics	F value	P value	Post hoc	Adjusted p-values
	*Kcnk*9KO^{mat}	Cultures					*Kcnk*9KO^{mat} vs. DMSO
1.000 ± 0.0656	DMSO	9					
2.586 ± 0.3351	4 µM	2					***P < 0.001
3.642 ± 0.2920	20 µM	4	**one way ANOVA**	F (5, 22) = 75.51	P < 0.0001	Bonferroni's multiple comparisons test	****P < 0.0001
4.349 ± 0.1035	40 µM	4					****P < 0.0001
5.216 ± 0.2264	80 µM	4					****P < 0.0001
3.636 ± 0.2824	WT DMSO	5					****P < 0.0001

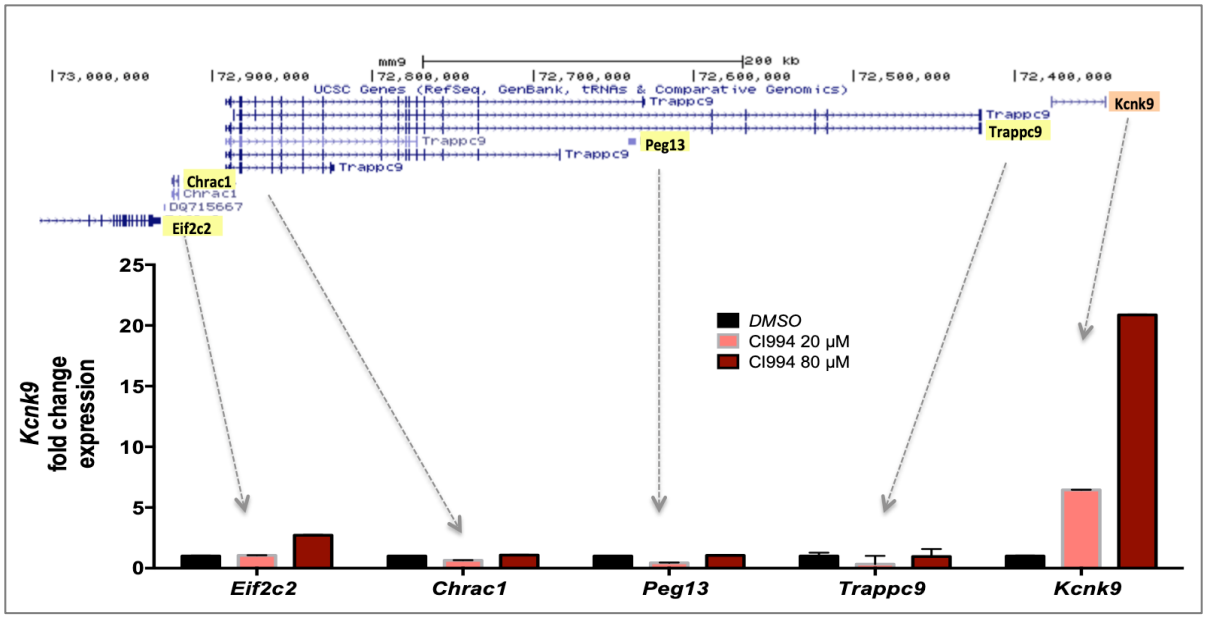

Figure 23: RT-qPCR expression analysis of *Kcnk9* and other nearby imprinted genes in the imprinting cluster on mouse chromosome 15. CI-994 treatment (20 µM and 80 µM CI-994) did not affect expression of *Trappc9, Peg13, Chrac1* and *Eif2c2* in mPCNs (n=2-3 cultures/group).

Table 20: RT-qPCR expression analysis of other nearby imprinted genes in the imprinting cluster on mouse chromosome 15

Gene	Mean ± SEM			Drug	Cultures
Eif2c2	1,050	±	0,014		2
Chrac1	0,646	±	0,014		3
Peg13	0,442	±	0,018	CI-994 20 µM	3
Trappc9	0,337	±	0,678		3
Kcnk9	6,448	±	0,016		2
Eif2c2	2,718	±	0,024		3
Chrac1	1,084	±	0,024		2
Peg13	1,060	±	0,024	CI-994 80 µM	3
Trappc9	0,965	±	0,608		3
Kcnk9	20,870	±	0,042		2

3.4 The HDAC inhibitor CI-994 Rescues the Behavioral Phenotype of *Kcnk9*KO^{mat} Animals

3.4.1 CI-994 Derepresses the Paternal *Kcnk9* Allele in the Brain

The expression of the paternal *Kcnk9* allele detected in several brain regions and the observation of intermediate phenotypes in *Kcnk9*KO^{mat} animals led us hypothesize that epigenetic manipulation could further stimulate paternal gene expression and thereby enhance the phenotypical rescue.

For testing, either DMSO (100 %) or CI-994 (30 mg/kg) were injected daily over 14 days in the peritoneum of *Kcnk9*KO^{mat} and WT animals (Fig. 24a). After injections, paternal expression was induced up to ~3 fold in several brain regions of CI-994-treated *Kcnk9*KO^{mat} mice compared to those of DMSO-treated *Kcnk9*KO^{mat} mice including the cerebellum, hippocampus, pons, hypothalamus, olfactory bulb, and locus coeruleus (Fig. 24b, Table 21). Importantly, this drug-induced rescue also included brain regions like the hippocampus, where only a small degree (< 1%) of spontaneous expression from paternal alleles was observed in the maternal KO. No up-regulation of *Kcnk9* expression was seen in WT animals after CI-994 treatment (Fig. 24c, Table 22).

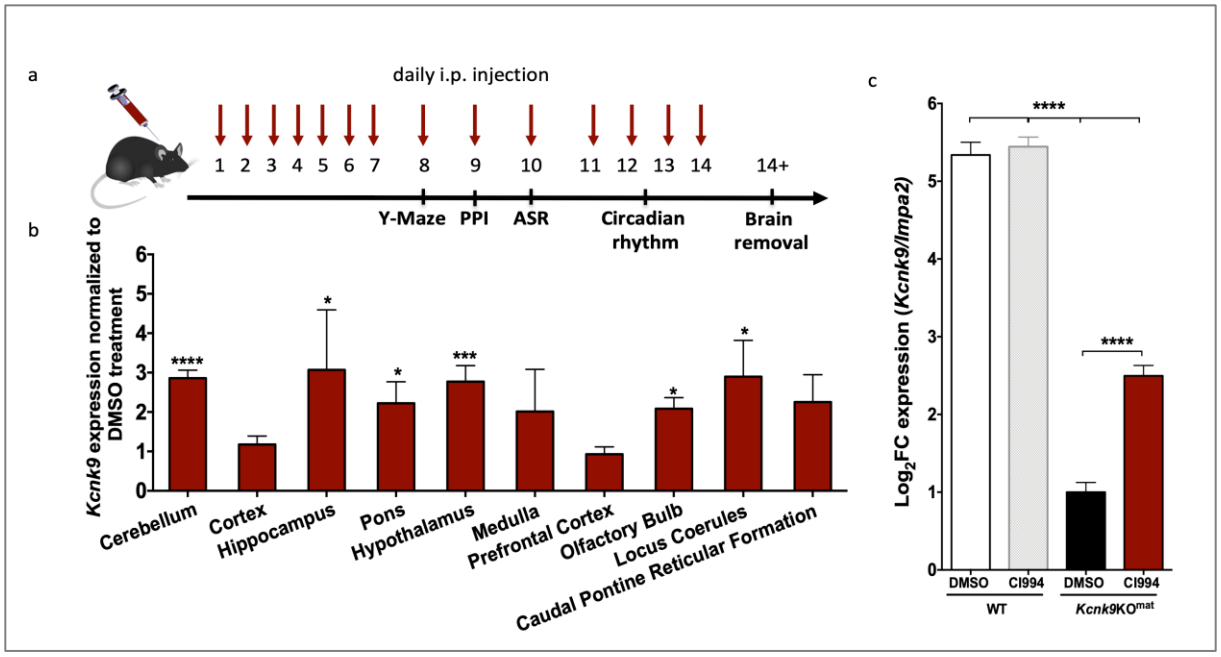

Figure 24: Effects of CI-994 histone deacetylase inhibitor treatment *in vivo*. (a) Experimental design of the mouse study. CI-994 was intraperitoneally injected every day starting 7 days before behavioral tests. DMSO was used as a vehicle control**. (b)** Significant up-regulation of *Kcnk9* after CI-994 treatment in several brain regions normalized to DMSO treatment, Mann-Whitney test. **(c)** Up-regulation of *Kcnk9* in the cerebellum of CI-994-treated *Kcnk9*KO^{mat} mice, but not in the cerebellum of CI-994-treated WT mice, each compared to DMSO-treated *Kcnk9*KO^{mat} and WT mice. 2-way ANOVA, interaction: $F(1, 42) = 26.16$, $P < 0.0001$; treatment: $F(1, 42) = 34.92$, $P < 0.0001$; genotype: $F(1, 42) = 719.1$, $P < 0.0001$; followed by Bonferroni's multiple comparison post hoc test, ****P<0.0001. Values are means ± SEM.

Table 21: *Kcnk9* expression in all brain regions after CI-994 treatment

Mean ± SEM	Region	N	Statistics	P value
DMSO vs CI-994				DMSO vs CI-994
2.89 ± 0,20	Cerebellum	DMSO: 12 CI-994: 13		P < 0.0001
1,18 ± 0,21	Cortex	DMSO: 6 CI-994: 9		P= 0,3251
2,94 ± 1,52	Hippocampus	DMSO: 7 CI-994: 9		P= 0,0164
2,22 ± 0,55	Pons	DMSO: 7 CI-994: 8		P= 0,0002
2,77 ± 0,41	Hypothalamus	DMSO: 9 CI-994: 12	**Mann-Whitney U** **DMSO vs CI-994**	P= 0,0003
2,01 ± 1,07	Medulla	DMSO: 6 CI-994: 6		P= 0,3961
0,96 ± 0,19	Prefrontal cortex	DMSO: 9 CI-994: 9		P= 0,7319
2,08 ± 0,28	Olfactory bulb	DMSO: 6 CI-994: 6		P= 0,0022
2,90 ± 0,92	Locus coeruleus	DMSO: 7 CI-994: 8		P= 0,0401
2,25 ± 0,69	Caudal Pontine Reticular Formation	DMSO: 7 CI-994: 4		P= 0,1409

Table 22: *Kcnk9* expression in cerebellum after CI-994 treatment

Mean ± SEM	Genotype	N	Statistics	Interaction	F value	P value	Post hoc	Adjusted p-values
5.337 ± 0.165	WT DMSO	9	**2-way-ANOVA**	Interaction	F (1, 42) = 26.16	P < 0.0001	Bonferroni's multiple comparisons test	*****P<0.0001 (all comparisons except DMSO: WT vs CI994: WT)*
5.445 ± 0.123	WT CI-994	12		Treatment	F (1, 42) = 34.92	P < 0.0001		
1.000 ± 0.125	*Kcnk*9KO^{mat} DMSO	12		Genotype	F (1, 42) = 719.1	P < 0.0001		
2.497 ± 0.133	*Kcnk*9KO^{mat} CI-994	13						

3.4.2 CI-994 Promotes Behavioral Recovery

A previous study reported that intraperitoneal administration of CI-994 in wildtype mice resulted in long-lasting CI-994 levels in the brain without affecting the overall behavioral phenotype of mice (Graff et al., 2014). Thus, to assess whether CI-994 treatment also promotes behavioral recovery, WT and *Kcnk9*KO^{mat} mice were subjected to behavioral testing after treatment (Fig. 24a) with either DMSO (100%) or CI-994 (30 mg/kg).

3.4.2.1 Pre-Pulse Inhibition after CI-994 Treatment

In the initial pre-pulse inhibition (PPI) experiments (chapter 3.1.3) *Kcnk9*KO^{mat} and *Kcnk9*KO^{hom} mice displayed decreased PPI compared to WT mice. After daily injections with DMSO, WT and *Kcnk9*KO^{mat} did not show a significant difference in PPI as described in previous experiments. Injections with CI-994 showed a slight decrease in PPI in WT and *Kcnk9*KO^{mat} mice compared to DMSO-treated littermates within the same genotype. Bonferroni's multiple comparisons test did not determine a significant difference between genotypes and treatment (Fig. 25, Table 23).

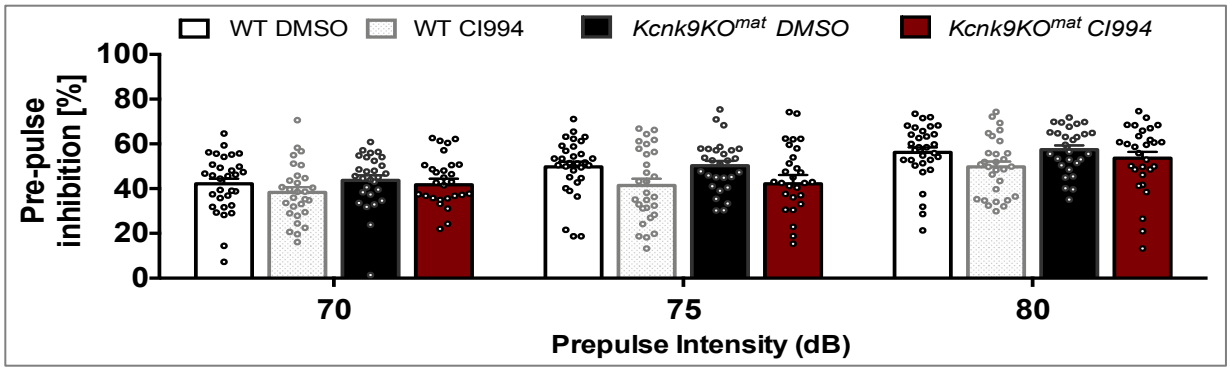

Figure 25: Pre-pulse inhibition (PPI) after CI994 treatment. Graph depicts PPI values for DMSO-treated WT mice (n=29), CI994-treated WT mice (n=27), DMSO-treated *Kcnk9*KO^{mat} mice (n=29) and CI994-treated *Kcnk9*KO^{mat} mice (n=27) mice at three different pre-pulse intensities (70, 75, and 80 dB). CI994 treated WT mice display decreased PPI compared to DMSO injected WT mice (p=0.0219) and *Kcnk9*KO^{mat} mice (p=0.0052). Data are expressed as means ± SEM.

Table 23: PPI after CI-994 treatment

Mean ± SEM		Genotype	N	Statistics	Interaction	F value	P value	Post hoc	Adjusted p-values
70dB	43.377 ± 2.639								
75dB	50.792 ± 2.477	DMSO: WT	31		Interaction	F (6, 216) = 1.291	P = 0.2623		
80dB	54.826 ± 2.530								
70dB	37.625 ± 2.002								
75dB	40.228 ± 3.057	CI-994: WT	29		Pre-pulse intensity	F (2, 216) = 75.23	P < 0.0001	Bonferroni's multiple comparisons test (within each row, compare columns)	
80dB	48.758 ± 2.390			**RM 2-way-ANOVA**					n.s.
70dB	43.755 ± 2.230								
75dB	50.262 ± 2.078	DMSO: *Kcnk*9KO^{mat}	28		Genotype	F (3, 108) = 3.025	P = 0.0328		
80dB	57.620 ± 1.886								
70dB	43.085 ± 2.331								
75dB	45.241 ± 2.909	CI-994: *Kcnk*9KO^{mat}	29		Subjects (matching)	F (108, 216) = 6.812	P < 0.0001		
80dB	55.500 ± 2.493								

3.4.2.2 Y-Maze after CI-994 Treatment

In the Y-maze task, CI-994 treatment led to a significant increase of spontaneous alternation in the *Kcnk9*KO^{mat} mice compared to DMSO-treated *Kcnk9*KO^{mat} control mice (Fig. 26, Table 24). Post hoc testing for multiple comparisons showed no difference between CI-994-treated *Kcnk9*KO^{mat} animals and either DMSO- or CI-994-treated WT animals (Table 24). Thus, CI-994-treated *Kcnk9*KO^{mat} mice just as WT mice treated with either DMSO or CI-994 did not exhibit deficits in working memory and significant differences in the Y-maze.

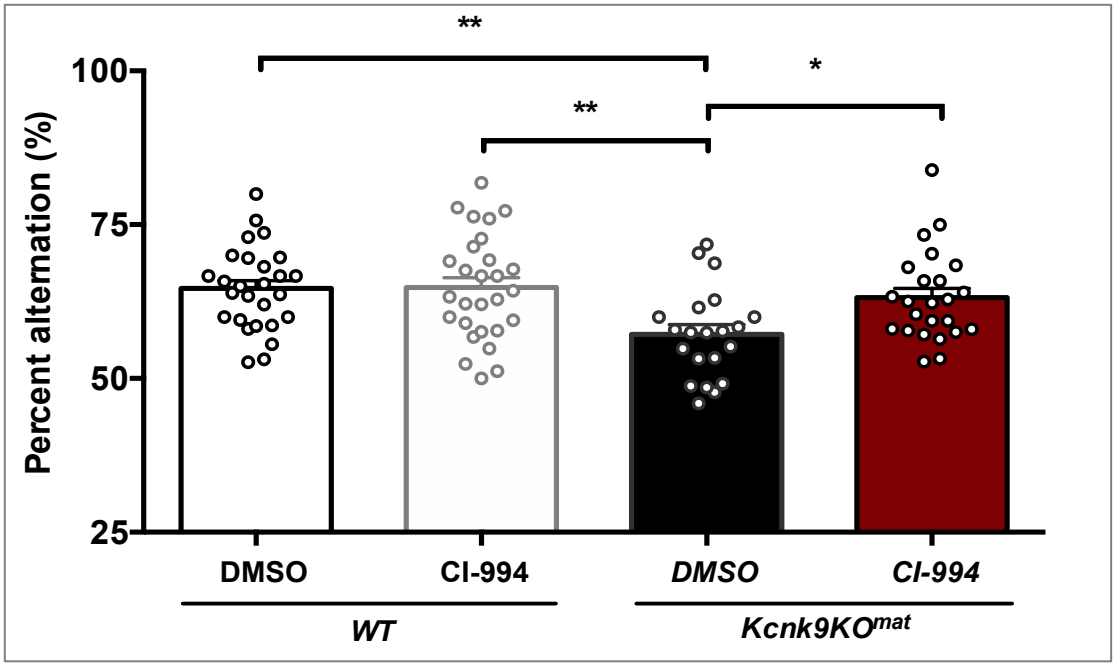

Figure 26: Y-Maze after CI-994 treatment. Y-maze percentage alteration was examined for DMSO-treated WT mice (n=27), CI-994-treated WT mice (n=28), DMSO-treated Kcnk9KO^{mat} mice (n=21) and CI-994 treated *Kcnk9*KO^{mat} mice (n=24). CI-994- or DMSO-treated WT mice and CI-994-treated *Kcnk9*KO^{mat} mice did not exhibit deficits in working memory and showed no significant differences in the Y-maze. CI-994-treated *Kcnk9*KO^{mat} mice showed a significant increase in percent spontaneous alteration and thus a rescue of working memory compared to DMSO-treated *Kcnk9*KO^{mat} mice. 2-way ANOVA, interaction: $F(1, 96) = 3.700$, $P = 0.0574$; treatment: $F(1, 96) = 4.096$, $P = 0.0458$; genotype: $F(1, 96) = 8.992$, $P = 0.0035$; followed by Tukey multiple comparison post hoc test, *P<0.05, **P<0.01. Values are means ± SEM.

Table 24: Y-Maze after CI-994 treatment

Mean ± SEM	Genotype	N	Statistics	Interaction	F value	P value	Post hoc	Adjusted p-values
64.62772 ± 1.290	DMSO: WT	27	**2-way-ANOVA**	Interaction	F (1, 96) = 3.700	P = 0.0574	Tukey multiple comparisons test	***P<0.01 (WT:DMSO vs. Kcnk9KO^{mat}:DMSO)*
64.77955 ±1.614	CI-994: WT	28		Treatment	F (1, 96) = 4.096	P = 0.0458		***P<0.01 (WT:CI994 vs. Kcnk9KO^{mat}:DMSO)*
57.179977 ± 1.584	DMSO*:* *Kcnk*9KO^{mat}	21		Genotype	F (1, 96) = 8.992	P = 0.0035		**P<0.05 (Kcnk9KO^{mat}: CI994 vs. Kcnk*9KO^{mat} :DMSO)
63.15288 ± 1.493	CI-994*:* *Kcnk*9KO^{mat}	24						

3.4.2.3 Acoustic Startle Response after CI-994 treatment

Next, acoustic startle response (ASR) was assessed after drug treatment. CI-994-injected *Kcnk9*KO^{mat} mice showed a significant increase in ASR compared to DMSO-treated *Kcnk9*KO^{mat} controls (Fig. 27, Table 25). A repeated measures 2 way-ANOVA showed no difference between DMSO-treated WT mice and CI-994-treated *Kcnk9*KO^{mat} animals suggesting full rescue of the ASR phenotype in the CI-994-treated *Kcnk9*KO^{mat} mice.

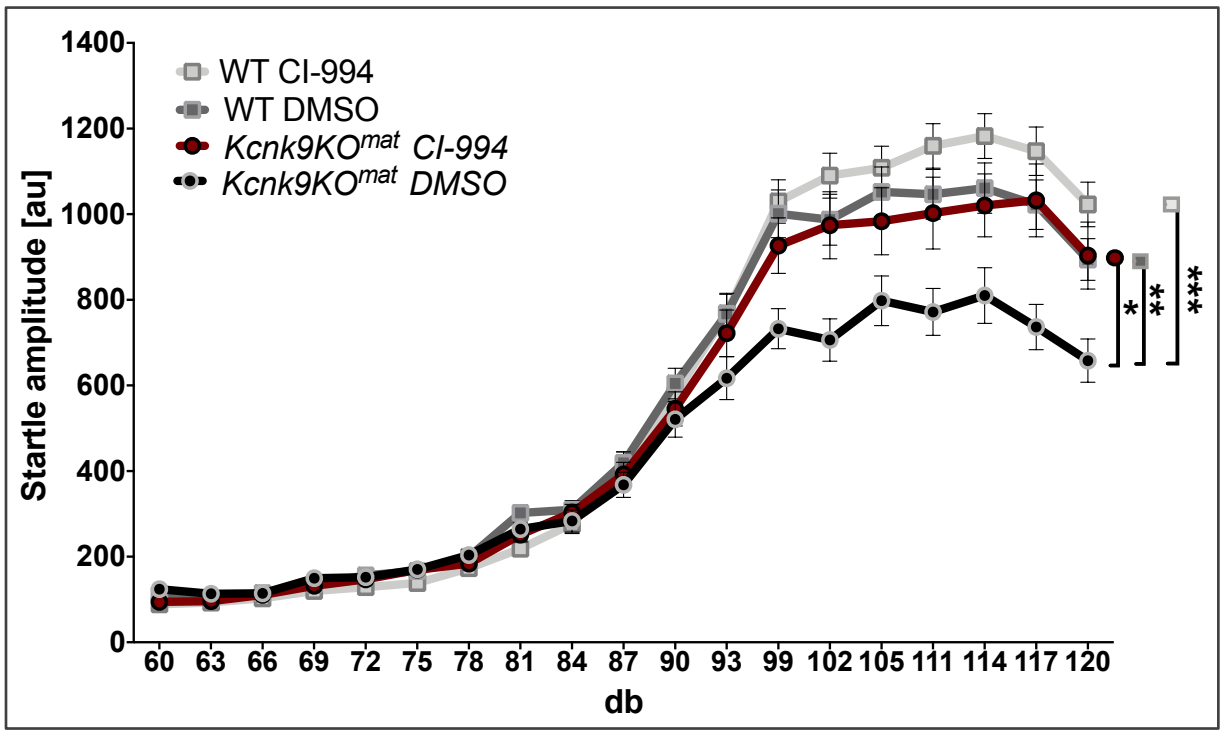

Figure 27: Acoustic startle response (ASR) after CI-994 treatment. ASR of DMSO-treated WT mice (n=31), CI-994-treated WT mice (n=28), DMSO-treated *Kcnk9*KO^{mat} mice (n=27) and CI-994-treated *Kcnk9*KO^{mat} mice (n=27). CI-994-injected *Kcnk9*KO^{mat} mice showed a significant increase in ASR compared to DMSO-treated *Kcnk9*KO^{mat} controls. The repeated measure two-way ANOVA showed a significant effect of genotype for *Kcnk9*KO^{mat}: CI-994 vs. *Kcnk9*KO^{mat}: DMSO = *P = 0.0439; WT:DMSO vs. *Kcnk9*KO^{mat} :DMSO= **P = 0.0025 and WT: CI-994 vs. *Kcnk9*KO^{mat} :DMSO= ***P = 0.0004. Values are means ± SEM.

Table 25: ASR after CI-994 treatment

Mean ± SEM	GT	N	Statistics	I	F value					
					Kcnk9KO^{mat}: CI994 vs. Kcnk9KO^{mat}:DMSO)	*WT:DMSO vs. Kcnk9KO^{mat}*:DMSO	*WT: CI994 vs. Kcnk9KO^{mat}*:DMSO	*WT: CI994 vs. Kcnk9KO^{mat}*:DMSO	*WT: CI994 vs WT*:DMSO	*WT: DMSO vs. Kcnk9KO^{mat}*:CI994
550,11 ± 25,39	DMSO: WT	31		Interaction	F (18, 936) = 6.320	F (18, 1008) = 9.048	F (18, 954) = 22.53	F (18, 954) = 2.285	F (18, 1026) = 2.646	F (18, 1008) = 0.3092
570,61 ± 29,66	CI994: WT	28		dB	F (18, 936) = 197.8	F (18, 1008) = 263.0	F (18, 954) = 349.5	F (18, 954) = 336.0	F (18, 1026) = 443.0	F (18, 1008) = 273.4
436,56 ± 31,27	DMSO*: Kcnk9KO^{mat}*	27	**RM 2- way ANOVA**	Genotype	F (1, 52) = 4.265	F (1, 56) = 10.01	F (1, 53) = 14.23	F (1, 53) = 1.117	F (1, 57) = 0.3409	F (1, 56) = 0.3328
525,87 ± 39,13	CI994*: Kcnk9KO^{mat}*	27		Subjects (matching)	F (52, 936) = 15.99	F (56, 1008) = 14.15	F (53, 954) = 15.77	F (53, 954) = 16.12	F (57, 1026) = 14.27	F (56, 1008) = 14.83
					P value					
					P < 0.0001	P < 0.0001	P < 0.0001	P = 0.0017	P = 0.0002	P = 0.9976
					P < 0.0001	P < 0.0001	P < 0.0001	P < 0.0001	P < 0.0001	P < 0.0001
					*P = 0.0439	**P = 0.0025	***P = 0.0004	P = 0.2954	P = 0.5616	P = 0.5664
					P < 0.0001	P < 0.0001	P < 0.0001	P < 0.0001	P < 0.0001	P < 0.0001

3.4.2.4 Circadian Rhythm after CI-994 Treatment

We then asked whether CI-994 treatment influences nocturnal activity in *Kcnk9*KO^{mat} mice. Indeed, *Kcnk9*KO^{mat} mice showed a significant decrease in horizontal nocturnal activity during the 12-hour dark phase after CI-994 treatment (Fig. 28, Table 26). Again, post hoc analysis of multiple comparisons showed no significant difference between CI-994-treated *Kcnk9*KO^{mat} and DMSO- or CI-994-treated WT animals suggesting full rescue of the nocturnal hyperactivity phenotype in the *Kcnk9*KO^{mat} animals. In contrast, total locomotor activity in the light phase was not altered by CI-994 treatment irrespective of the genotype of the animals (Fig. 28, Table 26).

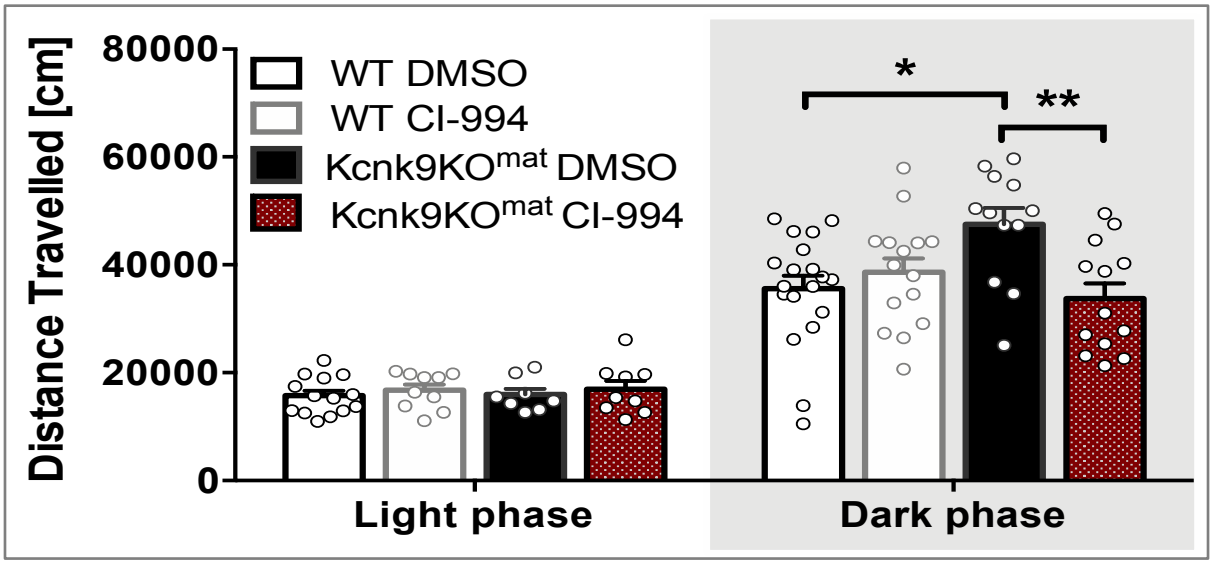

Figure 28: Total locomotor activity. Distance travelled in the home cage in light (12h) phase (left section) and the dark (12h) phase (right section). No differences between DMSO-treated WT (n=14), CI-994-treated WT (n=10), DMSO-treated *Kcnk9*KO^{mat} (n=8) and CI-994-treated *Kcnk9*KO^{mat} (n=9) mice in the distance travelled in the light phase were detected using the 2-way-ANOVA and subsequent multiple comparison tests. DMSO-treated *Kcnk9*KO^{mat} (n=12) mice displayed a significant increase of nocturnal activity compared to DMSO-treated WT mice (n=19) and CI-994-treated *Kcnk9*KO^{mat} mice (n=13) as well as a visible, but not significant increase of nocturnal activity compared to CI-994-treated WT mice (n=15). 2-way ANOVA (interaction: F (1, 55) = 9.582, P = 0.0031; treatment: F (1, 55) = 3.951, P = 0.0518; genotype: F (1, 55) = 1.713, P = 0.1960; followed by the Bonferroni's multiple comparison post hoc test, *P<0.05, **P<0.01.

Table 26: Circadian Rhythm after CI-994 treatment

Phase	Mean ± SEM	Genotype	N	Statistics	I	F value	P value	Post hoc	Adjusted p-values
Light	15731.143 ± 924.78	DMSO: WT	14	2-way-ANOVA	Interaction	F (1, 37) = 4.004e-005	P = 0.9950		
	16753.61 ± 1060.94	CI994: WT	10		Treatment	F (1, 37) = 0.7546	P = 0.3906		
	15950.41 ± 1073.25	DMSO: *Kcnk*9KO^{mat}	8						
	16958.10 ± 1556.50	CI994: *Kcnk*9KO^{mat}	9		Genotype	F (1, 37) = 0.03288	P = 0.8571		
Dark	35598.57± 2367.62	DMSO: WT	19	2-way-ANOVA	Interaction	F (1, 55) = 9.582	P = 0.0031	Bonferroni's multiple comparisons test	**P<0.05 (WT:DMSO vs. Kcnk*9KO^{mat} :DMSO)
	38600.70 ± 2630.08	CI994: WT	15		Treatment	F (1, 55) = 3.951	P = 0.0518		
	47535.23 ± 3015.68	DMSO: *Kcnk*9KO^{mat}	12						***P<0.01 (Kcnk9KO^{mat}: CI994 vs. Kcnk*9KO^{mat} :DMSO)
	33758.46 ± 2785.03	CI994: *Kcnk*9KO^{mat}	13		Genotype	F (1, 55) = 1.713	P = 0.1960		

3.5 CI-994 Interferes with H3K27 Acetylation but not with DNA Methylation at the *Peg13*-DMR

Imprinting of the *Kcnk9/KCNK9* gene has been proposed to be regulated by a maternally methylated germline differentially methylated region (DMR) in the promoter of the *Peg13/PEG13* gene (Ruf et al., 2007). Acetylation of histone 3 lysine 27 (H3K27ac), monomethylation of histone 3 lysine 4 (H3K4me1) as well as DNA methylation at the maternally methylated DMR in the human *PEG13* promoter region have been suggested to control human *KCNK9* expression (Court et al., 2014).

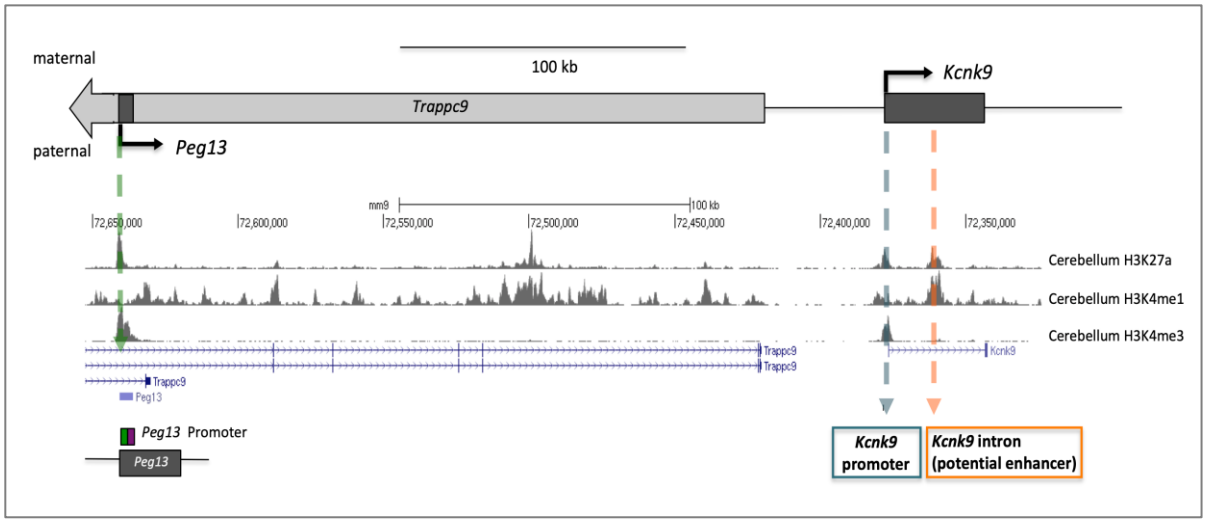

Figure 29: Schematic representation of the *Kcnk9* and *Peg13* loci on distal mouse chromosome 15. The murine *Kcnk9* and *Peg13* genes are shown with the corresponding H3K27ac, H3K4me1, and H3K4me3 enrichment peaks as well as the *Peg13*-DMR (UCSC Genome Browser on Mouse July 2007 (NCBI37/mm9) Assembly). The lower enlarged region of *Peg13* harbours two *Peg13*-DMR regions, *Peg13*-DMR1 (green) and *Peg13*-DMR2 (violet). Individual CpGs analyzed are depicted as lollipops. The orange and blue dotted lines indicate the localization of the two regions (*Kcnk9* promoter and *Kcnk9* intronic region) analyzed by ChIP-RTqPCR.

3.5.1 DNA Methylation Analysis of *Peg13*-DMRs

CI-994 is a second-generation class I histone deacetylase inhibitor inhibiting HDACs I and III with high specificity (Beckers et al., 2007). To clarify the epigenetic mechanism underlying the induction of the paternal *Kcnk9* allele through CI-994 we investigated the methylation status of two subregions of the *Peg13*-DMR (*Peg13*-DMR1 and *Peg13*-DMR2) in adult hippocampus and LC of DMSO- and CI-994-treated *Kcnk9*KO^{mat} mice using bisulphite pyrosequencing (Fig. 29). Methylation levels of about 40-50% typical for imprinted gene DMRs in somatic cells were determined for both DMRs in the two brain regions of *Kcnk9*KO^{mat} mice (Fig. 30, Fig. 31). These methylation levels were not significantly altered by CI-994 treatment of *Kcnk9*KO^{mat} mice (Fig. 31, Table 27). Our results indicate that the up-regulation of *Kcnk9* mRNA in various brain regions of *Kcnk9*KO^{mat} mice after CI-994 treatment is independent of the DNA methylation status at the *Peg13*-DMR.

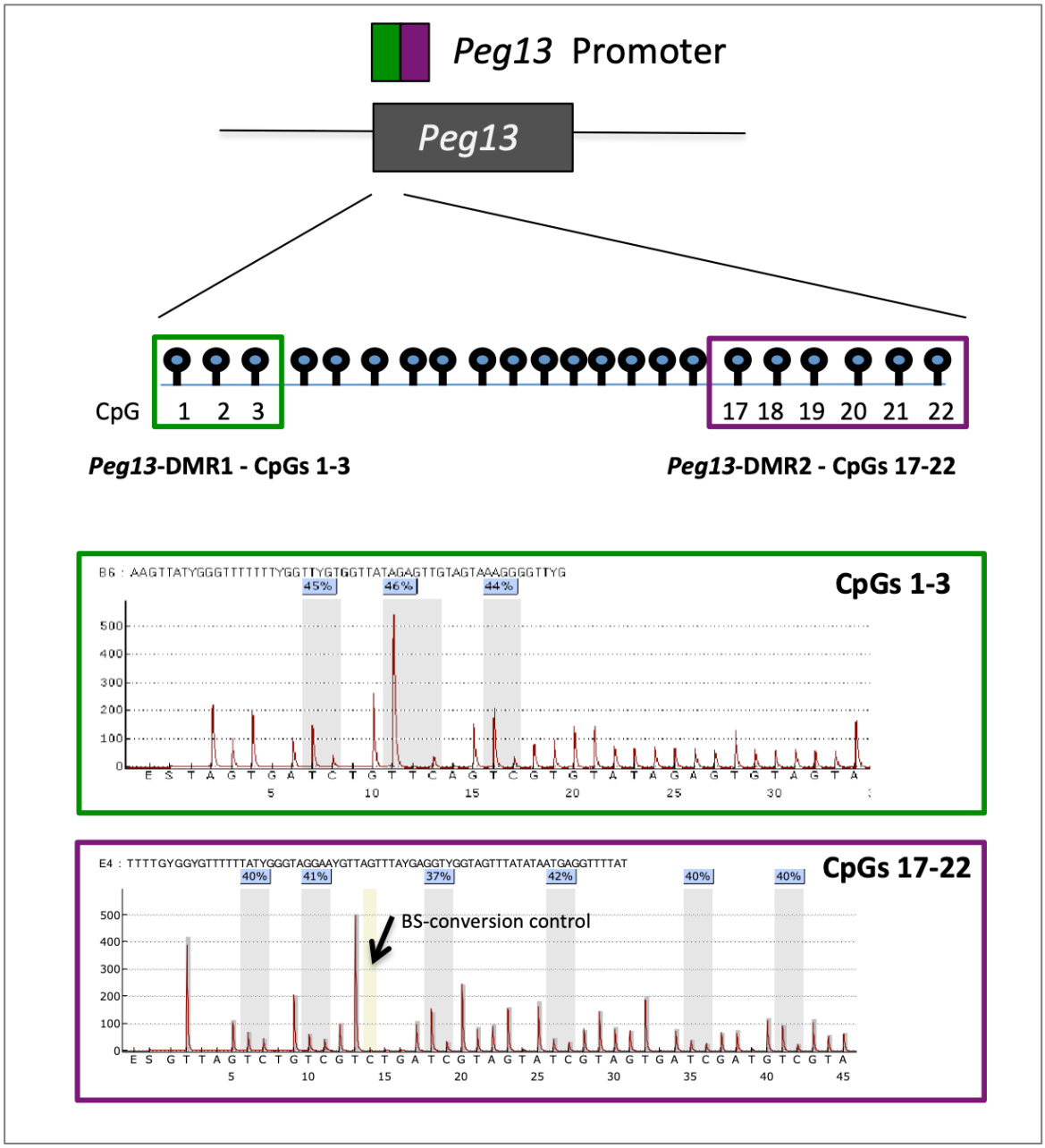

Figure 30: DNA methylation analysis. The *Peg13* differentially methylated region (*Peg13*-DMR) is analyzed in two separate assays. *Peg13*-DMR1 (green) and -DMR2 (violet). Individual CpGs analysed are depicted as lollipops. The pyrogram shows the methylation status of the *Peg13*-DMRs in the hippocampus. The Y-axis shows the intensity of the light emission. The X-axis shows the dispensing order of the added nucleotides. The CpGs are highlighted in gray. In the blue box the percentage of methylation is given. The bisulfite conversion control is highlighted yellow.

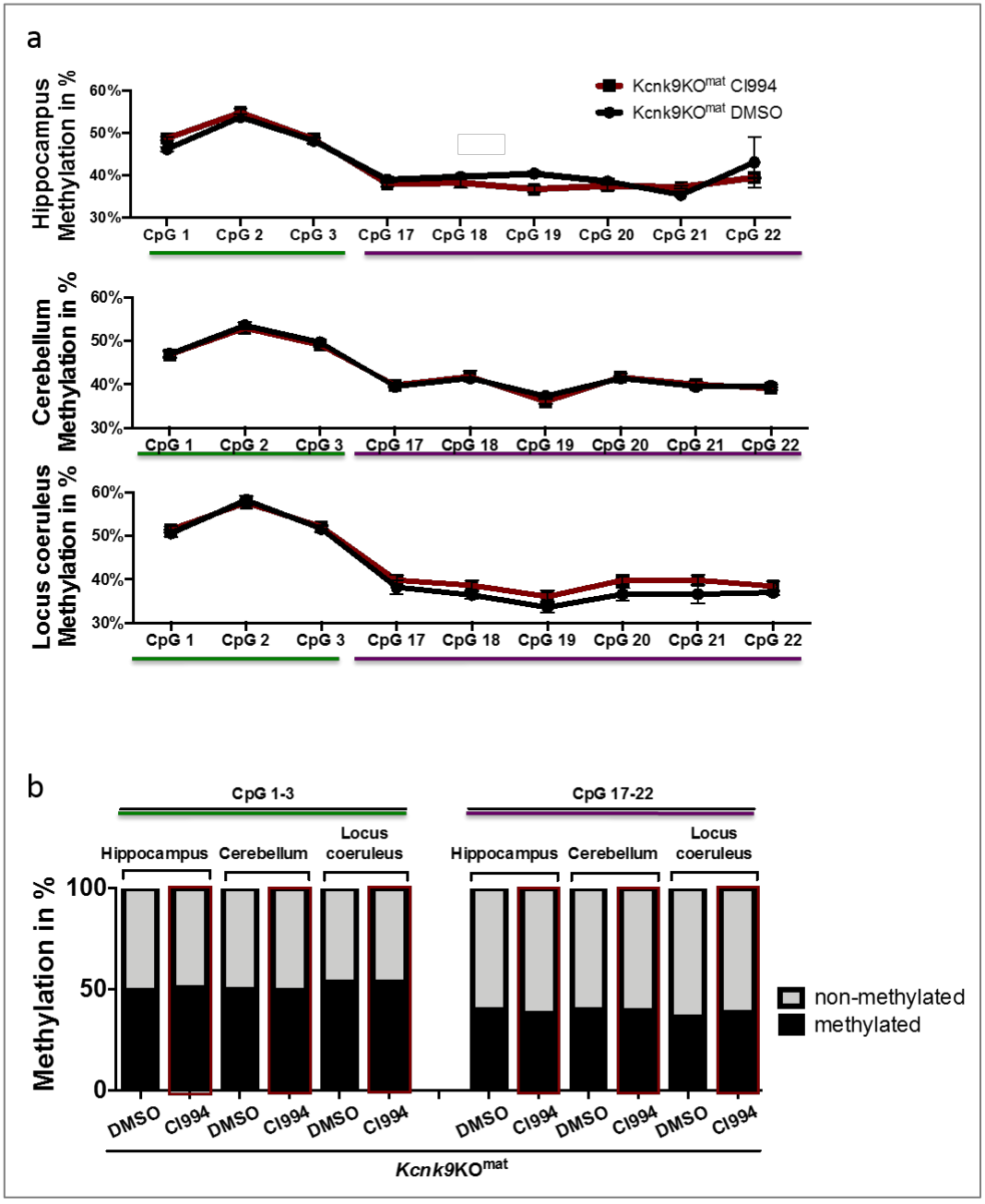

Figure 31: DNA methylation effects of CI-994 treatment in *Kcnk9*KO^{mat} mice. **(a)** Graph depicts methylation status of single CpG-sites in hippocampus, cerebellum and locus coeruleus. CI-994 did not significantly alter the DNA methylation status of *Peg13*-DMR1 (CpGs 1-3) and *Peg13*-DMR2 (CpGs 17-22) in hippocampus, cerebellum or locus coeruleus using the bisulfite pyrosequencing method. **(b)** Mean methylation values for *Peg13*-DMR1 and *Peg13*-DMR2 in comparison. Hippocampus (DMR1: P= 0.1348; DMR2: P= 0.2744), cerebellum (DMR1: P= 0.6190; DMR2: P=0.9366) and locus coeruleus (DMR1: P= 0.7135; DMR2: P=0.1840). Student's t-test).

Table 27: DNA methylation analysis of the *Peg13*-DMR1 and *Peg13*-DMR2

CpG	Mean ± SEM	Region	N	Statistics	P value
CpGs 1-3	49,37 ± 0,65	Hippocampus	DMSO: 3	**RM 2-way-ANOVA treated vs non-treated**	P= 0.1348
	50,71 ± 0,59		CI-994: 3		
CpGs 17-22	39,36 ± 1,34		DMSO: 3		P= 0.2744
	37,87 ± 2,67		CI-994: 3		
CpGs 1-3	50,05 ± 0,71	Cerebellum	DMSO: 4		P= 0.6190
	49,61 ± 0,51		CI-994: 3		
CpGs 17-22	39,77 ± 0,36		DMSO: 4		P= 0.9366
	39,72 ± 0,70		CI-994: 3		
CpGs 1-3	53,47 ± 0,81	LC	DMSO: 5		P= 0.7135
	53,72 ± 0,62		CI-994: 5		
CpGs 17-22	36,40 ± 1,30		DMSO: 5		P= 0.1840
	38,73 ± 1,18		CI-994: 5		

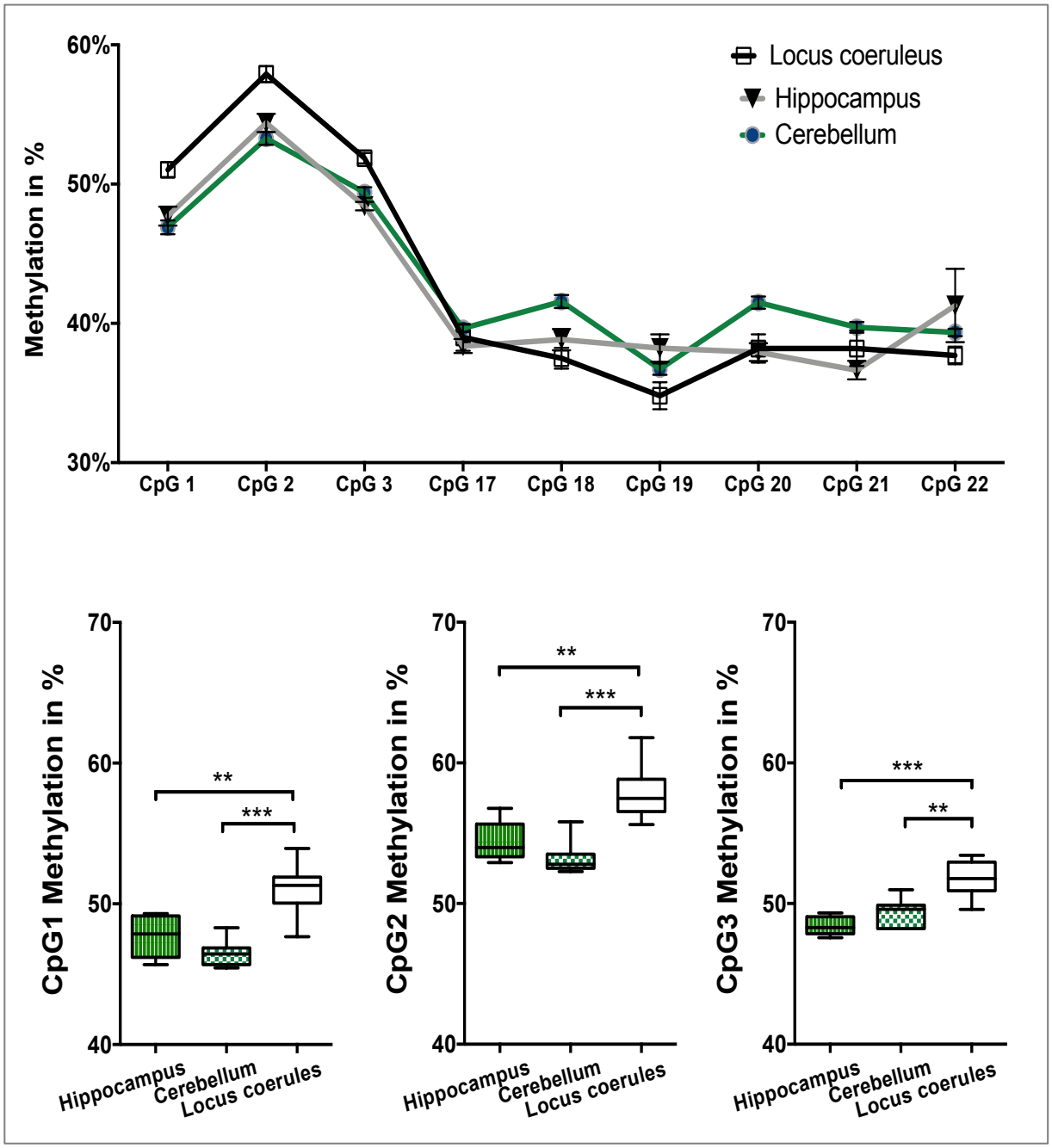

Figure 32: DNA methylation of CpGs at the *Peg13*-DMR1 in the hippocampus, cerebellum and locus coeruleus of CI-994- and DMSO-treated *Kcnk9*KO^{mat} mice taken together. Upper graph shows a summary of all mean methylation values at each CpG. Lower graphs depict methylation box plots for CpG1, CpG2 and CpG3 with significant methylation differences between LC and the other brain regions.

Interestingly, we could observe a significant difference in DNA methylation in the *Peg13*-DMR1 between the analyzed brain regions. The methylation analysis of the locus coeruleus tissue samples revealed a higher methylation status in comparison to cerebellum and hippocampus samples for *Peg13*-DMR1 CpG1-3 (Fig. 32, Table 28).

Table 28: DNA-Methylation *Peg13*-DMR1 CpG1-3 in different brain regions

CpG	Mean ± SEM			Region	N	Statistics	P value
CpGs 1	47,71	±	0,68	Hippocampus	6	Mann-Whitney U	vs LC P= 0.0047
	46,42	±	0,37	Cerebellum	10		vs LC P= 0.0002
	51,03	±	0,53	LC	7		
CpGs 2	54,39	±	0,65	Hippocampus	6		vs LC P= 0.0047
	53,29	±	0,46	Cerebellum	10		vs LC P= 0.0002
	57,90	±	0,58	LC	7		
CpGs 3	48,42	±	0,30	Hippocampus	6		vs LC P= 0.0007
	49,39	±	0,37	Cerebellum	10		vs LC P= 0.0031
	51,86	±	0,38	LC	7		

3.5.2 ChIP-qPCR Analysis of H3K27ac and H3K4me1 in the Promoter and Intronic Region of *Kcnk9*

The human *PEG13*-DMR has been further demonstrated to bind CTCF-cohesin which conveys chromatin looping between a brain-specific enhancer region, marked by H3K27ac and H3K4me1, and the *PEG13* and *KCNK9* promoters to supposedly control brain-specific *KCNK9* expression (Court et al., 2014). Next, we determined the effect of CI-994 on H3K27ac and H3K4me1 marks indicative for an enhancer chromatin signature at the mouse *Kcnk9* locus in the hippocampus and the LC of *Kcnk9*KO^{mat} mice by Chromatin immunoprecipitation (ChIP)-qPCR. Using several

mouse brain ChIP-seq datasets, we did not find an orthologous region in the mouse displaying a brain-specific enhancer chromatin signature similar to that identified at the human imprinted domain on chromosome 8q24. Thus, we focused our analysis on the promoter region and a region in the intron of the *Kcnk9* locus, which are enriched for both marks in the mouse brain ChIP-seq datasets (Fig. 33a). Due to the little amount of material generated from the LC we used an adapted low-input method for both regions (LC and hippocampus) and validated this by conventional ChIP-qPCR in the hippocampus (Fig 33b, Table 29). We observed a deposition of H3K27ac at the two *Kcnk9* regions in the hippocampus and LC of DMSO-treated *Kcnk9*KO^{mat} mice (Fig. 33c, Table 29). Upon CI-994 treatment, deposition of H3K27ac was significantly increased at the promoter region, but not at the intronic region in the hippocampus. By contrast, LC cells showed a significantly increased deposition of H3K27ac in both the intronic and the promoter region of *Kcnk9* after CI-994 treatment. Additionally, we tested the deposition of H3K4me1 in the LC to assess if histone acetylation inhibition leads to additional changes in other histone marks. Treatment with CI-994 led to only a slight, but not significant increase of H3K4me1 deposition at the *Kcnk9* promoter region (Fig. 33d, Table 29). Our findings indicate that CI-994 treatment affects consistently histone acetylation at the promoter of *Kcnk9*, but has diverging effects on histone acetylation at the *Kcnk9* intron region in different brain regions.

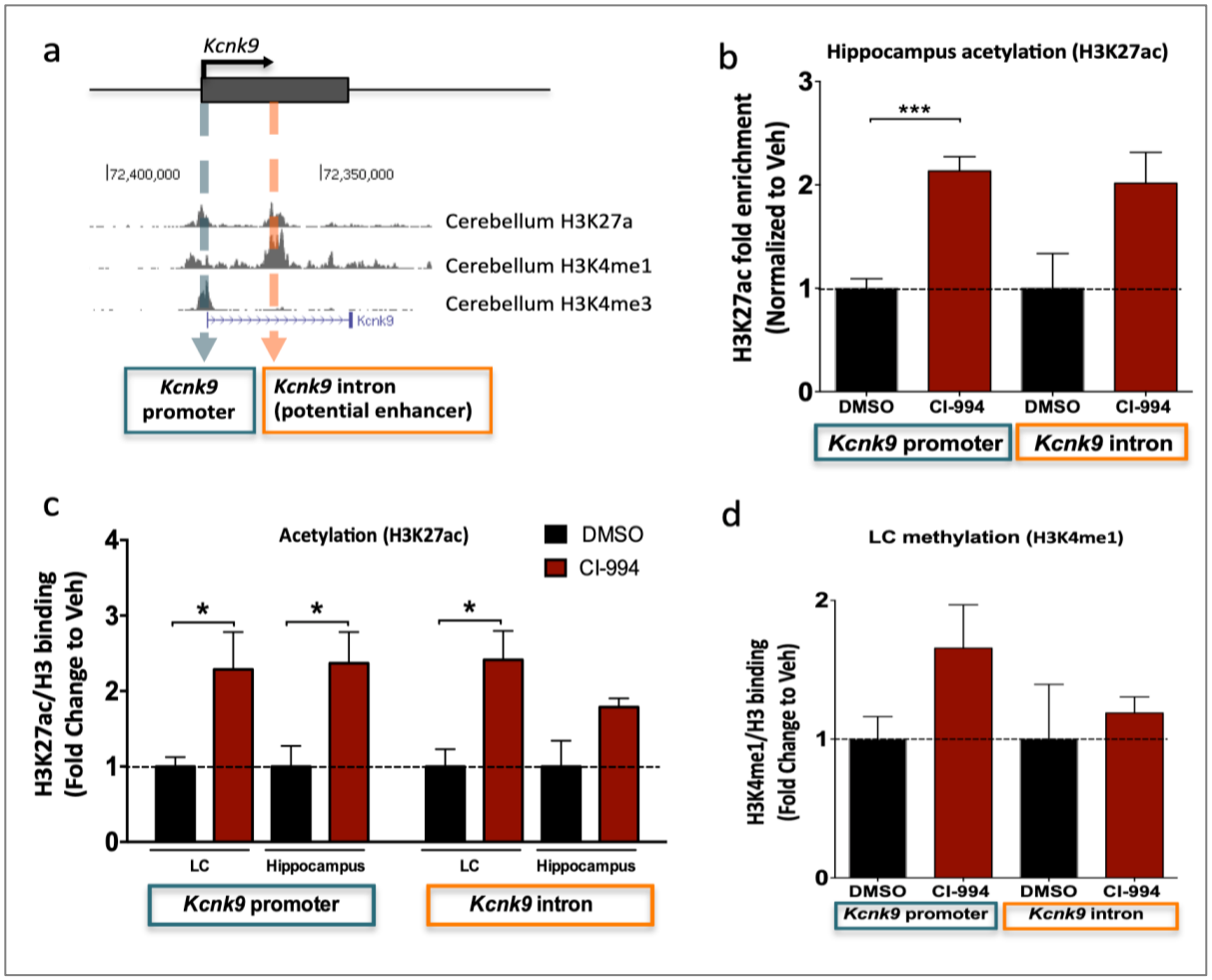

Figure 33: Effects of CI-994 treatment on H3K27ac and H3K4me1 in brain regions of *Kcnk9*KO^{mat} mice. (a) Schematic presentation of the *Kcnk9* and *Peg13* loci on distal mouse chromosome 15. The orange and blue dotted lines/boxes indicate the localization of the two regions (*Kcnk9* promoter and *Kcnk9* intronic region) analyzed by ChIP-RTqPCR**. (b)** Increased deposition of H3K27ac marks at the promoter and intronic region of *Kcnk9* in hippocampus following treatment with CI-994 (normalized to veh) using conventional ChIP method. **(c)** Increased deposition of H3K27ac marks at the promoter and intronic region of *Kcnk9* in hippocampus and LC following treatment with CI-994 (normalized to veh) using the low-input ChIP method. DMSO vs. CI-994: LC *Kcnk9* promoter P = 0.0450; *Kcnk9* intron P =0.0202. DMSO vs. CI-994: hippocampus *Kcnk9* promoter P = 0.0342; *Kcnk9* intron P = 0.1172 (n=3-4 animals/group) **(d)** CI-994 treatment did not significantly alter the H3K4me1 disposition at the promoter and intronic region of *Kcnk9* in locus coeruleus (LC) after treatment with CI-994 (normalized to veh). (n=3-4 animals/group). (b-d) Values are means ± SEM, *p≤ 0.05, ***p≤ 0.001 by Student's t test.

Table 29: ChIP results after CI-994 treatment

ChIP	Region		Mean ± SEM	N	Statistics	P value
Low-input ChIP H3K4me1	LC	***Kcnk9* prom**	1.000 ± 0.1624	DMSO: 4	**Student's t-test**	P = 0.1118
		***Kcnk9* prom**	1.656 ± 0.3125	CI-994: 4		
		***Kcnk9* intron**	1.000 ± 0.3949	DMSO: 4		P = 0.7092
		***Kcnk9* intron**	1.188 ±0.1161	CI-994: 3		
Conventional ChIP H3K27ac	Hippocampus	***Kcnk9* prom**	1.000 ± 0.09173	DMSO: 4		P = 0.0002
		***Kcnk9* prom**	2.135 ± 0.1373	CI-994: 4		
		***Kcnk9* intron**	1.000 ± 0.3358	DMSO: 4		P = 0.0648
		***Kcnk9* intron**	2.016 ± 0.2975	CI-994: 4		
Low-input ChIP H3K27ac	Hippocampus	***Kcnk9* prom**	1.000 ± 0.2726	DMSO: 4		P = 0.0342
		***Kcnk9* prom**	2.369 ± 0.4146	CI-994: 3		
		***Kcnk9* intron**	1.000 ± 0.3419	DMSO: 4		P = 0.1172
		***Kcnk9* intron**	1.787 ± 0.1179	CI-994: 3		
	LC	***Kcnk9* prom**	1.000 ± 0.1245	DMSO: 4		P = 0.0450
		***Kcnk9* prom**	2.288 ± 0.4945	CI-994: 4		
		***Kcnk9* intron**	1.000 ± 0.2305	DMSO: 4		P =0.0202
		***Kcnk9* intron**	2.414 ± 0.3838	CI-994: 3		

Taken together, these findings demonstrate that the paternal allele of *Kcnk9* is not fully silenced in the brain, further derepressed in the case of loss of the maternal allele and substantially activated upon exogenous epigenetic modulation. The data presented provide evidence for a promising therapeutic effect of the class I HDAC inhibitor CI-994, in a mouse model for BBIDS with maternal loss of *Kcnk9.*

4. Discussion

Kcnk9/KCNK9 is a maternally expressed and paternally silenced imprinted gene in the brain of man and mouse, whose heterozygous mutations are causative for the maternally inherited Birk-Barel intellectual disability syndrome (BBIDS or *KCNK9* imprinting syndrome), which is typically associated with developmental delay, congenital central hypotonia and intellectual disability (Barel et al., 2008; Ruf et al., 2007). The gene encodes a two-pore domain potassium (K2P)-channel, which controls resting membrane potential and excitability of neurons.

Using a BBIDS mouse model (*Kcnk9*KO^{mat}), a partial rescue of BBIDS-like behavioral phenotypes mediated via residual expression from the paternal *Kcnk9* allele was identified. This study demonstrates that the second-generation HDAC inhibitor CI-994 increases the expression from the paternally silenced *Kcnk9* allele and leads to a full rescue of the behavioral phenotype, proposing CI-994 as a promising molecule for BBIDS therapy.

4.1 Molecular and Behavioral Characterization of *Kcnk9* Knockout Mice

The first objective of this doctoral thesis was to characterize *Kcnk9* knockout mice genetically and phenotypically, and accentuate possible differences between heterozygous *Kcnk9*KO mice with inactivation of the maternal *Kcnk9* allele (*Kcnk9*KO^{mat}) and homozygous *Kcnk9*KO mice (*Kcnk9*KO^{hom}) in comparison to WT littermates. In order to investigate the neuropathology of BBIDS, a BBIDS mouse model compromising only the maternal *Kcnk9* allele (*Kcnk9*KO^{mat} mice) was utilized, mimicking the genetic condition of patients suffering from BBIDS.

4.1.1 Non-canonical Imprinting of *Kcnk9* in the Mouse Brain

The Birk-Barel intellectual disability dysmorphism syndrome is associated with heterozygous mutations on the maternal allele of the paternally imprinted *KCNK9*

gene in the brain (Ruf et al., 2007; Barel et al., 2008). Generally, numerous inherited DNA mutations for neuropsychiatric disorders are heterozygous in affected patients (Huguet et al., 2013). Therefore, is its essential to understand the effects of heterozygous, in particular allele-specific, gene expression in different cell and tissue types and to which extent it may impact progeny. Genomic imprinting is a process that is regulated epigenetically and effects approximately 250 genes in the mammalian genome, expressed monoallelically from one parental chromosome (Barlow and Bartolomei, 2014). Canonical imprinting describes the gene copy originating from one paternal allele to be fully silenced and the other allele to be entirely active. Conversely, previous studies observed non-canonical imprinting, the preferential expression towards the maternal or paternal allele, instead of complete silencing of one parental allele of an imprinted gene. Thorough investigations of imprinted genes implicate a more tissue- or development-dependent parental allelic bias rather than exclusive monoallelic expression (Martinez et al., 2014; Perez et al., 2016; Perez et al., 2015). One of the initial non-canonically imprinted genes described is the *UBE3A* gene, which is associated with the Angelman syndrome (see chapter 1.2.4 for more details) in humans (Sahoo et al., 2008). The murine *Ube3a* gene displays preferential or exclusive maternal-specific expression from the maternal allele in most brain regions, but biallelic expression in other brain areas(Albrecht et al., 1997). Moreover, parent-specific expression can differ even in individual cells within a tissue, resulting in monoallelic expression comprising a certain cell type, whereas other cell types exhibit biallelic gene activation (Gregg et al., 2010). It is estimated that the amount of genes expressed monoallelically is equal to the number of genes with parentally biased expression in the genome (Gregg, 2014; Khatib et al., 2007; Perez et al., 2016). Recent studies identified specific non-canonical imprinting mechanisms, which are distinguishable to those of canonical imprinting, influencing the highly tissue-specific expression of hundreds of imprinted genes (Bonthuis et al., 2015; Gregg, 2014). In essence, imprinting in the brain has gained more importance throughout the last years, with several studies proving that the majority of canonically and non-canonically imprinted genes are expressed in the

brain (Gregg et al., 2010; Perez et al., 2015).

In this study, various techniques were applied to investigate the overall and allele-specific expression of *Kcnk9* in different brain regions of WT and *Kcnk9*KO^{mat} mice. Accordingly, reciprocal crossbreeding between hybrid mouse strains and single nucleotide polymorphisms (SNPs), to differentiate between the two strains, were utilized to investigate the imprinting patterns of *Kcnk9* in the mouse brain. Quantification RT-qPCR expression analysis revealed a wide distribution of *Kcnk9* m-RNA throughout the brain, which is coherent with previous studies (Karschin et al., 2001; Marinc et al., 2014; Talley et al., 2001)(see table 30 for details).

Similar to a recent study, systematic pyrosequencing in mice revealed a parental expression bias towards maternal transcripts of *Kcnk9* in several brain regions analyzed. Allele-specific expression analysis of *Kcnk9* mRNA in (C57BL/6JxCast/Ei)F1 male mouse hybrids demonstrated residual *Kcnk9* expression from the paternal allele in some brain regions with a significant peak of 14 % in the locus coeruleus (LC) in *Kcnk9*KO^{mat} mice. In comparison, the study of Perez et al, (2015) observed an overall higher paternal expression in the all analyzed brain regions, which are detailed in table 31. However, this study used reciprocal crossbreeding of C57Bl/6J and Cast/EiJ mouse strains, with both, F1i (hybrid derived from a Cast/EiJ mother and C57Bl/6J father) and F1r (hybrid derived from a C57Bl/6J mother and Cast/EiJ father) female hybrids (Perez et al., 2015). Differences in biased parental expression levels of *Kcnk9* in both studies are most probably due to the diversity of sample origin (sex and F1-crossbreeding), which has also been described in a recent study (Bonthuis et al., 2015). Thus, it should be taken into consideration, that the mice used in this study for behavioral experiments have a C57BL/6 genetic background. In the light of these data, it is possible that mice with a C57BL/6 background compared to the F1^{male}, F1i^{female} and F1r^{female} hybrids described, exhibit a divergent paternal expression pattern of *Kcnk9*, which correlates more precisely to the behavioral phenotype of mice used in the presented behavioral experiments.

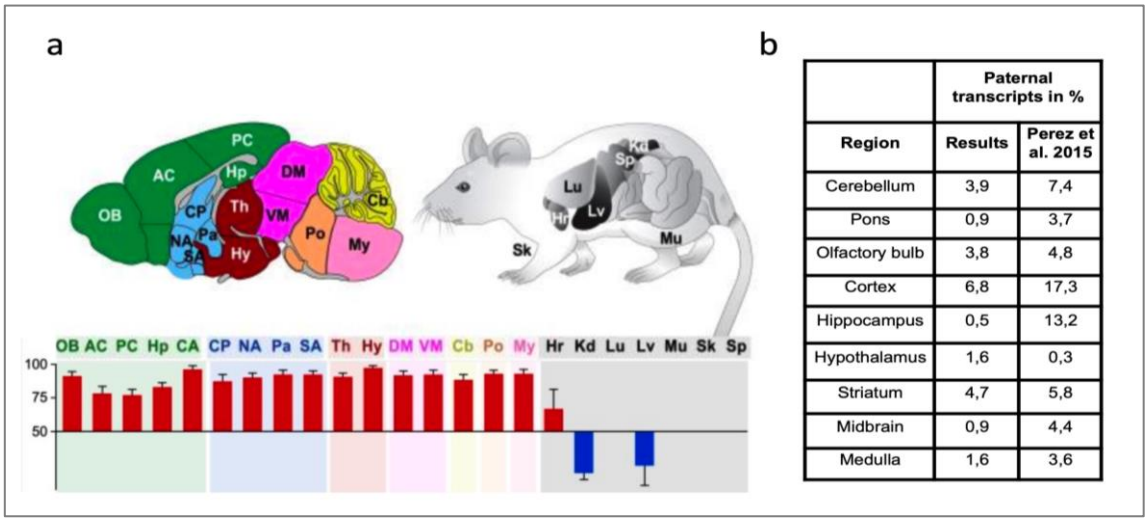

Region	Paternal transcripts in %	
	Results	Perez et al. 2015
Cerebellum	3,9	7,4
Pons	0,9	3,7
Olfactory bulb	3,8	4,8
Cortex	6,8	17,3
Hippocampus	0,5	13,2
Hypothalamus	1,6	0,3
Striatum	4,7	5,8
Midbrain	0,9	4,4
Medulla	1,6	3,6

Figure 34: Spatial regulation of *Kcnk9* expression. (a) Analyzed brain regions and body tissues. OB: Olfactory Bulb, AC: Anterior Cortex, PC: Posterior Cortex, Hp: Hippocampus, CA: Cortical Amygdala, CP: Caudate Putamen, NA: Nucleus Accumbens, Pa: Pallidum, SA: Striatum-like Amygdala, Th: Thalamus, Hy: Hypothalamus, DM: Dorsal Midbrain, VM: Ventral Midbrain, Cb: Cerebellum, Po: Pons, My: Medulla, Lg: Lung, Hr: Hearth, Sp: Spleen, Lv: Liver, Kd: Kidney, Sk: Skin, Mu: Muscle. Lower Panel demonstrates parental expression bias of *Kcnk9*. Red bars represent maternal biased expression, while blue bars represent expression biased towards paternal allele. **(b)** Comparison of paternal expression values of *Kcnk9* in adult mice obtained in this study and the study of Perez et al. (2015) (adapted from Perez et al., 2015).

Intriguingly, allele-specific expression analyses of *Kcnk9* revealed a high specificity for paternal activation in particular nuclei of certain brain regions. For instance, less than 1% paternal transcripts of *Kcnk9* were observed in the pons. However the LC, a nucleus within the pons, exhibited a total paternal expression of approximately 14%, which implies a specific function of KCNK9 within certain sub-regions of the brain. In the light of these data, is worthwhile to investigate additional nuclei to further elucidate the expression pattern and function of *Kcnk9* in the brain.

Nevertheless, it must also be mentioned that on the contrary, the paternal allele of *Kcnk9* is predominantly expressed in several analyzed peripheral body tissues, such as liver and kidneys (Fig. 34). Thus, the *Kcnk9* gene is not exclusively predominantly expressed by the maternal allele in all tissue types of the mouse (Perez et al., 2015).

Table 30: Localization of KCNK9 Protein in the Rat Brain (adapted from Marinc et al., 2014)

Brain region	Signal intensity: KCNK9	Brain region	Signal intensity: KCNK9
Bulbus olfactorius	+++	Laterodorsal thalamic ncl.	+/++
Neocortex	+/++/+++	**Midbrain, brainstem**	
Hippocampus		Superior colliculus	++
CA1	++	Substantia nigra, reticulata	+
CA2	++	Substantia nigra, compacta	-/+
CA3	++	VTA	+, few +++
Dentate gyrus	+++	Edinger-Westphal nucleus	+++
Basal forebrain		Caudal linear raphe	++
Caudate putamen	+, few +++	Red nucleus	++
Accumbens nucleus	++	Interpeduncular nucleus	+++
Globus pallidus	+	Interstitial nucleus	++
Basal nucleus of Meynert	+++	Oculomotor nucleus	++++
Ventral pallidum	+, few +++	Central gray, dorsal	++/+++
Island of Calleja	-/+	Trochlear nucleus	+++
Septohippocampal nucleus	++	Dorsal raphe	++++
Tenia tecta	+++	Median raphe	+++
Indusium griseum	++	Pontine reticular nucleus	++
		Pedunculopontine tegment. ncl.	++
Lateral septal nucleus	++	Ventral tegmental nucleus	++
Medial septal nucleus	+++	Dorsal tegmental nucleus	+
Diagonal band	+, few +++	Motor trigeminal nucleus	++++
Bed nucleus stria terminalis	++	Locus coeruleus	++++
Central amygdaloid ncl.	++	Central grey, pons	++
Basolateral amygdaloid ncl.	++	Raphe pontis	+++
Hypothalamus		Raphe magnus	++/+++
Preoptic nucleus	+++	Trapezoid body	++/+++
Supraoptic nucleus	+++	Mesencephalic trigeminal ncl.	-/+
Anterior hypoth. Area	+	Superior olivary nuclei	++/+++
Lateral hypoth. Area	++	Abducens nucleus	+++
Ventromedial hypoth. ncl.	++	Accessory facial nucleus	++++
Arcuate hypoth. Nucleus	+, few +++	Facial nucleus	++++
Periventricular hypoth. ncl.	++/+++	Vestibular nucleus	++
Dorsomedial hypoth. ncl.	++	Cerebellum	
Ventral tuberomammillary ncl.	++/+++	Molecular layer	++
Dorsal tuberomammillary ncl.	++	Purkinje cells	-/+
Lateral mammillary ncl.	++/+++	Granule cell layer	++
Medial mammillary ncl.	++	**Medulla/ and spinal cord**	
Medial habenula	+/++	Raphe pallidus	++
Lateral habenula	+/++	Spinal trigeminal nucleus	++
		Nucleus solitary tract	++
Thalamus			
Central thalamic ncl.	++	Ventral cochlear nucleus	++
Intermedial thalamic ncl.	++/+++	Ambiguus nucleus	++++
Anteroventral thalamic ncl.	++/+++	Inferior olivary nuclei	++/+++
Anterodorsal thalamic ncl.	+++	Hypoglossal nucleus	++++
Reticular thalamic ncl.	++/+++	Dorsal vagal motoneurons	++
Anteromedial thalamic ncl.	++	Cuneate nucleus	++
Paraventricular thalamic ncl.	++	Gracile nucleus	++
Entopeduncular ncl.	++	Raphe obscurus	++
Lateral geniculate ncl.	++	Nucleus solitary tract	++
Medial geniculate ncl.	++	Spinal motoneurons	++++

Interestingly, additional experiments show expression arising from the paternal allele is further increased in several brain regions in *Kcnk9*KO^{mat} mice compared to WT mice, suggesting a compensatory regulatory mechanism induced by the deletion of the maternal allele of *Kcnk9.* Genes regulated in this manner have been described in other studies. A comparable compensatory system was described in a mouse model of Prader-Willi syndrome, in which the deletion of the paternally expressed allele of the imprinted *Ndn* gene resulted in a loss of imprinting (silencing) of the maternal *Ndn* allele, introducing a partial rescue of the pathological phenotype, namely reduced birth lethality and breathing deficiency (Rieusset et al., 2013). However, it remains unclear which compensatory effect is to be expected in BBIDS patients.

4.1.2 Deletion of *Kcnk9* leads to Impaired Behavior

To date, two *Kcnk9* knockout mice models have been generated by homologous recombination, deleting either exon 1 or exon 2 of *Kcnk9* and hence disrupting the channel function (Brickley et al., 2007; Mulkey et al., 2007). Due to the high mRNA expression of *Kcnk9* and ubiquitous distribution of KCNK9 proteins in the brain (table 30), investigations of the phenotype of heterozygous *Kcnk9* knockout mice with maternal inherited knockout allele (*Kcnk9*KO^{mat}) and homozygous *Kcnk9* knockout mice (*Kcnk9*KO^{hom}) would assumedly lead to behavioral deficits in mice (Marinc et al., 2014; Talley et al., 2001). So far, only *Kcnk9*KO^{hom} mice with inactivation of both parental alleles, but not *Kcnk*9KO^{mat} mice with heterozygous deletion of the active maternal *Kcnk9* allele, thereby mimicking BBIDS, were phenotypically characterized (see chapter 1.3.3). It is conceivable, that a deletion of the maternally active *Kcnk9* allele in the *Kcnk9*KO^{mat} mouse would result in a phenotype comparable to *Kcnk9*KO^{hom} mice, taken into consideration that *Kcnk9* is predominantly maternally active. Indeed, whilst investigating *Kcnk9*KO^{mat} and *Kcnk9*KO^{hom} mice in a behavioral battery, both genotypes displayed behavioral deficits in working memory and sensorimotor gating to a similar extent in comparison to their wildtype littermates (WT). Unexpectedly, however, *Kcnk9*KO^{mat} mice exhibited an intermediate phenotype in tests regarding acoustic startle response and nocturnal locomotor activity, which

implies the involvement of the “silent” paternal allele in the behavioral phenotype.

4.1.2.1 Deficits in Motor Coordination

In comparison to other studies, describing modest motor deficits in the narrow horizontal beam test in male but not female *Kcnk9*KO^{hom} mice (Aller et al., 2005; Linden et al., 2007), the data provided by this study revealed no significant deficits in motor coordination performed in the rotarod test. *Kcnk9* is highly expressed in cerebellar granule neurons and partially in Purkinje cells of the cerebellum (Marinc et al., 2014; Talley et al., 2001), a region greatly associated with motor coordination and motor learning (Manto et al., 2012). However, although cerebellar granule cells without KCNK9 are not able to generate action potentials at high firing frequencies, a motor phenotype could not be observed in *Kcnk9*KO^{hom} and *Kcnk9*KO^{mat} in the rotarod test (Brickley et al., 2007; Linden et al., 2007). Interestingly, deletion of alpha 6 and delta subunits of extrasynaptic GABAA receptors in the cerebellar granule cells resulted in increased gene expression of *Kcnk3* and *Kcnk9* (Aller et al., 2005; Brickley et al., 2007). This type of counterbalancing process is common among ion-channels and in the case of *Kcnk9*KO^{hom} and *Kcnk9*KO^{mat} mice a similar compensatory mechanism is most probably operative in the cerebellum, leading to a full rescue of the behavioral motor phenotype.

4.1.2.2 Impairment of Working Memory

The Y-maze results demonstrate a clearly impaired working memory of the *Kcnk9*KO^{mat} and *Kcnk9*KO^{hom} mice is in comparison to WT mice, which are in line with results of the T-maze experiments with *Kcnk9*KO^{hom} mice performed in previous studies (Gotter et al., 2011; Linden et al., 2007). Spontaneous alternation, a parameter of spatial working memory assessed by the visuospatial Y-maze test, is driven by a native curiosity of rodents to investigate a novel environment. A mouse with intact working memory, and hence functional interaction between brain regions associated with this specific neural circuit, including prefrontal cortex, hippocampus

and locus coeruleus (LC), will recall the arms previously entered (Sara, 2015; Sarnyai et al., 2000; Swonger and Rech, 1972). In particular, the LC noradrenergic system has been proven to have an essential role in memory consolidation, long-term plasticity and cognitive flexibility (Khakpour-Taleghani et al., 2009; Sara, 2015). Noradrenergic efferent projections of the LC innervate virtually all brain regions (except the basal ganglia) throughout the sensory and pre-frontal cortex and subcortical brain regions, such as the hippocampus, hypothalamus, brainstem and cerebellum (Holstege, 1987; Kwiat and Basbaum, 1992; Schuerger and Balaban, 1993). Moreover, further studies proposed an essential role of LC-mediated dopamine release in hippocampus, which is associated with the formation of the episodic memory and is therefore implicated in higher cognitive functions (Takeuchi et al., 2016). LC projections into the hippocampus and the prefrontal cortex are strongly associated with the regulation of attention and arousal (Borodovitsyna et al., 2017). Immunocytochemistry with anti-KCNK9 antibodies in rat brain slices revealed a particular strong signal for KCNK9 in the hippocampus (dentate gyrus granule cells and hippocampal CA1 and CA3 pyramidal neurons), prefrontal cortex and locus coeruleus (see table 30) (Marinc et al., 2014), indicating an important role of these brain regions in neural processes involved in working memory. Consequently, it is expected that a lack of KCNK9 in hippocampus, prefrontal cortex and LC would lead to cognitive dysfunctions in mice. The presented results show that *Kcnk9*KO^{mat} and *Kcnk9*KO^{hom} mice exhibit similar deficits in working memory, which are consistent with the deficits in cognitive functions described in BBIDS patients.

4.1.2.3 Altered Acoustic Startle Response and Pre-Pulse Inhibition

The mammalian startle reflex is a rapid contraction of the skeletal and facial musculature evoked by a sudden intense tactile, visual or acoustic stimulus (Davis, 1980; Koch, 1999). The acoustic startle response (ASR) is a short-latency reaction induced by unexpected acoustic stimulus. ASR is affectivity-dependent and conduces as an indicator for several disorders and neuropsychiatric diseases such as anxiety, anhedonia, depression, schizophrenia and attention deficit hyperactivity disorder

(ADHD) (Borodovitsyna et al., 2017; Kaviani et al., 2004). The short latency of the ASR is mediated by a simple neuronal circuit involving, cochlear root neurons, giant neurons in the caudal pontine reticular formation (PnC) and motoneurons in the spinal cord (Davis, 1980; Koch, 1999; Lee et al., 1996). ASR can be modified within the simple pathway or modulated extrinsically, by innervation of higher order brain regions. In rodents, the startle amplitude is influenced by various factors, including habituation, shock stress, fear conditioning, pleasure attenuation, sensitization, pre-pulse inhibition and a variety of different active substances (Davis, 1980; Krase et al., 1994). *Kcnk9* is strongly expressed in 75% of PnC giant neurons and stabilizes their resting membrane potential. Furthermore, electrophysiological properties of PnC giant neurons, including high membrane time constant, wide action potentials and large cell surface, ensure a high cumulative integration of sensory inputs and modulatory signals from other brain regions (Koch, 1999; Wagner and Mack, 1998). A further study showed that inhibition of KCNK9 with acidification and ruthenium red increases the excitability in PnC giant neurons and modulates outgoing projections (Talley et al., 2003; Weber et al., 2008). Weber et al. (2008) proposed, that KCNK9 inhibition in rat PnC giant neurons is sufficient to reduce neuronal conductance, which forces the neurons to depolarize and respond quicker to excitatory input. Furthermore, serotonergic neurons from the nucleus raphe pallidus and magnus innervate the PnC giant neurons via serotonin 5-HT_{2C} receptors and generally inactivate KCNK9 channels, which is assumed to evoke startle response *in vivo* (Hornung, 2003; Weber et al., 2008). In addition, further studies demonstrated elevated acoustic startle response upon serotonergic transmission in neurons (Davis, 1986; Kehne et al., 1991). The ASR experiments performed in this study revealed for the first time a significantly reduced startle response amplitude across all pulse-intensities (dBs) in *Kcnk9*KO^{hom}, and to a smaller extent in *Kcnk9*KO^{mat} animals, each compared to WT littermates. The data presented in this work is not concordant with the proposed model by Weber et al (2008). However, exceptionally strong immunoreactivity of KCNK9 channels and very high levels of *Kcnk9* mRNA seen in neurons of the nucleus raphe magnus must be taken into consideration (Berg et al., 2004; Karschin et al., 2001; Marinc et al., 2011). The observed reduction of ASR in

Kcnk9 knockout animals could be the result of decreased serotonergic neurotransmission coming from raphe magnus to the PnC, due to lower amount of KCNK9 channels in raphe magnus neurons. Therefore, KCNK9 channels in the PnC giant neurons are less inhibited through 5-HT_{2C} receptors, resulting in decreased neuronal excitability and subsequently, reduced acoustic startle response. This hypothesis is supported by a recent study showing that inhibition of 5-HT_{2C} receptors reduces the startle response in mice (Kuznetsova et al., 2006).

Furthermore, these findings suggest that the intermediate phenotype in *Kcnk9*KO^{mat} animals is due to paternal expression of *Kcnk9* detected in brain regions associated with ASR, such as specific sub-regions in the pons (Fig. 17). Indeed, *Kcnk9* mRNA expression is high in the locus coeruleus (LC), which was also previously described to modulate the ASR. Thus, stimulation of the LC through pain leads to an increase of the signal coming from the caudal pontine reticular nucleus innervating motoneurons in the ASR circuit (Szabadi, 2012). Loss of LC neurons on the other hand in the parkin null mouse has been shown to result in a significant reduction of ASR (Von Coelln et al., 2004). In this present study, not only high *Kcnk9* expression levels in the LC but also elevated expression from the paternal *Kcnk9* allele were observed. In conclusion, increased paternal *Kcnk9* expression in maternal KO animals is correlated with an intermediate ASR phenotype, which further strengthens the role of the KCNK9 channel in the ASR axis *in vivo*.

As mentioned above, pre-pulse inhibition (PPI) is an extrinsic modifier of the ASR and plays an essential role in sensory gating mechanisms. This study also demonstrated for the first time that *Kcnk9*KO^{mat} and *Kcnk9*KO^{hom} mice exhibit to a similar extent a decrease of PPI, which implies severe deficits in sensory gating processes. Numerous studies strongly indicated that altered PPI is associated with several neuropsychiatric disorders including schizophrenia, obsessive-compulsive disorder, autism and ADHD (Braff et al., 1978; Kohl et al., 2013).

PPI describes the occurrence of reduced startle reflex after induction of a non-startling pre-pulse, evoking the ASR to the following startling stimulus (Koch and

Schnitzler, 1997). Theory concludes, that while processing the pre-pulse, the processing of the following pulse is disrupted, resulting in decreased startle, whilst filtering irrelevant stimuli in the process (Koch and Schnitzler, 1997). Numerous studies focusing on the elucidation of the PPI process have described the connectivity and neuronal network in the brain involved in PPI in detail. PPI is processed by an inhibitory pathway, in which cochlear root neurons innervate the superior and inferior colliculi, which subsequently project onto neurons in the pedunculopontine tegmental nucleus (PPT). Finally, the PPT sends inhibitory cholinergic projections to the PnC, which leads to a reduction of the startle response (Azzopardi et al., 2018; Fendt et al., 1994; Koch, 1999). Additionally, there are several other brain regions involved in an indirect modulation of the PPI response, such as projections from the substantia nigra, lateral globus pallidus, auditory cortex, and amygdala (Fendt et al., 1994; Fendt et al., 2001; Takahashi et al., 2011). Thus, it may be speculated that a deletion of *Kcnk9* alters the neuronal excitability in associated brain regions and that the paternal allele of *Kcnk9* is not significantly involved in the phenotypical outcome of *Kcnk9*KO^{mat} mice.

Thus, this study introduces two novel behavioral deficits of *Kcnk9* knockout mice, namely alterations in ASR and PPI, which have not been described in previous studies.

4.1.2.4 Elevated Nocturnal Activity

Disruption of *Kcnk9* expression in the mouse leads to neurophysiological and behavioral alterations concerning nocturnal locomotor activity (Gotter et al., 2011; Linden et al., 2007). In this study, no difference was seen in locomotor activity in the light phase. However a significant increase in nocturnal activity was seen in *Kcnk9*KO^{hom} mice and to a lesser intermediate extent in *Kcnk9*KO^{mat} mice, each compared to WT littermates, which is concurrent with investigations of circadian locomotor activity in previous studies (Gotter et al., 2011; Linden et al., 2007). The elevated nocturnal activity observed in these studies, was assumed to be a

consequence of modified membrane potential inducing a shift in neuronal excitability in the brain regions in which *Kcnk9* is expressed (Sabbadini and Yost, 2009).

Several neuronal nuclei are associated with the promotion of arousal and wakefulness mediated by specific neurotransmitters in two major pathways. The first pathway involves cholinergic neurons of the laterodorsal tegmental nucleus and pedunculopontine nucleus, which innervate thalamic relay neurons and subsequently activate the cortex (Saper et al., 2005). The second pathway arises from monoaminergic nuclei of the caudal hypothalamus and brainstem, including the raphe nuclei and locus coeruleus (LC), which excite neurons of the cerebral cortex and lateral hypothalamus (Jones, 2003). These associated brain regions are all highly active during wakefulness and inactive during rapid eye movement (REM) sleep. KCNK9 channels are highly present in these brain regions associated with the circadian rhythm and sleep-wake-cycle and are inhibited by monoaminergic neurotransmitters, such as serotonin and noradrenaline (Marinc et al., 2014; Talley et al., 2003). A lack of KCNK9 and absence of inhibition lead to hyperpolarized neurons in sleep-wake-cycle associated brain region ns, resulting in altered circadian-related behavior.

Concerning the first pathway, several studies have implicated KCNK9 in circadian-based thalamocortical neuronal network and hypothalamic orexin neuronal activity (Burdakov et al., 2006; Meuth et al., 2003; Pang et al., 2009). The maternal allele of *Kcnk9* is highly expressed in orexin-positive neurons, which are able to detect glucose levels in their membranes and subsequently modulate excitability of orexin neurons. Orexin neurons were described to regulate wakefulness and sleep and energy equilibrium *in vivo* (Burt et al., 2011). It was suggested that transition between sleep and wake phase is mediated by the release of acetylcholine in thalamic terminals onto muscarinic receptors, which subsequently inhibit KCNK3 and KCNK9 channels, resulting in depolarized thalamocortical relay neurons (Meuth et al., 2003). In addition, *Kcnk9* is highly expressed the neurons in the pedunculopontine nucleus, which play a crucial role in attention, arousal, learning and locomotion (French and Muthusamy, 2018; Tattersall et al., 2014). In the light of these data, it is possible that

a lack of KCNK9 in these regions is partially responsible for the described pathological phenotype in *Kcnk9* KO mice.

Regarding the second pathway, a previous study demonstrated that type two theta oscillations at a frequency range of 6–12 Hz, which are associated with sensory stimulation processes immediately before induction of locomotion, are disrupted in *Kcnk9*KO^{hom} mice (Pang et al., 2009). Electroencephalogram (EEG) recordings of *Kcnk9*KO^{hom} mice revealed fragmented suppression of REM sleep and inhibition of REM-associated theta waves, supporting enhanced locomotor activity in the dark phase (Gotter et al., 2011; Pang et al., 2009). The nucleus reticularis pontis caudalis suppresses muscle tone during REM sleep, inhibits sensory signals to the cerebral cortex and is thought to play an important role sleep.

Furthermore, recent studies demonstrated that the electrical activity of LC neurons are involved in arousal circuitry and sleep-wake transitions (Samuels and Szabadi, 2008; Szabadi, 2012; Von Coelln et al., 2004). The LC is a major noradrenergic nucleus in the pons, with the highest number and density of noradrenergic neurons in the brain (Dahlstrom and Fuxe, 1964). Activation of LC neurons via sustained 3-Hz neuronal stimulation increased locomotor activity by about 50%. Since the performed circadian rhythm experiments revealed an increase of spontaneous locomotion during the dark phase of *Kcnk9*KO^{hom} mice compared to wildtype controls, further experiments were executed to investigate possible KCNK9-related differences in LC pacemaker activity comparing the three genotypes. Electrophysiological analyses of tyrosine hydroxylase (TH)-positive neurons in the LC were performed in collaboration with the Institute of Neurophysiology, Goethe University Frankfurt, Germany. Their results showed a significantly increased spontaneous firing frequency during the active dark phase only for *Kcnk9*KO^{hom} and not for *Kcnk9*KO^{mat} mice, each compared to WT mice. This indicates that KCNK9 channel expression is necessary to selectively attenuate enhanced pacemaker activity during the dark phase in mice, which ultimately results in a higher firing frequency in *Kcnk9*KO^{hom} mice. Interestingly, no significant increase in pacemaker activity in the dark phase was observed in LC

neurons from *Kcnk9*KO^{mat} mice, suggesting that the functional expression of KCNK9 channels from the paternal *Kcnk9* allele in the LC is a sufficient to fully rescue the pacemaker frequency phenotype.

Taken together, *Kcnk9*KO^{mat} mice displayed no significant increase in pacemaker activity in the dark phase, but demonstrate an intermediate behavioral phenotype regarding dark-phase locomotion in the circadian rhythm experiment, leading to the assumption that the expression from the paternal allele of *Kcnk9* is not sufficient to fully dampen the nocturnal activity in *Kcnk9*KO^{mat} mice. However, there is a clear correlation of dark phase spontaneous locomotion of mice and intrinsic pacemaker frequency in the LC. Although electrophysiological recordings show full rescue of spontaneous pacemaker activity in LC neurons due to high paternal *Kcnk9* expression in the LC of *Kcnk9*KO^{mat} animals, only a fraction of the nocturnal activity is rescued. This demonstrates that the LC is involved, but not solely responsible for the regulation of neural networking regarding arousal and attention and that associated brain regions with distinctively lower paternal expression of *Kcnk9*, cannot sufficiently rescue the behavioral phenotype in the *Kcnk9*KO^{mat} mice.

Overall, the data obtained proves that the loss of *Kcnk9* in mice is causative for the impairment of several behavioral parameters that partially resembles the phenotype of patients suffering from Birk-Barel intellectual disability syndrome. In this doctoral thesis, novel behavioral deficits of *Kcnk9* KO mice such as reduced acoustic startle response and pre-pulse inhibition were demonstrated. Surprisingly, intermediate phenotypes for acoustic startle response and nocturnal locomotor activity in animals with a loss of only the expressed maternal allele (*Kcnk9*KO^{mat}) were detected, proposing the involvement of the epigenetically inactive paternal allele. Thus, this study provides clear evidence, that non-canonical imprinting of *Kcnk9* in specific brain regions affects brain function and behavioral phenotype in *Kcnk9*KO^{mat} animals.

4.2 Epigenetic Interference with CI-994 Rescues BBIDS in Mice

The second objective in this study was to identify molecules that are capable of derepressing the paternally silenced allele of *Kcnk9* and explore possibilities for an epigenetic therapy of Birk-Barel intellectual disability syndrome (BBIDS) using *Kcnk9*KO^{mat} mice. The observation of an intermediate phenotype in *Kcnk9*KO^{mat} animals and the expression arising from the paternal *Kcnk9* allele, led to the assumption that exogenous epigenetic manipulation could further increase paternal gene expression of *Kcnk9* in the brain. Thus, it may be speculated that this could compensate for the loss of the maternal allele and rescue the BBIDS-like phenotype in *Kcnk9*KO^{mat} animals. Several epigenetic modulators were identified in the course of this study, which further upregulated the paternal allele of the *Kcnk9* gene, in both murine primary cortical neurons (mPCNs) and the BBIDS mouse model (*Kcnk9*KO^{mat}), resulting in a successful rescue of the pathological phenotype in *Kcnk9*KO^{mat} mice.

An imprinting disorder is usually caused by a deficiency of the expressed genes in the imprinting cluster or imprinting control element (ICE), whereas the silenced gene is repressed epigenetically yet structurally unimpaired. Derepression of imprinted genes with exogenous epigenetic modulation provides an opportunity for epigenetic treatment of imprinting diseases. Generally, one would expect the mechanism behind epigenetic modulation to be unspecific throughout the genome, altering the chromatin confirmation and gene expression patterns unspecifically. Thus, it is of concern that the interference with epigenetic drugs results in numerous off-target effects, which are possibly causative for certain diseases such as tumor development, metabolic dysregulation and neurological dysfunction. In the majority of cases, epigenetic modulators are used for the treatment against cancer (See table 2) (Eckschlager et al., 2017). Several studies demonstrated that azacytidine and decitabine (or 5-aza-2'-deoxycytidine), two DNA methyltransferase inhibitors (DNMTi), which have been approved by the Food and Drug Administration (FDA) and European Medicines Agency (EMA), are an efficient treatment for myelodysplastic syndrome and acute

myeloid leukemia (Ades et al., 2013; Fenaux et al., 2010; Kantarjian et al., 2006). However, epigenetic drugs have also gained more importance for the treatment of neurological disorders throughout the last years (Treppendahl et al., 2014). In particular valproate (valproic acid), a first-generation HDACi, is used in anti-epileptic therapy without causing severe metabolic or tumorigenic side-effects (Perucca, 2002). Additional HDAC inhibitors approved by the FDA show great potential in the treatment of several neurological disorders (Bolden et al., 2006; Hahnen et al., 2008).

4.2.1 Epigenetic Modulators Derepresses Paternally Silenced *Kcnk9* Allele *in Vitro* and *in Vivo*

A previous study demonstrated induced derepression of maternal copies of paternally expressed Prader-Willi syndrome (PWS) candidate genes by injecting mouse pups with UNC0642, a selective inhibitor of euchromatic histone-lysine N-methyltransferase-2. UNC0642 affected the posttranslational histone modification of the imprint at the Prader-Willi syndrome locus and promoted growth and survival of the pups with a paternal deletion of the PWS region, without altering DNA methylation at the PWS-ICR, thereby suggesting histone methylation as a potential therapeutic target for PWS (Kim et al., 2017).

In this work, the investigation of the paternal *Kcnk9* transcripts after epigenetic drug administration revealed a significant upregulation of the paternal *Kcnk9* allele in *Kcnk9*KO^{mat} murine primary cortical neurons (mPCNs) after treatment with histone methyltransferase EZH2 inhibitor 3-deazaneplanocin A (DZNep) and the histone deacetylase inhibitors (HDACi) SAHA (suberoylanilide hydroxamic acid), valproic acid and CI-994. The RT-qPCR experiments demonstrated that SAHA, the active ingredient of the epigenetic drug Vorinostat, and CI994 induced a similar upregulation of *Kcnk9* in *Kcnk9*KO^{mat} mPCNs after treatment, compared to DMSO-treated mPCNs. Vorinostat is the first HDAC inhibitor approved by the United States (FDA) for the treatment of cutaneous T-cell lymphoma (CTCL) (Duvic et al., 2007). Despite SAHA being an FDA-approved drug, the action of SAHA is less specific than that of

CI-994 and is described to be a pan-inhibitor, targeting all types of HDACs. On the other hand, the benzamide-based second-generation class I HDAC inhibitor CI-994 is a selective inhibitor of class I HDACs, which is a potent inhibitor of HDAC1 and 3 isoenzymes relative to HDAC6 and HDAC8 (Ki values: 0.41 µM for HDAC1, 0.75 µM for HDAC3, and ≥ 100 µM for HDAC6 and HDAC8) (Beckers et al., 2007).

Due to overall stability of expression throughout the performed experiments, including dose response expression analysis, and high specificity described in previous literature (Beckers et al., 2007), CI-994 was applied in further *in vivo* experiments. Accumulating evidence has shown curative effects of CI-994 *in vitro* and *in vivo.* The drug Tacedinaline, with CI-994 as the active substance, has been demonstrated to inhibit apoptosis in susceptible tumor cells and was administered in several clinical trials for anti-cancer therapy, in particular against advanced myeloma and pancreatic cancer (Nemunaitis et al., 2003; Pauer et al., 2004; Prakash et al., 2001). Controversially, *KCNK9* has also been described as a key oncogene in the role of tumor formation with the finding that it is overexpressed in various human carcinoma tissues, e.g. lung, colon, breast and prostate cancers (Mu et al., 2003). However, CI-994 has proven inhibitory potency of epithelial-mesenchymal transition processes by restoring ErbB3 and E-cadherin expressions in ovarian, pancreatic and bladder carcinoma cells (Tang et al., 2016). In addition, a recent investigation provided therapeutic evidence by demonstrating that CI-994 inhibition of HDAC activity is involved in neuronal protection in the central nervous system, inflammatory suppression processes and cell survival *in vitro* and *in vivo* (Zhang et al., 2018). Furthermore, CI-994 has been proven to reduce neuronal loss and inhibit aggregation of neutrophils in spinal cord injuries (Zhang et al., 2018).

For *in vivo* testing, either DMSO or CI-994 was daily intraperitoneally injected over 14 days. Injections with CI-994 induced paternal *Kcnk9* expression about ~3 fold compared to DMSO-treated controls in the majority of analyzed brain regions. Interestingly, no upregulation of *Kcnk9* expression was observed in wildtype animals after CI-994 treatment, indicating the involvement of an allele-specific targeting

mechanism, which can discriminate parental alleles epigenetically. A recent study already demonstrated an allele-specific enrichment of specific histone marks on silenced (or actively expressed) imprinted genes, including the enrichment for H3K9me3 on the silenced alleles and absence of H3K9ac on the expressed alleles *of Plagl1, Magel2*, and *Meg3* (Bonthuis et al., 2015).

The mouse *Kcnk9* gene resides in an imprinted gene cluster on chromosome 15 that comprises further brain-specific maternally expressed protein-coding genes, including *Ago2*, *Chrac1* and *Trappc9*, and one paternally expressed non-coding gene, *Peg13* (Court et al., 2014; Ruf et al., 2007). To exclude off-target effects of CI-994 within the imprinting cluster, RT-qPCR gene expression analyses of the cluster genes were performed. Interestingly, CI-994 treatment increased *Kcnk9* expression from the paternal allele and did not influence the expression of adjacent imprinted genes within the imprinted cluster on mouse chromosome 15, implying specificity to *Kcnk9* as a target within the imprinted gene cluster.

Intriguingly, systematic administration of CI-994 in mice induced derepression of the paternal allele of *Kcnk9* in brain regions associated with the pathology of the BBIDS-phenotype, such as hippocampus and LC. Moreover, increase of paternal *Kcnk9* expression after CI-994 injections seems to be tissue-specific (Fig. 24b). In comparison to all other brain regions analyzed, an increase of *Kcnk9* expression was not observed in the cortex or prefrontal cortex of *Kcnk9*KO^{mat} mice after CI-994 treatment, implicating the presence of tissue-specific mechanisms in *Kcnk9* gene regulation *Kcnk9*, which still have to be identified.

Nevertheless, it must also be taken in to consideration, that CI-994 also influences the expression of other genes in the genome, which could have an impact on the described behavioral outcome. RNA sequencing of hippocampal tissue of CI-994-treated and control mice was performed in a previous study. 475 genes differentially expressed between CI-994- and vehicle-treated animals were found after one hour treatment. Furthermore, gene ontology and pathway analyses revealed that a great number of these differentially expressed genes are neuroplasticity-associated genes,

such as immediate-early genes *Arc* and *cFos*, that displayed enhanced histone acetylation in their promoter region, resulting in augmented neuroplasticity (Graff et al., 2014; Korb and Finkbeiner, 2011). These findings suggest that the epigenetic manipulation with CI-994 *in vivo* modulates the expression of genes interrelated with neuroplasticity, which could play an important role in the behavioral rescue of *Kcnk9*KO^{mat} mice, including working memory.

4.2.2 HDACi CI-994 Successfully Rescues Behavioral Phenotype in BBIDS

A previous study regarding the brain function of mice revealed that systematic administration of CI-994 leads to a long-lasting CI-994 concentration in the brain without interfering in the basic behavioral phenotype of wildtype mice (Graff et al., 2014). In our experiments, no significant behavioral abnormalities regarding ASR, working memory or circadian locomotor activity were observed after CI-994 injections in in wildtype animals. However, overall injections with DMSO and CI-994 seemed to have an influence on sensorimotor gating in the pre-pulse inhibition (PPI) test. Regions associated with PPI are possibly more sensitive to minor interferences, altering the equilibrium of the brain circuit involved in PPI, compared to brain regions associated with the other described behavioral phenotypes.

Overall, CI-994 treatment resulted in a full behavioral rescue of working memory, acoustic startle response and nocturnal activity in *Kcnk9*KO^{mat} mice. The presented results suggest CI-994 as a potential treatment for ADHS, Birk-Barel intellectual disability syndrome and other imprinting disorders with similar gene regulatory mechanisms. So far, two preclinical mouse studies provided compelling results implicating KCNK9 in the neuropathology of depression (Coburn et al., 2012; Gotter et al., 2011). Utilizing *Kcnk9* knockout mouse models, along with behavior, electrophysiological and genetic experiments, KCNK9 has also been proposed a promising target for therapy of depression and mood disorders (Borsotto et al., 2015).

To date, only adult *Kcnk9* knockout mice have been phenotypically described (Gotter et al., 2011; Linden et al., 2007; Pang et al., 2009). Fittingly, adult *Kcnk9* knockout mice were subjected to the epigenetic drug intervention with CI-994. Continuative studies are essential to determine whether the HDACi CI-994 might provide therapeutic benefits in younger *Kcnk9* knockout individuals, i.e. both neonatal and juvenile mice or even embryos to possibly allow earlier preventive treatment. So far, it is unclear at which developmental stage behavioral symptoms in *Kcnk9*KO^{mat} mice and *Kcnk9*KO^{hom} mice first appear. This issue should be investigated in further future studies.

In addition, it is also noteworthy that in contrast to the analyzed *Kcnk9*KO^{mat} animals with a deletion of exon 2 of the *Kcnk9* gene, previously described BBIDS mutations are missense mutations that lead to partially functional KCNK9 channels (Veale et al., 2014). Therefore, investigating a mouse model with the known human BBIDS mutations could give a more BBIDS-specific insight into the neuronal and behavioral phenotypes before and after epigenetic drug treatment with CI-994, than that provided by the *Kcnk9* knockout mice examined in this study. The co-existence of a fully functional paternal KCNK9 potassium channel and a modified maternal KCNK9 protein, with reduced functionality, could lead to a divergent phenotype compared to the phenotype described in this work.

4.2.3 CI-994 Interferes with H3K27 Acetylation but not with DNA Methylation in *Kcnk9/Peg13* loci

The differentially methylated region (DMR) associated with the promoter region of the non-coding *Peg13* gene on mouse chromosome 15 is methylated on the maternal allele and was proposed to be involved in the regulation of the maternally expressed *Kcnk9* gene (Singh et al., 2011; Xie et al., 2012). In contrast, the CpG islands overlapping the *Kcnk9* promoter are biallelically hypomethylated (Ruf et al., 2007). Reciprocal brain-specific imprinted expression of the *KCNK9* and *PEG13* genes accompanied by the enrichment of CTCF-cohesin on the unmethylated paternal

PEG13 allele was also identified for the human gene orthologues on chromosome 8q24, (Court et al., 2014). Concordantly to the murine gene orthologues, *KCNK9* is maternally and *PEG13* paternally expressed in brain tissue (Court et al., 2014; Ruf et al., 2007). Furthermore, it was shown that CTCF mediates allele-specific chromatin looping, which occurs between a shared brain-specific enhancer and the *KCNK9* and *PEG13* promoter regions, indicating the involvement of the *PEG13*-DMR as an enhancer-blocker controlling element (Court et al., 2014). These findings are consistent with a methylation-sensitive enhancer-blocker mechanism mediated by CTCF, similar to that regulating the reciprocal imprinting at the *Igf2/H19* locus (Hark et al., 2000). In addition, the *KCNK9* promoter and intronic region displayed high levels of active histone H3 lysine 27 acetylation (H3K27ac) and histone H3 lysine 4 monomethylation (H3K4me1) chromatin marks in brain tissues.

As shown in figure 31, the derepression of the paternal *Kcnk9* allele after CI-994 treatment was not accompanied by changes in the DNA methylation status at the *Peg13*-DMR, which is proposed to be involved in regulation of *Kcnk9* expression (Ruf et al., 2007). However, it is important to mention that the bisulfite sequencing technique used in this study does not discriminate between 5-methylcytosine and 5-hydroxymethylcytosine modifications. Thus, minor modifications of cytosine affected by CI-994 cannot be excluded (Booth et al., 2012). Surprisingly, the LC exhibits a significantly higher DNA methylation status of the *Peg13*-DMR1 CpG1-3 compared to the analyzed cerebellum and hippocampus samples, which correlates with the elevated paternal expression.

The data presented in chapter 3.5.2 provides strong evidence that CI-994-mediated activation of the paternal *Kcnk9* allele is induced by an increase of H3K27ac at regulatory elements in the promoter and intronic region of the *Kcnk9* gene. CI-994 as a histone deacetylase inhibitor did not only significantly increase H3K27ac but also caused a slightly elevated deposition of H3K4me1 at the *Kcnk9* promoter region. These types of cross-talk mechanisms between histone-modifying enzymes are not unusual. Several studies have described an increase of histone methylation marks

through downregulation of histone deacetylases (Calo and Wysocka, 2013; Huang et al., 2011).

CI-994 introduces a brain region-specific deposition of H3K27ac at the *Kcnk9* promoter and intronic region of the hippocampus and LC. In comparison, the hippocampus exclusively shows significantly increased deposition of H3K27ac at the *Kcnk9* promoter, but not at the intronic region, whereas the LC exhibits significant deposition of H3K27ac at both genomic positions. These observations indicate that the investigated intronic region of *Kcnk9* is a brain region-specific enhancer element in mouse, which has not been described to date. The data suggests that histone modifications in this particular intronic sub-region, is highly sensitive to exogenous and most probably also to endogenous effectors resulting in changes in the higher chromatin structure at the paternal allele.

Taken together, the increased residual expression of the paternal *Kcnk9* gene in the LC of *Kcnk9*KO^{mat} mice could be explained by a combination of increased DNA methylation at the *Peg13*-DMR1-CpG1-3 and increased chromatin accessibility at the promoter and intronic region of the paternal *Kcnk9* allele in the LC compared to other analyzed brain regions. The data shown lead to the assumption, that with the introduction of the *Kcnk9* knockout on the maternal allele, the paternal locus is subsequently highly susceptible to histone modifications mediated by CI-994.

In summary, the epigenetic activity of CI-994 seems to act rather specifically on the paternal allele of *Kcnk9* in the mouse chromosome 15 imprinting cluster of *Kcnk9*KO^{mat} animals. This is an essential feature if CI-994 were to be considered an active substance for medication, making the drug possibly safe for the use in BBIDS patients. However, the potential risk of off-target effects, which occur with administration of epigenetic drugs, should be a serious concern and investigated thoroughly in drug development processes. The presented results, together with data of a previous study, demonstrate that CI-994 treatment in mice does not influence basic behavior (Graff et al., 2014), indicating a high tolerability and low toxicity of the drug in the individual. Although the overall picture displays a successful treatment,

each particular case should be assessed individually with consideration to the duration, dose and developmental stage of drug administration. Overall, based on the promising results in this study and in preclinical trails, therapeutic potential of CI-994 should be further explored for the treatment of Birk-Barel ID syndrome.

5. Conclusion

To date no general curative therapy has been identified for imprinting disorders. Moreover, the impact of the silenced allele on the phenotype has not been thoroughly investigated. In this interdisciplinary study, *Kcnk9* expression and the behavioral phenotype of mice with heterozygous deletion of the active maternal *Kcnk9* allele (*Kcnk9*KO^{mat}) were analyzed.

The results presented reveal brain region-specific upregulation of the paternally silenced *Kcnk9* allele particularly in the LC of *Kcnk9*KO^{mat} mice, which is sufficient to substantially influence the behavioral phenotype and modulate acoustic startle response and nocturnal activity, a central phenotype of *Kcnk9* knockout animals.

Furthermore, results arising from this thesis demonstrate that the systematic administration of the class I second-generation HDAC inhibitor CI-994 serves as a potential treatment for imprinting disorders such as Birk-Barel intellectual disability syndrome. CI-994 treatment of *Kcnk9*KO^{mat} mice substantially derepressed the paternal allele of *Kcnk9* in several brain regions resulting in a significant increase in paternal *Kcnk9* expression and full rescue of the neurodevelopmental behavioral phenotype in *Kcnk9*KO^{mat} animals. The rescue is mediated by an increase of H3K27 histone acetylation, but not by changes in DNA methylation at the DMR (differentially methylated region) in the *Peg13/Kcnk9* locus.

In conclusion, the data presented shows the first successful phenotypic rescue of cognitive dysfunctions in a mouse model for an imprinting disorder and suggests epigenetic modulation by CI-994 as a promising therapeutic strategy for patients with Birk-Barel ID syndrome or possibly other imprinting disorders.

6. References

Ades, L., Sekeres, M.A., Wolfromm, A., Teichman, M.L., Tiu, R.V., Itzykson, R., Maciejewski, J.P., Dreyfus, F., List, A.F., Fenaux, P.*, et al.* (2013). Predictive factors of response and survival among chronic myelomonocytic leukemia patients treated with azacitidine. Leukemia research *37*, 609-613.

Akhtar, J., More, P., Kulkarni, A., Marini, F., Kaiser, W., and Berger, C. (2018). TAF-ChIP: An ultra-low input approach for genome wide chromatin immunoprecipitation assay. Preprint at https://biorxivorg/content/early/2018/04/12/299727, 299727.

Albrecht, U., Sutcliffe, J.S., Cattanach, B.M., Beechey, C.V., Armstrong, D., Eichele, G., and Beaudet, A.L. (1997). Imprinted expression of the murine Angelman syndrome gene, Ube3a, in hippocampal and Purkinje neurons. Nature genetics *17*, 75-78.

Aller, M.I., Veale, E.L., Linden, A.M., Sandu, C., Schwaninger, M., Evans, L.J., Korpi, E.R., Mathie, A., Wisden, W., and Brickley, S.G. (2005). Modifying the subunit composition of TASK channels alters the modulation of a leak conductance in cerebellar granule neurons. The Journal of neuroscience : the official journal of the Society for Neuroscience *25*, 11455-11467.

Angulo, M.A., Butler, M.G., and Cataletto, M.E. (2015). Prader-Willi syndrome: a review of clinical, genetic, and endocrine findings. Journal of endocrinological investigation *38*, 1249-1263.

Azzopardi, E., Louttit, A.G., DeOliveira, C., Laviolette, S.R., and Schmid, S. (2018). The Role of Cholinergic Midbrain Neurons in Startle and Prepulse Inhibition. The Journal of neuroscience : the official journal of the Society for Neuroscience *38*, 8798-8808.

Bando, Y., Hirano, T., and Tagawa, Y. (2014). Dysfunction of KCNK potassium channels impairs neuronal migration in the developing mouse cerebral cortex.

Cerebral cortex *24*, 1017-1029.

Bannister, A.J., and Kouzarides, T. (2011). Regulation of chromatin by histone modifications. Cell research *21*, 381-395.

Barel, O., Shalev, S.A., Ofir, R., Cohen, A., Zlotogora, J., Shorer, Z., Mazor, G., Finer, G., Khateeb, S., Zilberberg, N.*, et al.* (2008). Maternally inherited Birk Barel mental retardation dysmorphism syndrome caused by a mutation in the genomically imprinted potassium channel KCNK9. American journal of human genetics *83*, 193-199.

Barlow, D.P. (2011). Genomic imprinting: a mammalian epigenetic discovery model. Annual review of genetics *45*, 379-403.

Barlow, D.P., and Bartolomei, M.S. (2014). Genomic imprinting in mammals. Cold Spring Harbor perspectives in biology *6*.

Barlow, D.P., Stoger, R., Herrmann, B.G., Saito, K., and Schweifer, N. (1991). The mouse insulin-like growth factor type-2 receptor is imprinted and closely linked to the Tme locus. Nature *349*, 84-87.

Barr, M.L., and Bertram, E.G. (1949). A morphological distinction between neurones of the male and female, and the behaviour of the nucleolar satellite during accelerated nucleoprotein synthesis. Nature *163*, 676.

Bartolomei, M.S., Webber, A.L., Brunkow, M.E., and Tilghman, S.M. (1993). Epigenetic mechanisms underlying the imprinting of the mouse H19 gene. Genes & development *7*, 1663-1673.

Bartolomei, M.S., Zemel, S., and Tilghman, S.M. (1991). Parental imprinting of the mouse H19 gene. Nature *351*, 153-155.

Beckers, T., Burkhardt, C., Wieland, H., Gimmnich, P., Ciossek, T., Maier, T., and Sanders, K. (2007). Distinct pharmacological properties of second generation HDAC

inhibitors with the benzamide or hydroxamate head group. International journal of cancer *121*, 1138-1148.

Beckwith (1963). Extreme cytomegaly of the adrenal fetal cortex, omphalocele, hyperplasia of kidneys and pancreas, and Leydig-cell hyperplasia: Another syndrome? Western Society for Pediatric Research (abstract), Los Angeles.

Bell, A.C., and Felsenfeld, G. (2000). Methylation of a CTCF-dependent boundary controls imprinted expression of the Igf2 gene. Nature *405*, 482-485.

Berg, A.P., Talley, E.M., Manger, J.P., and Bayliss, D.A. (2004). Motoneurons express heteromeric TWIK-related acid-sensitive K+ (TASK) channels containing TASK-1 (KCNK3) and TASK-3 (KCNK9) subunits. The Journal of neuroscience : the official journal of the Society for Neuroscience *24*, 6693-6702.

Berger, S.L. (2002). Histone modifications in transcriptional regulation. Current opinion in genetics & development *12*, 142-148.

Binder, G., Begemann, M., Eggermann, T., and Kannenberg, K. (2011). Silver-Russell syndrome. Best practice & research Clinical endocrinology & metabolism *25*, 153-160.

Bird, A.P., and Wolffe, A.P. (1999). Methylation-induced repression--belts, braces, and chromatin. Cell *99*, 451-454.

Bird, L.M. (2014). Angelman syndrome: review of clinical and molecular aspects. The application of clinical genetics *7*, 93-104.

Bliek, J., Maas, S.M., Ruijter, J.M., Hennekam, R.C., Alders, M., Westerveld, A., and Mannens, M.M. (2001). Increased tumour risk for BWS patients correlates with aberrant H19 and not KCNQ1OT1 methylation: occurrence of KCNQ1OT1 hypomethylation in familial cases of BWS. Human molecular genetics *10*, 467-476.

Bolden, J.E., Peart, M.J., and Johnstone, R.W. (2006). Anticancer activities of histone

deacetylase inhibitors. Nature reviews Drug discovery *5*, 769-784.

Bonaldi, A. (2017). Mining Novel Candidate Imprinted Genes Using Genome-Wide Methylation Screening and Literature Review. Epigenomes.

Bonasio, R., Tu, S., and Reinberg, D. (2010). Molecular signals of epigenetic states. Science *330*, 612-616.

Bonthuis, P.J., Huang, W.C., Stacher Horndli, C.N., Ferris, E., Cheng, T., and Gregg, C. (2015). Noncanonical Genomic Imprinting Effects in Offspring. Cell reports *12*, 979-991.

Booth, M.J., Branco, M.R., Ficz, G., Oxley, D., Krueger, F., Reik, W., and Balasubramanian, S. (2012). Quantitative sequencing of 5-methylcytosine and 5-hydroxymethylcytosine at single-base resolution. Science *336*, 934-937.

Bordone, L., and Guarente, L. (2005). Calorie restriction, SIRT1 and metabolism: understanding longevity. Nature reviews Molecular cell biology *6*, 298-305.

Borisenko, V., Sansom, M.S., and Woolley, G.A. (2000). Protonation of lysine residues inverts cation/anion selectivity in a model channel. Biophysical journal *78*, 1335-1348.

Borodovitsyna, O., Flamini, M., and Chandler, D. (2017). Noradrenergic Modulation of Cognition in Health and Disease. Neural plasticity *2017*, 6031478.

Borsotto, M., Veyssiere, J., Moha Ou Maati, H., Devader, C., Mazella, J., and Heurteaux, C. (2015). Targeting two-pore domain K(+) channels TREK-1 and TASK-3 for the treatment of depression: a new therapeutic concept. British journal of pharmacology *172*, 771-784.

Bourc'his, D., and Bestor, T.H. (2004). Meiotic catastrophe and retrotransposon reactivation in male germ cells lacking Dnmt3L. Nature *431*, 96-99.

Braff, D., Stone, C., Callaway, E., Geyer, M., Glick, I., and Bali, L. (1978). Prestimulus effects on human startle reflex in normals and schizophrenics. Psychophysiology *15*, 339-343.

Brickley, S.G., Aller, M.I., Sandu, C., Veale, E.L., Alder, F.G., Sambi, H., Mathie, A., and Wisden, W. (2007). TASK-3 two-pore domain potassium channels enable sustained high-frequency firing in cerebellar granule neurons. The Journal of neuroscience : the official journal of the Society for Neuroscience *27*, 9329-9340.

Buiting, K. (2010). Prader-Willi syndrome and Angelman syndrome. American journal of medical genetics Part C, Seminars in medical genetics *154C*, 365-376.

Burdakov, D., Jensen, L.T., Alexopoulos, H., Williams, R.H., Fearon, I.M., O'Kelly, I., Gerasimenko, O., Fugger, L., and Verkhratsky, A. (2006). Tandem-pore K+ channels mediate inhibition of orexin neurons by glucose. Neuron *50*, 711-722.

Burt, J., Alberto, C.O., Parsons, M.P., and Hirasawa, M. (2011). Local network regulation of orexin neurons in the lateral hypothalamus. American journal of physiology Regulatory, integrative and comparative physiology *301*, R572-580.

Calo, E., and Wysocka, J. (2013). Modification of enhancer chromatin: what, how, and why? Molecular cell *49*, 825-837.

Cattanach, B.M., and Kirk, M. (1985). Differential activity of maternally and paternally derived chromosome regions in mice. Nature *315*, 496-498.

Cedar, H., and Bergman, Y. (2009). Linking DNA methylation and histone modification: patterns and paradigms. Nature reviews Genetics *10*, 295-304.

Clements, A., Poux, A.N., Lo, W.S., Pillus, L., Berger, S.L., and Marmorstein, R. (2003). Structural basis for histone and phosphohistone binding by the GCN5 histone acetyltransferase. Molecular cell *12*, 461-473.

Coburn, C.A., Luo, Y., Cui, M., Wang, J., Soll, R., Dong, J., Hu, B., Lyon, M.A.,

Santarelli, V.P., Kraus, R.L., *et al.* (2012). Discovery of a pharmacologically active antagonist of the two-pore-domain potassium channel K2P9.1 (TASK-3). ChemMedChem *7*, 123-133.

Cooper, W.N., Luharia, A., Evans, G.A., Raza, H., Haire, A.C., Grundy, R., Bowdin, S.C., Riccio, A., Sebastio, G., Bliek, J., *et al.* (2005). Molecular subtypes and phenotypic expression of Beckwith-Wiedemann syndrome. European journal of human genetics : EJHG *13*, 1025-1032.

Court, F., Camprubi, C., Garcia, C.V., Guillaumet-Adkins, A., Sparago, A., Seruggia, D., Sandoval, J., Esteller, M., Martin-Trujillo, A., Riccio, A., *et al.* (2014). The PEG13-DMR and brain-specific enhancers dictate imprinted expression within the 8q24 intellectual disability risk locus. Epigenetics & chromatin *7*, 5.

Cowley, M., and Oakey, R.J. (2010). Retrotransposition and genomic imprinting. Briefings in functional genomics *9*, 340-346.

Csankovszki, G., Nagy, A., and Jaenisch, R. (2001). Synergism of Xist RNA, DNA methylation, and histone hypoacetylation in maintaining X chromosome inactivation. The Journal of cell biology *153*, 773-784.

Czirjak, G., and Enyedi, P. (2003). Ruthenium red inhibits TASK-3 potassium channel by interconnecting glutamate 70 of the two subunits. Molecular pharmacology *63*, 646-652.

Dahlstrom, A., and Fuxe, K. (1964). Localization of monoamines in the lower brain stem. Experientia *20*, 398-399.

Davis, M. (1980). Neurochemical modulation of sensory-motor reactivity: acoustic and tactile startle reflexes. Neuroscience and biobehavioral reviews *4*, 241-263.

Davis, M. (1986). Pharmacological and anatomical analysis of fear conditioning using the fear-potentiated startle paradigm. Behavioral neuroscience *100*, 814-824.

DeChiara, T.M., Robertson, E.J., and Efstratiadis, A. (1991). Parental imprinting of the mouse insulin-like growth factor II gene. Cell *64*, 849-859.

DeVeale, B., van der Kooy, D., and Babak, T. (2012). Critical evaluation of imprinted gene expression by RNA-Seq: a new perspective. PLoS genetics *8*, e1002600.

Duprat, F., Lesage, F., Fink, M., Reyes, R., Heurteaux, C., and Lazdunski, M. (1997). TASK, a human background K+ channel to sense external pH variations near physiological pH. The EMBO journal *16*, 5464-5471.

Duvic, M., Talpur, R., Ni, X., Zhang, C., Hazarika, P., Kelly, C., Chiao, J.H., Reilly, J.F., Ricker, J.L., Richon, V.M.*, et al.* (2007). Phase 2 trial of oral vorinostat (suberoylanilide hydroxamic acid, SAHA) for refractory cutaneous T-cell lymphoma (CTCL). Blood *109*, 31-39.

Eckschlager, T., Plch, J., Stiborova, M., and Hrabeta, J. (2017). Histone Deacetylase Inhibitors as Anticancer Drugs. International journal of molecular sciences *18*.

Egger, G., Liang, G., Aparicio, A., and Jones, P.A. (2004). Epigenetics in human disease and prospects for epigenetic therapy. Nature *429*, 457-463.

Eggermann, T., Perez de Nanclares, G., Maher, E.R., Temple, I.K., Tumer, Z., Monk, D., Mackay, D.J., Gronskov, K., Riccio, A., Linglart, A.*, et al.* (2015). Imprinting disorders: a group of congenital disorders with overlapping patterns of molecular changes affecting imprinted loci. Clinical epigenetics *7*, 123.

El Hachmane, M.F., Rees, K.A., Veale, E.L., Sumbayev, V.V., and Mathie, A. (2014). Enhancement of TWIK-related acid-sensitive potassium channel 3 (TASK3) two-pore domain potassium channel activity by tumor necrosis factor alpha. The Journal of biological chemistry *289*, 1388-1401.

Emanuele, S., Lauricella, M., and Tesoriere, G. (2008). Histone deacetylase inhibitors: apoptotic effects and clinical implications (Review). International journal of

oncology *33*, 637-646.

Fenaux, P., Mufti, G.J., Hellstrom-Lindberg, E., Santini, V., Gattermann, N., Germing, U., Sanz, G., List, A.F., Gore, S., Seymour, J.F.*, et al.* (2010). Azacitidine prolongs overall survival compared with conventional care regimens in elderly patients with low bone marrow blast count acute myeloid leukemia. Journal of clinical oncology : official journal of the American Society of Clinical Oncology *28*, 562-569.

Fendt, M., Koch, M., and Schnitzler, H.U. (1994). Lesions of the central gray block the sensitization of the acoustic startle response in rats. Brain research *661*, 163-173.

Fendt, M., Li, L., and Yeomans, J.S. (2001). Brain stem circuits mediating prepulse inhibition of the startle reflex. Psychopharmacology *156*, 216-224.

Ferguson-Smith, A.C. (2011). Genomic imprinting: the emergence of an epigenetic paradigm. Nature reviews Genetics *12*, 565-575.

Fire, A., Xu, S., Montgomery, M.K., Kostas, S.A., Driver, S.E., and Mello, C.C. (1998). Potent and specific genetic interference by double-stranded RNA in Caenorhabditis elegans. Nature *391*, 806-811.

Fischle, W., Wang, Y., and Allis, C.D. (2003). Histone and chromatin cross-talk. Current opinion in cell biology *15*, 172-183.

Fournier, C., Goto, Y., Ballestar, E., Delaval, K., Hever, A.M., Esteller, M., and Feil, R. (2002). Allele-specific histone lysine methylation marks regulatory regions at imprinted mouse genes. The EMBO journal *21*, 6560-6570.

Fraga, M.F., Ballestar, E., Paz, M.F., Ropero, S., Setien, F., Ballestar, M.L., Heine-Suner, D., Cigudosa, J.C., Urioste, M., Benitez, J.*, et al.* (2005). Epigenetic differences arise during the lifetime of monozygotic twins. Proceedings of the National Academy of Sciences of the United States of America *102*, 10604-10609.

Franklin, K.B.J., & Paxinos, G. (1997). The mouse brain in stereotaxic coordinates.

French, I.T., and Muthusamy, K.A. (2018). A Review of the Pedunculopontine Nucleus in Parkinson's Disease. Frontiers in aging neuroscience *10*, 99.

Frommer, M., McDonald, L.E., Millar, D.S., Collis, C.M., Watt, F., Grigg, G.W., Molloy, P.L., and Paul, C.L. (1992). A genomic sequencing protocol that yields a positive display of 5-methylcytosine residues in individual DNA strands. Proceedings of the National Academy of Sciences of the United States of America *89*, 1827-1831.

Gibney, E.R., and Nolan, C.M. (2010). Epigenetics and gene expression. Heredity *105*, 4-13.

Goldstein, S.A., Bockenhauer, D., O'Kelly, I., and Zilberberg, N. (2001). Potassium leak channels and the KCNK family of two-P-domain subunits. Nature reviews Neuroscience *2*, 175-184.

Gotter, A.L., Santarelli, V.P., Doran, S.M., Tannenbaum, P.L., Kraus, R.L., Rosahl, T.W., Meziane, H., Montial, M., Reiss, D.R., Wessner, K.*, et al.* (2011). TASK-3 as a potential antidepressant target. Brain research *1416*, 69-79.

Goudarzi, A., Zhang, D., Huang, H., Barral, S., Kwon, O.K., Qi, S., Tang, Z., Buchou, T., Vitte, A.L., He, T.*, et al.* (2016). Dynamic Competing Histone H4 K5K8 Acetylation and Butyrylation Are Hallmarks of Highly Active Gene Promoters. Molecular cell *62*, 169-180.

Graff, J., Joseph, N.F., Horn, M.E., Samiei, A., Meng, J., Seo, J., Rei, D., Bero, A.W., Phan, T.X., Wagner, F.*, et al.* (2014). Epigenetic priming of memory updating during reconsolidation to attenuate remote fear memories. Cell *156*, 261-276.

Graham, J.M., Jr., Zadeh, N., Kelley, M., Tan, E.S., Liew, W., Tan, V., Deardorff, M.A., Wilson, G.N., Sagi-Dain, L., and Shalev, S.A. (2016). KCNK9 imprinting syndrome-further delineation of a possible treatable disorder. American journal of medical

genetics Part A *170*, 2632-2637.

Gregg, C. (2014). Known unknowns for allele-specific expression and genomic imprinting effects. F1000prime reports *6*, 75.

Gregg, C., Zhang, J., Butler, J.E., Haig, D., and Dulac, C. (2010). Sex-specific parent-of-origin allelic expression in the mouse brain. Science *329*, 682-685.

Gruenbaum, Y., Stein, R., Cedar, H., and Razin, A. (1981). Methylation of CpG sequences in eukaryotic DNA. FEBS letters *124*, 67-71.

Grunstein, M. (1997). Histone acetylation in chromatin structure and transcription. Nature *389*, 349-352.

Guibert, S., Forne, T., and Weber, M. (2012). Global profiling of DNA methylation erasure in mouse primordial germ cells. Genome research *22*, 633-641.

Guyon, A., Tardy, M.P., Rovere, C., Nahon, J.L., Barhanin, J., and Lesage, F. (2009). Glucose inhibition persists in hypothalamic neurons lacking tandem-pore K+ channels. The Journal of neuroscience : the official journal of the Society for Neuroscience *29*, 2528-2533.

Hahnen, E., Hauke, J., Trankle, C., Eyupoglu, I.Y., Wirth, B., and Blumcke, I. (2008). Histone deacetylase inhibitors: possible implications for neurodegenerative disorders. Expert opinion on investigational drugs *17*, 169-184.

Hajkova, P., Ancelin, K., Waldmann, T., Lacoste, N., Lange, U.C., Cesari, F., Lee, C., Almouzni, G., Schneider, R., and Surani, M.A. (2008). Chromatin dynamics during epigenetic reprogramming in the mouse germ line. Nature *452*, 877-881.

Hark, A.T., Schoenherr, C.J., Katz, D.J., Ingram, R.S., Levorse, J.M., and Tilghman, S.M. (2000). CTCF mediates methylation-sensitive enhancer-blocking activity at the H19/Igf2 locus. Nature *405*, 486-489.

Hayashi, K., and Surani, M.A. (2009). Self-renewing epiblast stem cells exhibit continual delineation of germ cells with epigenetic reprogramming in vitro. Development *136*, 3549-3556.

Heintzman, N.D., Hon, G.C., Hawkins, R.D., Kheradpour, P., Stark, A., Harp, L.F., Ye, Z., Lee, L.K., Stuart, R.K., Ching, C.W.*, et al.* (2009). Histone modifications at human enhancers reflect global cell-type-specific gene expression. Nature *459*, 108-112.

Henckel, A., and Arnaud, P. (2010). Genome-wide identification of new imprinted genes. Briefings in functional genomics *9*, 304-314.

Holstege, J.C. (1987). Brainstem projections to lumbar motoneurons in rat--II. An ultrastructural study by means of the anterograde transport of wheat germ agglutinin coupled to horseradish peroxidase and using the tetramethyl benzidine reaction. Neuroscience *21*, 369-376.

Hornung, J.P. (2003). The human raphe nuclei and the serotonergic system. Journal of chemical neuroanatomy *26*, 331-343.

Horsthemke, B., and Buiting, K. (2006). Imprinting defects on human chromosome 15. Cytogenetic and genome research *113*, 292-299.

Horsthemke, B., and Buiting, K. (2008). Genomic imprinting and imprinting defects in humans. Advances in genetics *61*, 225-246.

Hotchkiss, R.D. (1948). The quantitative separation of purines, pyrimidines, and nucleosides by paper chromatography. The Journal of biological chemistry *175*, 315-332.

Huang, P.H., Plass, C., and Chen, C.S. (2011). Effects of Histone Deacetylase Inhibitors on Modulating H3K4 Methylation Marks - A Novel Cross-Talk Mechanism between Histone-Modifying Enzymes. Molecular and cellular pharmacology *3*, 39-43.

Huguet, G., Ey, E., and Bourgeron, T. (2013). The genetic landscapes of autism

spectrum disorders. Annual review of genomics and human genetics *14*, 191-213.

Hull, E.E., Montgomery, M.R., and Leyva, K.J. (2016). HDAC Inhibitors as Epigenetic Regulators of the Immune System: Impacts on Cancer Therapy and Inflammatory Diseases. BioMed research international *2016*, 8797206.

Irizarry, R.A., Wu, H., and Feinberg, A.P. (2009). A species-generalized probabilistic model-based definition of CpG islands. Mammalian genome : official journal of the International Mammalian Genome Society *20*, 674-680.

Jones, B.E. (2003). Arousal systems. Frontiers in bioscience : a journal and virtual library *8*, s438-451.

Kaneda, M., Sado, T., Hata, K., Okano, M., Tsujimoto, N., Li, E., and Sasaki, H. (2004). Role of de novo DNA methyltransferases in initiation of genomic imprinting and X-chromosome inactivation. Cold Spring Harbor symposia on quantitative biology *69*, 125-129.

Kang, D., Han, J., Talley, E.M., Bayliss, D.A., and Kim, D. (2004). Functional expression of TASK-1/TASK-3 heteromers in cerebellar granule cells. The Journal of physiology *554*, 64-77.

Kantarjian, H., Issa, J.P., Rosenfeld, C.S., Bennett, J.M., Albitar, M., DiPersio, J., Klimek, V., Slack, J., de Castro, C., Ravandi, F.*, et al.* (2006). Decitabine improves patient outcomes in myelodysplastic syndromes: results of a phase III randomized study. Cancer *106*, 1794-1803.

Karschin, C., Wischmeyer, E., Preisig-Muller, R., Rajan, S., Derst, C., Grzeschik, K.H., Daut, J., and Karschin, A. (2001). Expression pattern in brain of TASK-1, TASK-3, and a tandem pore domain K(+) channel subunit, TASK-5, associated with the central auditory nervous system. Molecular and cellular neurosciences *18*, 632-648.

Kaviani, H., Gray, J.A., Checkley, S.A., Raven, P.W., Wilson, G.D., and Kumari, V. (2004). Affective modulation of the startle response in depression: influence of the

severity of depression, anhedonia, and anxiety. Journal of affective disorders *83*, 21-31.

Kebede, A.F., Schneider, R., and Daujat, S. (2015). Novel types and sites of histone modifications emerge as players in the transcriptional regulation contest. FEBS Journal *282*, 1658-1674.

Kehne, J.H., Boulis, N.M., and Davis, M. (1991). Effects of the phosphodiesterase inhibitor rolipram on the acoustic startle response in rats. Psychopharmacology *105*, 27-36.

Kelsey, G., and Feil, R. (2013). New insights into establishment and maintenance of DNA methylation imprints in mammals. Philosophical transactions of the Royal Society of London Series B, Biological sciences *368*, 20110336.

Keverne, E.B., and Curley, J.P. (2008). Epigenetics, brain evolution and behaviour. Frontiers in neuroendocrinology *29*, 398-412.

Khakpour-Taleghani, B., Lashgari, R., Motamedi, F., and Naghdi, N. (2009). Effect of reversible inactivation of locus ceruleus on spatial reference and working memory. Neuroscience *158*, 1284-1291.

Khatib, H., Zaitoun, I., and Kim, E.S. (2007). Comparative analysis of sequence characteristics of imprinted genes in human, mouse, and cattle. Mammalian genome : official journal of the International Mammalian Genome Society *18*, 538-547.

Kim, Y., Bang, H., and Kim, D. (2000). TASK-3, a new member of the tandem pore K(+) channel family. The Journal of biological chemistry *275*, 9340-9347.

Koch, M. (1999). The neurobiology of startle. Progress in neurobiology *59*, 107-128.

Koch, M., and Schnitzler, H.U. (1997). The acoustic startle response in rats--circuits mediating evocation, inhibition and potentiation. Behavioural brain research *89*, 35-

49.

Kohl, S., Heekeren, K., Klosterkotter, J., and Kuhn, J. (2013). Prepulse inhibition in psychiatric disorders--apart from schizophrenia. Journal of psychiatric research *47*, 445-452.

Kono, T. (2006). Genomic imprinting is a barrier to parthenogenesis in mammals. Cytogenetic and genome research *113*, 31-35.

Korb, E., and Finkbeiner, S. (2011). Arc in synaptic plasticity: from gene to behavior. Trends Neurosci *34*, 591-598.

Kornberg, R.D., and Thomas, J.O. (1974). Chromatin structure; oligomers of the histones. Science *184*, 865-868.

Kotzot, D., Schmitt, S., Bernasconi, F., Robinson, W.P., Lurie, I.W., Ilyina, H., Mehes, K., Hamel, B.C., Otten, B.J., Hergersberg, M.*, et al.* (1995). Uniparental disomy 7 in Silver-Russell syndrome and primordial growth retardation. Human molecular genetics *4*, 583-587.

Kouzarides, T. (2007). Chromatin Modifications and Their Function. Cell *128*, 693-705.

Krase, W., Koch, M., and Schnitzler, H.U. (1994). Substance P is involved in the sensitization of the acoustic startle response by footshocks in rats. Behavioural brain research *63*, 81-88.

Kuznetsova, E.G., Amstislavskaya, T.G., Shefer, E.A., and Popova, N.K. (2006). Effect of 5-HT2C receptor antagonist RS 102221 on mouse behavior. Bulletin of experimental biology and medicine *142*, 76-79.

Kwiat, G.C., and Basbaum, A.I. (1992). The origin of brainstem noradrenergic and serotonergic projections to the spinal cord dorsal horn in the rat. Somatosensory &

motor research *9*, 157-173.

Lawrence, M., Daujat, S., and Schneider, R. (2016). Lateral Thinking: How Histone Modifications Regulate Gene Expression. Trends in genetics : TIG *32*, 42-56.

Lee, Y., Lopez, D.E., Meloni, E.G., and Davis, M. (1996). A primary acoustic startle pathway: obligatory role of cochlear root neurons and the nucleus reticularis pontis caudalis. The Journal of neuroscience : the official journal of the Society for Neuroscience *16*, 3775-3789.

Leighton, P.A., Saam, J.R., Ingram, R.S., Stewart, C.L., and Tilghman, S.M. (1995). An enhancer deletion affects both H19 and Igf2 expression. Genes & development *9*, 2079-2089.

Lesage, F., and Lazdunski, M. (2000). Molecular and functional properties of two-pore-domain potassium channels. American journal of physiology Renal physiology *279*, F793-801.

Leszinski, G., Gezer, U., Siegele, B., Stoetzer, O., and Holdenrieder, S. (2012). Relevance of histone marks H3K9me3 and H4K20me3 in cancer. Anticancer research *32*, 2199-2205.

Li, E., Bestor, T.H., and Jaenisch, R. (1992). Targeted mutation of the DNA methyltransferase gene results in embryonic lethality. Cell *69*, 915-926.

Li, E., and Zhang, Y. (2014). DNA methylation in mammals. Cold Spring Harbor perspectives in biology *6*, a019133.

Li, G., Margueron, R., Hu, G., Stokes, D., Wang, Y.H., and Reinberg, D. (2010). Highly compacted chromatin formed in vitro reflects the dynamics of transcription activation in vivo. Molecular cell *38*, 41-53.

Li, Z.K., Wang, L.Y., Wang, L.B., Feng, G.H., Yuan, X.W., Liu, C., Xu, K., Li, Y.H., Wan, H.F., Zhang, Y.*, et al.* (2018). Generation of Bimaternal and Bipaternal Mice

from Hypomethylated Haploid ESCs with Imprinting Region Deletions. Cell stem cell *23*, 665-676 e664.

Linden, A.M., Sandu, C., Aller, M.I., Vekovischeva, O.Y., Rosenberg, P.H., Wisden, W., and Korpi, E.R. (2007). TASK-3 knockout mice exhibit exaggerated nocturnal activity, impairments in cognitive functions, and reduced sensitivity to inhalation anesthetics. The Journal of pharmacology and experimental therapeutics *323*, 924-934.

Lister, R., Pelizzola, M., Dowen, R.H., Hawkins, R.D., Hon, G., Tonti-Filippini, J., Nery, J.R., Lee, L., Ye, Z., Ngo, Q.M.*, et al.* (2009). Human DNA methylomes at base resolution show widespread epigenomic differences. Nature *462*, 315-322.

Livak, K.J., and Schmittgen, T.D. (2001). Analysis of relative gene expression data using real-time quantitative PCR and the 2(-Delta Delta C(T)) Method. Methods *25*, 402-408.

Local, A., Huang, H., Albuquerque, C.P., Singh, N., Lee, A.Y., Wang, W., Wang, C., Hsia, J.E., Shiau, A.K., Ge, K.*, et al.* (2018). Identification of H3K4me1-associated proteins at mammalian enhancers. Nature genetics *50*, 73-82.

Lucifero, D., Mertineit, C., Clarke, H.J., Bestor, T.H., and Trasler, J.M. (2002). Methylation dynamics of imprinted genes in mouse germ cells. Genomics *79*, 530-538.

Luethy, A., Boghosian, J.D., Srikantha, R., and Cotten, J.F. (2017). Halogenated Ether, Alcohol, and Alkane Anesthetics Activate TASK-3 Tandem Pore Potassium Channels Likely through a Common Mechanism. Molecular pharmacology *91*, 620-629.

Luger, K., Mäder, A.W., Richmond, R.K., Sargent, D.F., and Richmond, T.J. (1997). Crystal structure of the nucleosome core particle at 2.8 Å resolution. Nature *389*, 251.

Mahadevan, L.C., Willis, A.C., and Barratt, M.J. (1991). Rapid histone H3

phosphorylation in response to growth factors, phorbol esters, okadaic acid, and protein synthesis inhibitors. Cell *65*, 775-783.

Maingret, F., Patel, A.J., Lazdunski, M., and Honore, E. (2001). The endocannabinoid anandamide is a direct and selective blocker of the background K(+) channel TASK-1. The EMBO journal *20*, 47-54.

Mancini-Dinardo, D., Steele, S.J., Levorse, J.M., Ingram, R.S., and Tilghman, S.M. (2006). Elongation of the Kcnq1ot1 transcript is required for genomic imprinting of neighboring genes. Genes & development *20*, 1268-1282.

Mandel, J.L., and Chambon, P. (1979). DNA methylation: organ specific variations in the methylation pattern within and around ovalbumin and other chicken genes. Nucleic acids research *7*, 2081-2103.

Manto, M., Bower, J.M., Conforto, A.B., Delgado-Garcia, J.M., da Guarda, S.N., Gerwig, M., Habas, C., Hagura, N., Ivry, R.B., Marien, P.*, et al.* (2012). Consensus paper: roles of the cerebellum in motor control--the diversity of ideas on cerebellar involvement in movement. Cerebellum *11*, 457-487.

Margueron, R., Trojer, P., and Reinberg, D. (2005). The key to development: interpreting the histone code? Current opinion in genetics & development *15*, 163-176.

Marinc, C., Derst, C., Pruss, H., and Veh, R.W. (2014). Immunocytochemical localization of TASK-3 protein (K2P9.1) in the rat brain. Cellular and molecular neurobiology *34*, 61-70.

Marinc, C., Preisig-Muller, R., Pruss, H., Derst, C., and Veh, R.W. (2011). Immunocytochemical localization of TASK-3 (K(2P)9.1) channels in monoaminergic and cholinergic neurons. Cellular and molecular neurobiology *31*, 323-335.

Martienssen, R., and Moazed, D. (2015). RNAi and heterochromatin assembly. Cold

Spring Harbor perspectives in biology *7*, a019323.

Martinez, F.P., Cruz, R., Lu, F., Plasschaert, R., Deng, Z., Rivera-Molina, Y.A., Bartolomei, M.S., Lieberman, P.M., and Tang, Q. (2014). CTCF binding to the first intron of the major immediate early (MIE) gene of human cytomegalovirus (HCMV) negatively regulates MIE gene expression and HCMV replication. Journal of virology *88*, 7389-7401.

McGhee, J.D., and Ginder, G.D. (1979). Specific DNA methylation sites in the vicinity of the chicken beta-globin genes. Nature *280*, 419-420.

McGrath, J., and Solter, D. (1984a). Completion of mouse embryogenesis requires both the maternal and paternal genomes. Cell *37*, 179-183.

McGrath, J., and Solter, D. (1984b). Inability of mouse blastomere nuclei transferred to enucleated zygotes to support development in vitro. Science *226*, 1317-1319.

Meadows, H.J., and Randall, A.D. (2001). Functional characterisation of human TASK-3, an acid-sensitive two-pore domain potassium channel. Neuropharmacology *40*, 551-559.

Meehan, R.R., Lewis, J.D., McKay, S., Kleiner, E.L., and Bird, A.P. (1989). Identification of a mammalian protein that binds specifically to DNA containing methylated CpGs. Cell *58*, 499-507.

Meuth, S.G., Budde, T., Kanyshkova, T., Broicher, T., Munsch, T., and Pape, H.C. (2003). Contribution of TWIK-related acid-sensitive K+ channel 1 (TASK1) and TASK3 channels to the control of activity modes in thalamocortical neurons. The Journal of neuroscience : the official journal of the Society for Neuroscience *23*, 6460-6469.

Mochida, G.H., Mahajnah, M., Hill, A.D., Basel-Vanagaite, L., Gleason, D., Hill, R.S., Bodell, A., Crosier, M., Straussberg, R., and Walsh, C.A. (2009). A truncating mutation of TRAPPC9 is associated with autosomal-recessive intellectual disability

and postnatal microcephaly. American journal of human genetics *85*, 897-902.

Moore, T., and Haig, D. (1991). Genomic imprinting in mammalian development: a parental tug-of-war. Trends in genetics : TIG *7*, 45-49.

Morison, I.M., Ramsay, J.P., and Spencer, H.G. (2005). A census of mammalian imprinting. Trends in genetics : TIG *21*, 457-465.

Mu, D., Chen, L., Zhang, X., See, L.H., Koch, C.M., Yen, C., Tong, J.J., Spiegel, L., Nguyen, K.C., Servoss, A.*, et al.* (2003). Genomic amplification and oncogenic properties of the KCNK9 potassium channel gene. Cancer cell *3*, 297-302.

Mulkey, D.K., Talley, E.M., Stornetta, R.L., Siegel, A.R., West, G.H., Chen, X., Sen, N., Mistry, A.M., Guyenet, P.G., and Bayliss, D.A. (2007). TASK channels determine pH sensitivity in select respiratory neurons but do not contribute to central respiratory chemosensitivity. The Journal of neuroscience : the official journal of the Society for Neuroscience *27*, 14049-14058.

Nakamura, T., Liu, Y.J., Nakashima, H., Umehara, H., Inoue, K., Matoba, S., Tachibana, M., Ogura, A., Shinkai, Y., and Nakano, T. (2012). PGC7 binds histone H3K9me2 to protect against conversion of 5mC to 5hmC in early embryos. Nature *486*, 415-419.

Nemunaitis, J.J., Orr, D., Eager, R., Cunningham, C.C., Williams, A., Mennel, R., Grove, W., and Olson, S. (2003). Phase I study of oral CI-994 in combination with gemcitabine in treatment of patients with advanced cancer. Cancer journal *9*, 58-66.

Nicholls, R.D., Knoll, J.H., Butler, M.G., Karam, S., and Lalande, M. (1989). Genetic imprinting suggested by maternal heterodisomy in nondeletion Prader-Willi syndrome. Nature *342*, 281-285.

Nyren, P., Pettersson, B., and Uhlen, M. (1993). Solid phase DNA minisequencing by an enzymatic luminometric inorganic pyrophosphate detection assay. Analytical

biochemistry *208*, 171-175.

Olins, A.L., and Olins, D.E. (1974). Spheroid chromatin units (v bodies). Science *183*, 330-332.

Otto, S.P., and Gerstein, A.C. (2008). The evolution of haploidy and diploidy. Current biology : CB *18*, R1121-1124.

Oudet, P., Gross-Bellard, M., and Chambon, P. (1975). Electron microscopic and biochemical evidence that chromatin structure is a repeating unit. Cell *4*, 281-300.

Pang, D.S., Robledo, C.J., Carr, D.R., Gent, T.C., Vyssotski, A.L., Caley, A., Zecharia, A.Y., Wisden, W., Brickley, S.G., and Franks, N.P. (2009). An unexpected role for TASK-3 potassium channels in network oscillations with implications for sleep mechanisms and anesthetic action. Proceedings of the National Academy of Sciences of the United States of America *106*, 17546-17551.

Papazian, D.M., Schwarz, T.L., Tempel, B.L., Jan, Y.N., and Jan, L.Y. (1987). Cloning of genomic and complementary DNA from Shaker, a putative potassium channel gene from Drosophila. Science *237*, 749-753.

Pask, A.J., Papenfuss, A.T., Ager, E.I., McColl, K.A., Speed, T.P., and Renfree, M.B. (2009). Analysis of the platypus genome suggests a transposon origin for mammalian imprinting. Genome biology *10*, R1.

Patel, A.J., and Honore, E. (2001a). Anesthetic-sensitive 2P domain K+ channels. Anesthesiology *95*, 1013-1021.

Patel, A.J., and Honore, E. (2001b). Molecular physiology of oxygen-sensitive potassium channels. The European respiratory journal *18*, 221-227.

Pauer, L.R., Olivares, J., Cunningham, C., Williams, A., Grove, W., Kraker, A., Olson, S., and Nemunaitis, J. (2004). Phase I study of oral CI-994 in combination with carboplatin and paclitaxel in the treatment of patients with advanced solid tumors.

Cancer investigation *22*, 886-896.

Payer, B., and Lee, J.T. (2008). X chromosome dosage compensation: how mammals keep the balance. Annual review of genetics *42*, 733-772.

Peall, K.J., Smith, D.J., Kurian, M.A., Wardle, M., Waite, A.J., Hedderly, T., Lin, J.P., Smith, M., Whone, A., Pall, H.*, et al.* (2013). SGCE mutations cause psychiatric disorders: clinical and genetic characterization. Brain : a journal of neurology *136*, 294-303.

Perez, J.D., Rubinstein, N.D., and Dulac, C. (2016). New Perspectives on Genomic Imprinting, an Essential and Multifaceted Mode of Epigenetic Control in the Developing and Adult Brain. Annual review of neuroscience *39*, 347-384.

Perez, J.D., Rubinstein, N.D., Fernandez, D.E., Santoro, S.W., Needleman, L.A., Ho-Shing, O., Choi, J.J., Zirlinger, M., Chen, S.K., Liu, J.S.*, et al.* (2015). Quantitative and functional interrogation of parent-of-origin allelic expression biases in the brain. eLife *4*, e07860.

Perucca, E. (2002). Pharmacological and therapeutic properties of valproate: a summary after 35 years of clinical experience. CNS drugs *16*, 695-714.

Portela, A., and Esteller, M. (2010). Epigenetic modifications and human disease. Nature biotechnology *28*, 1057-1068.

Prakash, S., Foster, B.J., Meyer, M., Wozniak, A., Heilbrun, L.K., Flaherty, L., Zalupski, M., Radulovic, L., Valdivieso, M., and LoRusso, P.M. (2001). Chronic oral administration of CI-994: a phase 1 study. Investigational new drugs *19*, 1-11.

Radyushkin, K., Anokhin, K., Meyer, B.I., Jiang, Q., Alvarez-Bolado, G., and Gruss, P. (2005). Genetic ablation of the mammillary bodies in the Foxb1 mutant mouse leads to selective deficit of spatial working memory. The European journal of neuroscience *21*, 219-229.

Radyushkin, K., El-Kordi, A., Boretius, S., Castaneda, S., Ronnenberg, A., Reim, K., Bickeboller, H., Frahm, J., Brose, N., and Ehrenreich, H. (2010). Complexin2 null mutation requires a 'second hit' for induction of phenotypic changes relevant to schizophrenia. Genes, brain, and behavior *9*, 592-602.

Rajan, S., Preisig-Müller, R., Wischmeyer, E., Nehring, R., Hanley, P.J., Renigunta, V., Musset, B., Schlichthörl, G., Derst, C., Karschin, A.*, et al.* (2002). Interaction with 14-3-3 proteins promotes functional expression of the potassium channels TASK-1 and TASK-3. The Journal of physiology *545*, 13-26.

Rajan, S., Wischmeyer, E., Xin Liu, G., Preisig-Muller, R., Daut, J., Karschin, A., and Derst, C. (2000). TASK-3, a novel tandem pore domain acid-sensitive K+ channel. An extracellular histiding as pH sensor. The Journal of biological chemistry *275*, 16650-16657.

Reik, W., and Walter, J. (2001). Genomic imprinting: parental influence on the genome. Nature reviews Genetics *2*, 21-32.

Renfree, M.B., Hore, T.A., Shaw, G., Graves, J.A., and Pask, A.J. (2009a). Evolution of genomic imprinting: insights from marsupials and monotremes. Annual review of genomics and human genetics *10*, 241-262.

Renfree, M.B., Papenfuss, A.T., Shaw, G., and Pask, A.J. (2009b). Eggs, embryos and the evolution of imprinting: insights from the platypus genome. Reproduction, fertility, and development *21*, 935-942.

Reppert, S.M., and Weaver, D.R. (2002). Coordination of circadian timing in mammals. Nature *418*, 935-941.

Rieusset, A., Schaller, F., Unmehopa, U., Matarazzo, V., Watrin, F., Linke, M., Georges, B., Bischof, J., Dijkstra, F., Bloemsma, M.*, et al.* (2013). Stochastic loss of silencing of the imprinted Ndn/NDN allele, in a mouse model and humans with prader-willi syndrome, has functional consequences. PLoS genetics *9*, e1003752.

Robinson, M.D., Stirzaker, C., Statham, A.L., Coolen, M.W., Song, J.Z., Nair, S.S., Strbenac, D., Speed, T.P., and Clark, S.J. (2010). Evaluation of affinity-based genome-wide DNA methylation data: effects of CpG density, amplification bias, and copy number variation. Genome research *20*, 1719-1729.

Roth, S.Y., Denu, J.M., and Allis, C.D. (2001). Histone acetyltransferases. Annual review of biochemistry *70*, 81-120.

Rougier, N., Bourc'his, D., Gomes, D.M., Niveleau, A., Plachot, M., Paldi, A., and Viegas-Pequignot, E. (1998). Chromosome methylation patterns during mammalian preimplantation development. Genes & development *12*, 2108-2113.

Ruf, N., Bahring, S., Galetzka, D., Pliushch, G., Luft, F.C., Nurnberg, P., Haaf, T., Kelsey, G., and Zechner, U. (2007). Sequence-based bioinformatic prediction and QUASEP identify genomic imprinting of the KCNK9 potassium channel gene in mouse and human. Human molecular genetics *16*, 2591-2599.

Russell, A. (1954). A syndrome of intra-uterine dwarfism recognizable at birth with cranio-facial dysostosis, disproportionately short arms, and other anomalies (5 examples). Proceedings of the Royal Society of Medicine *47*, 1040-1044.

Sabari, B.R., Zhang, D., Allis, C.D., and Zhao, Y. (2017). Metabolic regulation of gene expression through histone acylations. Nature reviews Molecular cell biology *18*, 90-101.

Sabbadini, M., and Yost, C.S. (2009). Molecular biology of background K channels: insights from K(2P) knockout mice. Journal of molecular biology *385*, 1331-1344.

Sadakierska-Chudy, A., Kostrzewa, R.M., and Filip, M. (2015). A comprehensive view of the epigenetic landscape part I: DNA methylation, passive and active DNA demethylation pathways and histone variants. Neurotoxicity research *27*, 84-97.

Sahoo, T., del Gaudio, D., German, J.R., Shinawi, M., Peters, S.U., Person, R.E.,

Garnica, A., Cheung, S.W., and Beaudet, A.L. (2008). Prader-Willi phenotype caused by paternal deficiency for the HBII-85 C/D box small nucleolar RNA cluster. Nature genetics *40*, 719-721.

Samuels, E.R., and Szabadi, E. (2008). Functional neuroanatomy of the noradrenergic locus coeruleus: its roles in the regulation of arousal and autonomic function part II: physiological and pharmacological manipulations and pathological alterations of locus coeruleus activity in humans. Current neuropharmacology *6*, 254-285.

Santoro, F., and Barlow, D.P. (2011). Developmental control of imprinted expression by macro non-coding RNAs. Seminars in cell & developmental biology *22*, 328-335.

Santos, F., and Dean, W. (2004). Epigenetic reprogramming during early development in mammals. Reproduction *127*, 643-651.

Saper, C.B., Scammell, T.E., and Lu, J. (2005). Hypothalamic regulation of sleep and circadian rhythms. Nature *437*, 1257-1263.

Sara, S.J. (2015). Locus Coeruleus in time with the making of memories. Current opinion in neurobiology *35*, 87-94.

Sarnyai, Z., Sibille, E.L., Pavlides, C., Fenster, R.J., McEwen, B.S., and Toth, M. (2000). Impaired hippocampal-dependent learning and functional abnormalities in the hippocampus in mice lacking serotonin(1A) receptors. Proceedings of the National Academy of Sciences of the United States of America *97*, 14731-14736.

Saxonov, S., Berg, P., and Brutlag, D.L. (2006). A genome-wide analysis of CpG dinucleotides in the human genome distinguishes two distinct classes of promoters. Proceedings of the National Academy of Sciences of the United States of America *103*, 1412-1417.

Schanen, N.C. (2006). Epigenetics of autism spectrum disorders. Human molecular

genetics *15 Spec No 2*, R138-150.

Schuerger, R.J., and Balaban, C.D. (1993). Immunohistochemical demonstration of regionally selective projections from locus coeruleus to the vestibular nuclei in rats. Experimental brain research *92*, 351-359.

Schultz, D.C., Ayyanathan, K., Negorev, D., Maul, G.G., and Rauscher, F.J., 3rd (2002). SETDB1: a novel KAP-1-associated histone H3, lysine 9-specific methyltransferase that contributes to HP1-mediated silencing of euchromatic genes by KRAB zinc-finger proteins. Genes & development *16*, 919-932.

Seki, Y., Hayashi, K., Itoh, K., Mizugaki, M., Saitou, M., and Matsui, Y. (2005). Extensive and orderly reprogramming of genome-wide chromatin modifications associated with specification and early development of germ cells in mice. Developmental biology *278*, 440-458.

Shahbazian, M.D., and Grunstein, M. (2007). Functions of site-specific histone acetylation and deacetylation. Annual review of biochemistry *76*, 75-100.

Singh, P., Wu, X., Lee, D.H., Li, A.X., Rauch, T.A., Pfeifer, G.P., Mann, J.R., and Szabo, P.E. (2011). Chromosome-wide analysis of parental allele-specific chromatin and DNA methylation. Molecular and cellular biology *31*, 1757-1770.

Sleutels, F., Zwart, R., and Barlow, D.P. (2002). The non-coding Air RNA is required for silencing autosomal imprinted genes. Nature *415*, 810-813.

Smith, Z.D., Chan, M.M., Mikkelsen, T.S., Gu, H., Gnirke, A., Regev, A., and Meissner, A. (2012). A unique regulatory phase of DNA methylation in the early mammalian embryo. Nature *484*, 339-344.

Soejima, H., and Higashimoto, K. (2013). Epigenetic and genetic alterations of the imprinting disorder Beckwith-Wiedemann syndrome and related disorders. Journal of human genetics *58*, 402-409.

Stadler, M.B., Murr, R., Burger, L., Ivanek, R., Lienert, F., Scholer, A., van Nimwegen, E., Wirbelauer, C., Oakeley, E.J., Gaidatzis, D., *et al.* (2011). DNA-binding factors shape the mouse methylome at distal regulatory regions. Nature *480*, 490-495.

Strahl, B.D., and Allis, C.D. (2000). The language of covalent histone modifications. Nature *403*, 41-45.

Surani, M.A., Barton, S.C., and Norris, M.L. (1984). Development of reconstituted mouse eggs suggests imprinting of the genome during gametogenesis. Nature *308*, 548-550.

Surani, M.A., Barton, S.C., and Norris, M.L. (1986). Nuclear transplantation in the mouse: heritable differences between parental genomes after activation of the embryonic genome. Cell *45*, 127-136.

Suzuki, S., Renfree, M.B., Pask, A.J., Shaw, G., Kobayashi, S., Kohda, T., Kaneko-Ishino, T., and Ishino, F. (2005). Genomic imprinting of IGF2, p57(KIP2) and PEG1/MEST in a marsupial, the tammar wallaby. Mechanisms of development *122*, 213-222.

Swonger, A.K., and Rech, R.H. (1972). Serotonergic and cholinergic involvement in habituation of activity and spontaneous alternation of rats in a Y maze. Journal of comparative and physiological psychology *81*, 509-522.

Szabadi, E. (2012). Modulation of physiological reflexes by pain: role of the locus coeruleus. Frontiers in integrative neuroscience *6*, 94.

Taft, R.J., Pang, K.C., Mercer, T.R., Dinger, M., and Mattick, J.S. (2010). Non-coding RNAs: regulators of disease. The Journal of pathology *220*, 126-139.

Tahiliani, M., Koh, K.P., Shen, Y., Pastor, W.A., Bandukwala, H., Brudno, Y., Agarwal, S., Iyer, L.M., Liu, D.R., Aravind, L., *et al.* (2009). Conversion of 5-methylcytosine to 5-hydroxymethylcytosine in mammalian DNA by MLL partner TET1. Science *324*,

930-935.

Takahashi, H., Hashimoto, R., Iwase, M., Ishii, R., Kamio, Y., and Takeda, M. (2011). Prepulse inhibition of startle response: recent advances in human studies of psychiatric disease. Clinical psychopharmacology and neuroscience : the official scientific journal of the Korean College of Neuropsychopharmacology *9*, 102-110.

Takai, D., and Jones, P.A. (2002). Comprehensive analysis of CpG islands in human chromosomes 21 and 22. Proceedings of the National Academy of Sciences of the United States of America *99*, 3740-3745.

Takeuchi, T., Duszkiewicz, A.J., Sonneborn, A., Spooner, P.A., Yamasaki, M., Watanabe, M., Smith, C.C., Fernandez, G., Deisseroth, K., Greene, R.W.*, et al.* (2016). Locus coeruleus and dopaminergic consolidation of everyday memory. Nature *537*, 357-362.

Talley, E.M., Sirois, J.E., Lei, Q., and Bayliss, D.A. (2003). Two-pore-Domain (KCNK) potassium channels: dynamic roles in neuronal function. The Neuroscientist : a review journal bringing neurobiology, neurology and psychiatry *9*, 46-56.

Talley, E.M., Solorzano, G., Lei, Q., Kim, D., and Bayliss, D.A. (2001). Cns distribution of members of the two-pore-domain (KCNK) potassium channel family. The Journal of neuroscience : the official journal of the Society for Neuroscience *21*, 7491-7505.

Tan, L., and Shi, Y.G. (2012). Tet family proteins and 5-hydroxymethylcytosine in development and disease. Development *139*, 1895-1902.

Tang, H.M., Kuay, K.T., Koh, P.F., Asad, M., Tan, T.Z., Chung, V.Y., Lee, S.C., Thiery, J.P., and Huang, R.J. (2016). An epithelial marker promoter induction screen identifies histone deacetylase inhibitors to restore epithelial differentiation and abolishes anchorage independence growth in cancers. Cell death discovery *2*,

16041.

Tattersall, T.L., Stratton, P.G., Coyne, T.J., Cook, R., Silberstein, P., Silburn, P.A., Windels, F., and Sah, P. (2014). Imagined gait modulates neuronal network dynamics in the human pedunculopontine nucleus. Nature neuroscience *17*, 449-454.

Tempel, B.L., Papazian, D.M., Schwarz, T.L., Jan, Y.N., and Jan, L.Y. (1987). Sequence of a probable potassium channel component encoded at Shaker locus of Drosophila. Science *237*, 770-775.

Thorvaldsen, J.L., Duran, K.L., and Bartolomei, M.S. (1998). Deletion of the H19 differentially methylated domain results in loss of imprinted expression of H19 and Igf2. Genes & development *12*, 3693-3702.

Tomizawa, S., Kobayashi, H., Watanabe, T., Andrews, S., Hata, K., Kelsey, G., and Sasaki, H. (2011). Dynamic stage-specific changes in imprinted differentially methylated regions during early mammalian development and prevalence of non-CpG methylation in oocytes. Development *138*, 811-820.

Torborg, C.L., Berg, A.P., Jeffries, B.W., Bayliss, D.A., and McBain, C.J. (2006). TASK-like conductances are present within hippocampal CA1 stratum oriens interneuron subpopulations. The Journal of neuroscience : the official journal of the Society for Neuroscience *26*, 7362-7367.

Treppendahl, M.B., Kristensen, L.S., and Gronbaek, K. (2014). Predicting response to epigenetic therapy. The Journal of clinical investigation *124*, 47-55.

Tropberger, P., and Schneider, R. (2013). Scratching the (lateral) surface of chromatin regulation by histone modifications. Nature structural & molecular biology *20*, 657-661.

Ubeda, F., and Gardner, A. (2015). Mother and offspring in conflict: why not? PLoS biology *13*, e1002084.

Varmuza, S., and Mann, M. (1994). Genomic imprinting--defusing the ovarian time bomb. Trends in genetics : TIG *10*, 118-123.

Veale, E.L., Hassan, M., Walsh, Y., Al-Moubarak, E., and Mathie, A. (2014). Recovery of current through mutated TASK3 potassium channels underlying Birk Barel syndrome. Molecular pharmacology *85*, 397-407.

Von Coelln, R., Thomas, B., Savitt, J.M., Lim, K.L., Sasaki, M., Hess, E.J., Dawson, V.L., and Dawson, T.M. (2004). Loss of locus coeruleus neurons and reduced startle in parkin null mice. Proceedings of the National Academy of Sciences of the United States of America *101*, 10744-10749.

Waddington (1942). The epigenotype.

Wagner, T., and Mack, A. (1998). Membrane properties of giant neurons in the caudal pontine reticular formation in vitro. Neuroreport *9*, 1211-1215.

Walsh, C.P., Chaillet, J.R., and Bestor, T.H. (1998). Transcription of IAP endogenous retroviruses is constrained by cytosine methylation. Nature genetics *20*, 116-117.

Wan, L.B., and Bartolomei, M.S. (2008). Regulation of imprinting in clusters: noncoding RNAs versus insulators. Advances in genetics *61*, 207-223.

Watt, F., and Molloy, P.L. (1988). Cytosine methylation prevents binding to DNA of a HeLa cell transcription factor required for optimal expression of the adenovirus major late promoter. Genes & development *2*, 1136-1143.

Weber, M., Schmitt, A., Wischmeyer, E., and Doring, F. (2008). Excitability of pontine startle processing neurones is regulated by the two-pore-domain K+ channel TASK-3 coupled to 5-HT2C receptors. The European journal of neuroscience *28*, 931-940.

Weksberg, R., Shuman, C., and Beckwith, J.B. (2010). Beckwith-Wiedemann syndrome. European journal of human genetics : EJHG *18*, 8-14.

Wiedemann (1964). Complexe malformatif familial avec hernie ombilicale et macroglossie. Un syndrome nouveau ?". Journal de genetique humaine *13: 223-232.*

Wilkins, J.F., and Haig, D. (2003). What good is genomic imprinting: the function of parent-specific gene expression. Nature reviews Genetics *4*, 359-368.

Williams, C.A., and Frias, J.L. (1982). The Angelman ("happy puppet") syndrome. American journal of medical genetics *11*, 453-460.

Wolf, J.B., and Hager, R. (2006). A maternal-offspring coadaptation theory for the evolution of genomic imprinting. PLoS biology *4*, e380.

Wong, C.M., Wong, C.C., Ng, Y.L., Au, S.L., Ko, F.C., and Ng, I.O. (2011). Transcriptional repressive H3K9 and H3K27 methylations contribute to DNMT1-mediated DNA methylation recovery. PloS one *6*, e16702.

Wright, P.D., Veale, E.L., McCoull, D., Tickle, D.C., Large, J.M., Ococks, E., Gothard, G., Kettleborough, C., Mathie, A., and Jerman, J. (2017). Terbinafine is a novel and selective activator of the two-pore domain potassium channel TASK3. Biochemical and biophysical research communications *493*, 444-450.

Wutz, A., and Jaenisch, R. (2000). A shift from reversible to irreversible X inactivation is triggered during ES cell differentiation. Molecular cell *5*, 695-705.

Wutz, A., Smrzka, O.W., Schweifer, N., Schellander, K., Wagner, E.F., and Barlow, D.P. (1997). Imprinted expression of the Igf2r gene depends on an intronic CpG island. Nature *389*, 745-749.

Wysocka, J., Swigut, T., Xiao, H., Milne, T.A., Kwon, S.Y., Landry, J., Kauer, M., Tackett, A.J., Chait, B.T., Badenhorst, P.*, et al.* (2006). A PHD finger of NURF couples histone H3 lysine 4 trimethylation with chromatin remodelling. Nature *442*, 86-90.

Xie, W., Barr, C.L., Kim, A., Yue, F., Lee, A.Y., Eubanks, J., Dempster, E.L., and Ren, B. (2012). Base-resolution analyses of sequence and parent-of-origin dependent

DNA methylation in the mouse genome. Cell *148*, 816-831.

Yang, X.J., and Seto, E. (2003). Collaborative spirit of histone deacetylases in regulating chromatin structure and gene expression. Current opinion in genetics & development *13*, 143-153.

Zanzouri, M., Lauritzen, I., Duprat, F., Mazzuca, M., Lesage, F., Lazdunski, M., and Patel, A. (2006). Membrane potential-regulated transcription of the resting K+ conductance TASK-3 via the calcineurin pathway. The Journal of biological chemistry *281*, 28910-28918.

Zhang, S., Fujita, Y., Matsuzaki, R., and Yamashita, T. (2018). Class I histone deacetylase (HDAC) inhibitor CI-994 promotes functional recovery following spinal cord injury. Cell death & disease *9*, 460.

Zilberman, D., and Henikoff, S. (2007). Genome-wide analysis of DNA methylation patterns. Development *134*, 3959-3965.

Zimprich, A., Grabowski, M., Asmus, F., Naumann, M., Berg, D., Bertram, M., Scheidtmann, K., Kern, P., Winkelmann, J., Muller-Myhsok, B.*, et al.* (2001). Mutations in the gene encoding epsilon-sarcoglycan cause myoclonus-dystonia syndrome. Nature genetics *29*, 66-69.

7. Attachment

7.1 List of Figures

7.2 List of Tables

7.3 Abbreviations

C. H.	Conrad Hal
° C	Degree Celsius
5-HAT	5-hydroxytryptamine
5hmC	5-hydroxymethylcytosine
5mC	5-methylcytosine
ADHD	Attention deficit hyperactivity disorder
AS	Angelman syndrome
ASR	Acoustic startle response
BBIDS	Birk-Barel intellectual disability syndrome
BDNF	Brain-derived neurotrophic factor
BER	Base excision repair
Bp	Base pair
BWS	Beckwith-Wiedemann Syndrome
C	Cytosin
C-terminal	C-terminus
cAMP	Cyclic adenosine monophosphate
Cast/Ei	Mus musculus castaneus
ChIP	Chromatin immunoprecipitation
CO_2	Carbon dioxide
CpG	5'—Cytosine—phosphate—Guanine—3'
Ct	Cycles to threshold
CTCF	CCCTC binding factor
CTCL	Cutaneous T-cell lymphoma
dB	Decibel
DMEM	Dulbecco's Modified Eagle's Medium
DMR	Differentially methylated region
DMSO	Dimethyl sulfoxide
DNA	Deoxyribonucleic acid
DNMTi	DNA methyltransferase inhibitors
DNMTs	DNA methyltransferases
dNTP	Dideoxynucleotide
dNTP	Deoxynucleotide triphosphates
DZNep	3-Deazaneplanocin A
EDTA	Ethylenediaminetetraacetic acid
EEG	Electroencephalogram
EMA	European Medicines Agency

EPM	Elevated Plus Maze
ESTs	Expressed sequence tags
EtOH	Ethanol
FBS	Fetal bovine serum
FDA	Food and Drug Administration
g	Gramm
GABA	Gamma aminobutyric acid
GPCR	G protein-coupled receptors
h	Hour
H_2O	Water
H3K27ac	Acectylation on lysine 27 of histone H3
H3K27me3	Trimethylation on lysine 27 of histone H3
H3K9me3	Trimethylation on lysine 9 of histone H3
ICE	Imprinting control element
ICR	Imprinting control region
Igf2	Insulin Like Growth Factor 2
Igf2r	Insulin Like Growth Factor 2 Receptor
K	Lysine
K+	Potassium
K+ channel	Potassium channels
K2P	Two-pore domain potassium channel
Kb	Kilobase
Kcnk9	Potassium Two Pore Domain Channel Subfamily K Member 9
*Kcnk9*KO^{hom}	*Kcnk9* knockout animals
KO	Knockout
l	Liter
LC	Locus coeruleus
lncRNA	long non-coding RNA
LTR	Long terminal repeat
min	Minutes
ml	Mililiter
mPCNs	Murine primary cortical neurons
mRNA	Messenger Ribunucleic acid
$NaHSO_3$	Sodium bisulfite
NaOH	Sodium hydroxide
Ncl.	Nucleus
NMDA	N-Methyl-D-aspartic acid
OB	Olfactory bulb
PBS	Phosphate buffered saline
PCR	Polymerase chain reaction

PGCs	Primordial germ cells
pH	Potentia Hydrogenii
piRNA	Piwi-interacting RNA
PnC	Caudal pontine reticular formation
PPI	Pre-pulse inhibition
PPi	Pyrophosphate
PPT	Pedunculopontine tegmental nucleus
PWS	Prader–Willi syndrome
QUASEP	Quantification of Allele-Specific Expression by Pyrosequencing
R	Arginine
REM	Rapid eye movement
RNA	Ribunucleic acid
RNAi	RNA interference
Rpm	Rounds per minute
RT	Room temperature
RT-PCR	Reverse transcription polymerase chain reaction
S	Serine
SAHA	Suberanilohydroxamic acid
SDS	Sodium dodecyl sulfate
SEM	Standard error of the mean
shRNA	Short hairpin RNA
siRNA	Small interfering RNA
SNPs	Single nucleotide polymorphisms
SPF	Specific-pathogen-free
SRS	Silver-Russell syndrome
T	Threonine
TET	Ten-eleven translocation
TH	Tyrosine hydroxylase
TM	Transmembrane domains
TRIS	Tris(hydroxymethyl)aminomethane
VPA	Valproic acid
WT / wt	Wild-type
µl	Mikroliter (10^{-6}l)

7.4 Conference Contributions and Publication

Conference Contributions

Cooper, A., Inhibition of histone deacetylation improves Birk-Barel intellectual disability dysmorphism syndrome in mice.

- Oral presentation at the German Society of Human Genetics, Weimar, Germany, March, 2019

Cooper, A., Inhibition of histone deacetylation up-regulates the repressed paternal allele of the imprinted *Kcnk9* gene and improves the behavioral phenotype of a mouse model of Birk-Barel syndrome.

- Poster presentation at the Forum of Neuroscience by the Federation of European Neuroscience Societies (FENS), Berlin, Germany, July, 2018
- Oral presentation and electronic poster in “Best Poster Session“ at the European Human Genetics Conference, Milan, Italy, June, 2018
- Poster presentation at the Rhine-Main Neuroscience Network Meeting, Oberwesel, Germany, June, 2018

Cooper, A., Inhibition of histone deacetylation up-regulates the repressed paternal allele of the imprinted *Kcnk9* gene towards improving the behavioral phenotype of a mouse model of Birk-Barel syndrome. Oral presentation at the German Society of Human Genetics, Münster, Germany, March, 2018

Cooper, A., Characterization of the expression of the imprinted *Kcnk9*-gene in specific brain regions and the phenotypic analysis of *Kcnk9*-knockout mice**.** Oral presentation and electronic poster delivered at the European Human Genetics Conference, Copenhagen, Denmark, June, 2017

Cooper, A., The paternal allele in Birk-Barel syndrome: chances for a rescue in a

maternal loss of function phenotype. Data presented in oral presentation at the Symposium on Translational Epigenetics by Susann Schweiger, Institute of Molecular Biology, Mainz, Germany, May, 2017

Cooper, A., Characterization of the expression of the imprinted *Kcnk9* gene in specific brain regions of mice.

- Poster presentation delivered at the German Society of Human Genetics, Bochum, March. 2017 Germany and Lübeck, Germany, March, 2016
- Poster presentation delivered at the German Society of Neurogenetics, Bonn, Germany, March, 2015

Cooper, A., The role of MTHFR in the molecular pathogenesis of varicose vein disease - global and gene-specific DNA methylation analyses in varicose veins. Poster presentation delivered at the IMB Conference “DNA Demethylation, DNA Repair and Beyond”, Mainz, Germany, May, 2012

PUBLICATIONS

- **Cooper, A,** Butto T., Jagannath, S., Akhtar, J., Lesage L., Radyushkin, K., Roeper, J., Schweiger S., Zechner. Inhibition of histone deacetylation rescues Birk-Barel - Intellectual Disability syndrome in mice. *In preparation (2019)*
- Motzek A., Knežević J., Switzeny O.J., **Cooper A.**, Barić I., Beluzić R., et al. (2016) Abnormal Hypermethylation at Imprinting Control Regions in Patients with S-Adenosylhomocysteine Hydrolase (AHCY) Deficiency. PLoS ONE 11(3): e0151261.
- Wilmanns C., **Cooper A.**, Wockner L., et al. Morphology and Progression in Primary Varicose Vein Disorder Due to 677C>T and 1298A>C Variants of *MTHFR*. *EBioMedicine*. 2015;2(2):158-164. doi:10.1016/j.ebiom.2015.01.006.

7.5 Statement of Authorship (Selbstständigkeitserklärung)

Hiermit erkläre ich, Alexis Cooper (geboren am 27.11.1985 in Kansas Fort Riley, USA), die hier vorliegende Arbeit selbstständig und ohne unerlaubte Hilfe angefertigt zu haben und alle verwendeten Hilfsmittel und Inhalte aus anderen Quellen als solche kenntlich gemacht zu haben. Zudem versichere ich, dass die vorliegende Arbeit noch an keiner anderen Fakultät oder Universität zur Prüfung vorgelegen hat.

Mir ist der Inhalt der Promotionsordnung bekannt.

Alexis Cooper